Strained Ferrocenophanes Bridged by Silicon for New Metallopolymers

A Thesis Submitted to the College of

Graduate and Postdoctoral Studies

in Partial Fulfilment of the Requirements

for the Degree of Master of Science

in the Department of Chemistry

University of Saskatchewan

Saskatoon

By

JOSÉ ESTEBAN FLORES

Permission to use

In presenting this thesis in partial fulfillment of the requirements for a Postgraduate degree from the University of Saskatchewan, I agree that the Libraries of this University may make it freely available for inspection. I further agree that permission for copying of this thesis in any manner, in whole or in part, for scholarly purposes may be granted by Professor Jens Müller who supervised my thesis work or, in his absence, by the Head of the Department or the Dean of the College in which my thesis work was done. It is understood that any copying or publication or use of this thesis or parts thereof for financial gain shall not be allowed without my written permission. It is also understood that due recognition shall be given to me and to the University of Saskatchewan in any scholarly use which may be made of any material in my thesis.

Requests for permission to copy or to make other uses of materials in this thesis in whole or part should be addressed to:

Head of the Chemistry Department
165-110 Science Place
University of Saskatchewan
Saskatoon, Saskatchewan S7N 5C9 Canada

ABSTRACT

In recent years, the Müller group has developed a route to strained ferrocenophanes (FCPs) with planar-chirality. Alkyl groups are usually incorporated into the ferrocene moiety to increase the solubility of the resulting polymers. Unfortunately, thermal ring-opening polymerization (T-ROP) of S_p,S_p-**39** (Figure i) equipped with two *i*Pr groups resulted in an insoluble polymer (S_p,S_p-**39**)$_n$. In order to increase the solubility of the polymers and study the primary structure of the polymers, some alterations have been made either in the monomer or in the ROP process. The *i*Pr groups have been replaced by Et groups, which have a higher conformational freedom. On the other hand, transition-metal-catalyzed ROP (TMC-ROP) of FCPs equipped with *i*Pr groups have been explored. Following the well-known "Ugi's amine" chemistry, new dibromoferrocene derivatives with planar-chirality were prepared to access new metallopolymers. The syntheses and characterization of C_1- and C_2-symmetric, new dibromoferrocene derivatives are described. Dibromoferrocene species *rac*-1,1'-dibromo-2-ethylferrocene (*rac*-**41**), and (S_p,S_p)-1,1'-dibromo-2,2'-diethylferrocene (S_p,S_p-**42**), *rac*-1,1'-dibromo-2-(hydroxyethyl)ferrocene (*rac*-**46**) were prepared and fully characterized (Figure ii).

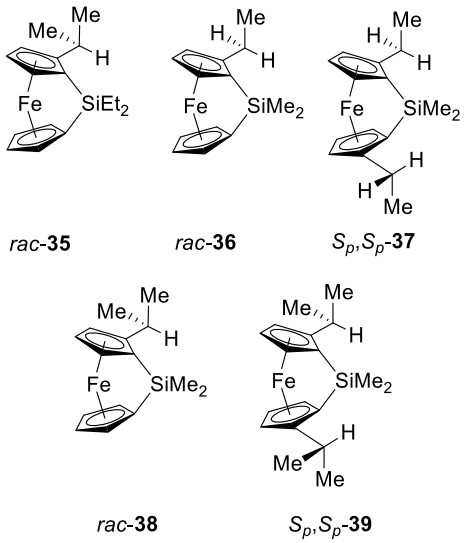

Figure i. Prepared sila[1]ferrocenophanes.

Salt-metathesis reactions of the dilithio derivatives of *rac*-**41** and S_p,S_p-**42** with Me_2SiCl_2 afforded novel silicon-bridged [1]FCPs *rac*-**36** and S_p,S_p-**37**, respectively (Figure i). New sila[1]ferrocenophane *rac*-**35** and known sila[1]ferrocenophanes *rac*-**38** and S_p,S_p-**39** were also prepared (Figure i).

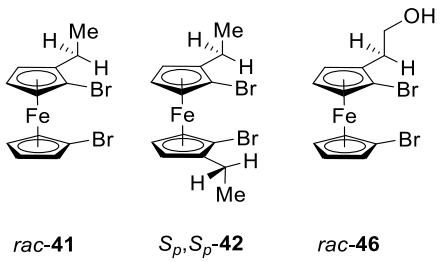

rac-**41** S_p,S_p-**42** *rac*-**46**

Figure ii. Prepared dibromoferrocenes.

T-ROP of *rac*-**35**, *rac*-**36**, and S_p,S_p-**37** afforded polymers (*rac*-**35**)$_n$, (*rac*-**36**)$_n$, and (S_p,S_p-**37**)$_n$, respectively. Polymers (*rac*-**35**)$_n$ and (*rac*-**36**)$_n$ are soluble in thf and benzene. Therefore, they were fully characterized by nuclear magnetic resonance (NMR) and gel-permeation-chromatography (GPC) analysis. Polymer (S_p,S_p-**37**)$_n$ could not be characterized due to its poor solubility. Copolymers **49** and **50**, which were obtained from mixtures of *rac*-**38** and S_p,S_p-**39** in ratios of 90 : 10 and 70 : 30, respectively, have also been prepared.

TMC-ROP of *rac*-**38** and S_p,S_p-**39** yielded polymers (*rac*-**38**)$_n$ and (S_p,S_p-**39**)$_n$, respectively. Polymer (*rac*-**38**)$_n$ is soluble in thf and benzene and was fully characterized by GPC analysis and NMR spectroscopy. However, polymer (S_p,S_p-**39**)$_n$ could not be characterized due to its poor solubility.

Polyferrocenylsilane (PFS) (S_p,S_p-**37**)$_n$ was not significantly more soluble in common organic solvents than PFS (S_p,S_p-**39**)$_n$, which means that replacing *i*Pr groups by Et groups did not increase the solubility of the respective polymer. The decrease of the steric bulkiness in the ferrocene moieties of the polymer (*rac*-**36**)$_n$ did not affect the weight average molar mass (M_w),

whereas the increase of the steric bulkiness on silicon in (*rac*-**35**)$_n$ resulted in a significant decrease of the M_w. TMC-ROP of *rac*-**38** gave a more regular PFS than that obtained from T-ROP, which means that the addition of new monomers to the propagating chain end occurred with a higher selectivity.

ACKNOWLEDGMENTS

I would like to express how grateful I am to my supervisor Professor Jens Müller for his support on my M.Sc. studies and related research. His guidance and immense knowledge helped me in all the time of research and writing this thesis.

I would like to thank the University of Saskatchewan and the Department of Chemistry for providing me the opportunity to study here and providing financial support. I am grateful for the advice of my advisory committee and the assistance of the staff at the Saskatchewan Structural Science Centre: Dr. Keith C. Brown for his help with NMR measurements, Ken Thoms for measuring mass spectra, and Dr. Jianfeng Zhu for his help with NMR measurements and X-ray diffraction analysis. I am thankful to Dr. Marcelo Sales for being the best lab manager I could have asked for. Also, I would like to thank Leah Hildebrandt for having the answers to all my questions. I would like to acknowledge all past and present members of the Müller Research group for their support and comradery throughout my studies with a special mention to Dr. Elaheh Khozeimeh Sarbisheh.

I must undoubtedly express my very profound gratitude to my parents María Inés Flores Navarrete and José Esteban Marcos, my siblings Rosa María Esteban Flores and Daniel Esteban Flores, and my niece Leyla Esteban Flores for providing me with unfailing support, unconditional love, and continuous encouragement throughout my years of study.

I am immensely grateful to my friends, especially María de la Torre Romero, María Hevia Azcue, and María García Fernández, who have showed me that friendship can last a lifetime.

Finally, I would like to convey my special thanks to Manuel Andrés Sanz for all the unequivocal support and encouragement.

José Esteban Flores

TABLE OF CONTENTS

LIST OF FIGURES

page

LIST OF SCHEMES

page

LIST OF TABLES

page

LIST OF ABBREVIATIONS

Ar′……....2-(Me_2NCH_2)C_6H_4

cod……..……1,5-cyclooctadiene

Cp……...……...…..cyclopentadienyl

Cp^H…….C_5H_4

Cp^{Et}…….....EtC_5H_3

Cp^{iPr}……...*i*PrC_5H_3

Đ……...dispersity

Da……..……..dalton

Fc……...…….(C_5H_4)FeCp

FCP……ferrocenophane

GPC……..….gel-permeation-chromatography

Mamx……2,4-*t*Bu_2-6-(Me_2NCH_2)C_6H_2

MCP…….…….metallocenophane

Me_2Ntsi…….….$C(SiMe_3)_2SiMe_2NMe_2$

M_n……...……number average molar mass

M_w……..…….……weight average molar mass

ODG…….*ortho*-directing group

PFS……..….poly(ferrocenylsilane)

PS……polystyrene

Pytsi……$C(SiMe_3)_2SiMe_2$(2-C_5H_4N)

r.t……room temperature

ROP……..……ring-opening polymerization

TCB……..…..1,2,4-trichlorobenzene

T-ROP…….……...…..…thermal ring-opening polymerization

TMC-ROP…….....…transition-metal-catalyzed ring-opening polymerization

tmeda……...……N,N,N′,N′-tetramethylethylenediamine

Vol…….....……volume

XRD……..…….…….X-ray diffraction

CHAPTER 1

INTRODUCTION

The development of synthetic organic polymers during the last century had an extraordinary impact on the growth of society.[1] Polymers, commonly comprised of C, N and H atoms, are literally everywhere e.g. in containers, cooking utensils, clothes, glasses, and cars. Nonetheless, metals cover approximately 80% of the elements of the periodic table, so a huge potential for the application of metallopolymers is currently untapped.[1] Metallopolymers are inorganic or organometallic polymers that contain metal atoms in the polymer chain. If transition metals are incorporated into the main chain of a polymer, it will offer a unique potential for the preparation of materials with properties that are significantly different from those of conventional organic polymers. In addition, the diverse range of coordination numbers and geometries which exist for transition elements offers the possibility of accessing polymers with unusual conformational, mechanical, and morphological characteristics.[2]

Metallopolymers can be used as precursors to ceramics[3] and in catalysis[4] due to their ability to activate organic molecules. Moreover, they present magnetic, electronic, redox, and optical properties which organic polymers do not.[5] The majority of organic compounds are diamagnetic, however, metal ions may have unpaired electrons whose magnetic moments can align in the solid state in different ways resulting in ferromagnetic, antiferromagnetic or superparamagnetic properties. Metallopolymers can be either side-chain metal-containing polymers or main-chain metal-containing polymers (Figure 1-1).[5] Main-chain metal-containing polymers show more diverse properties that can be used to obtain some improved materials due to the proximity of the metal ions, which results in metal-metal interactions. For this class of metallopolymers several synthetic methods are known. The most used and common route to obtain metallopolymers is the

ROP of [*n*]metallocyclophanes, whereby the thermodynamic driving force for the ROP process is the presence of ring strain.[5]

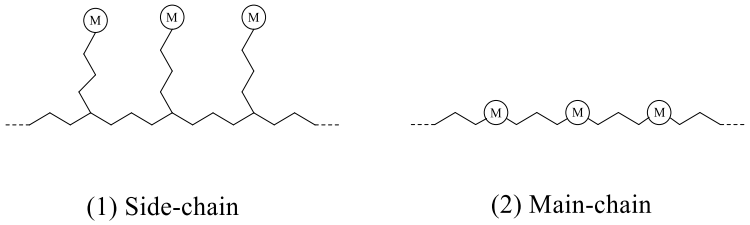

Figure 1-1. Structural classes of linear metallopolymers: (1) side-chain and (2) main-chain metallopolymers.

[*n*]Metallocyclophanes are strained cyclic organometallic compounds with a transition metal between two π-hydrocarbon rings (Figure 1-2).[2] These sandwich compounds can be homoleptic (e.g. **1** and **2**), with two identical π-hydrocarbon rings, or heteroleptic (e.g. **3** and **4**), with two different π-hydrocarbon rings. In both cases the two rings are linked together by *n* atoms in the bridge.

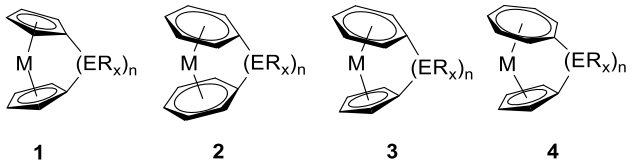

Figure 1-2. Generic forms of [*n*]metallocyclophanes.

Many [*n*]metallocyclophanes have been discovered, with the largest class of strained cyclic organometallic compounds being [*n*]metallocenophanes. In this class, a transition metal M is bound to two η^5-cyclopentadienyl (Cp) rings, which are linked by a bridging chain with *n* atoms in its backbone. In metallocenes the two Cp rings are parallel to each other (**5**; Figure 1-3). Nonetheless, in [*n*]metallocenophanes the two Cp rings are linked by a short bridging moiety,

which results in a ring-tilted structure. Due to the tilt, the system bears some strain (**6**; Figure 1-3).[6] The tilt within [1]FCPs is described *via* the tilt angle α.[7, 8] The α angle is the dihedral angle between the two Cp rings and an increase of this angle results in an increase of the total energy of the molecule.[6] In addition to the α angle, structural distortions in [*n*]FCPs are described with the angles β ($Cp_{centroid}$-C_{ipso}-E angle), θ (C_{ipso}-E-C'_{ipso} angle), and δ ($Cp_{centroid}$-M-$Cp'_{centroid}$) (**6**, Figure 1-3).[7]

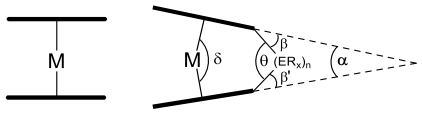

5 **6**

Figure 1-3. Representation of metallocenes (**5**) and geometric parameters α, β, δ, and θ in [*n*]metallocenophanes (**6**).

1.1. [1]Ferrocenophanes

The most widely investigated class of [*n*]metallocyclophanes is that of [*n*]ferrocenophanes (**6**, M = Fe). In fact, the first [*n*]metallocenophane that was discovered was a [3]ferrocenophane ([3]FCP) (**7**; Figure 1-4), which was reported by Rinehart Jr. *et al*. in 1957.[9] Shortly after, a [2]FCP (**8**; Figure 1-4) with C_2Me_4 bridge was reported by the same research group.[10] These two FCPs contained a hydrocarbon bridge that linked the two Cp rings together.

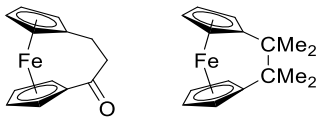

7 **8**

Figure 1-4. The first [*n*]ferrocenophanes containing a hydrocarbon bridge.

It was not until 1975 that Osborne and coworkers reported the synthesis of the first [1]FCPs with a silicon bridge (**9** and **10**; Figure 1-5).[11]

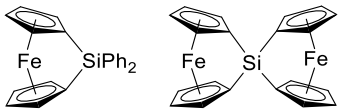

9 **10**

Figure 1-5. The first sila[*n*]ferrocenophanes.

The most common method to synthesize [*n*]FCPs is the salt-metathesis reaction. This method involves the deprotonation of the parent metallocene, allowing the dilithio derivative to react with an element dihalide R_xEX_2, whose R_xE moiety serves as a bridging unit between the two Cp rings (Scheme 1-1).[8] Several strained [1]FCPs, with bridging elements from group 13 (B, Al, Ga, In), group 14 (Si, Ge, Sn), group 15 (P, As), group 16 (S, Se), and group 4 (Ti, Zr, Hf) have been prepared by the salt-metathesis reaction.[8]

Scheme 1-1. Salt-metathesis reaction of 1,1'-dilithioferrocene with an element dihalide.

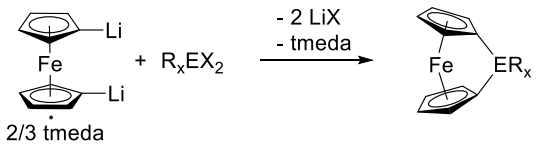

1.1.1. Aluminum- and Gallium-Bridged [1]Ferrocenophanes

The development of new metallopolymers containing Al and Ga has been an active research area for Dr. Müller's group.[12–16] In 2005, the first aluminum- and gallium-bridged [1]FCPs were reported. These species were equipped with bulky *trisyl*-derived ligands (Pytsi and Me_2Ntsi; Scheme 1-2),[13] as sterics plays a vital role for the outcome of the salt-metathesis reaction.

Scheme 1-2. Synthesis of gallium- and aluminum-bridged [1]FCPs with Pytsi or Me_2Ntsi ligand.

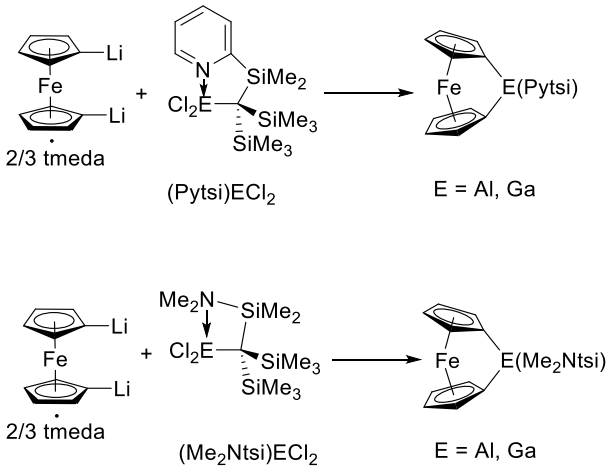

Sterics also plays a crucial role for the polymerizability of the resulting strained compounds. Attempts to polymerize these first aluminum- and gallium-bridged [1]FCPs were unsuccessful. It was concluded that the bulkiness of the ligands (Me_2Ntsi or Pytsi; Scheme 1-2) prevents the polymerization from occurring.[16, 17] On the other hand, if the bulkiness of the ligand is significantly reduced, as is the case of Ar' ligand, [1.1]FCPs form instead of the targeted [1]FCPs (Scheme 1-3).[18, 19] All these compounds form the *first generation* of strained aluminum- and gallium-bridged [1]metallocenophanes.[20]

Scheme 1-3. Formation of untargeted [1.1]FCPs instead of [1]FCPs.

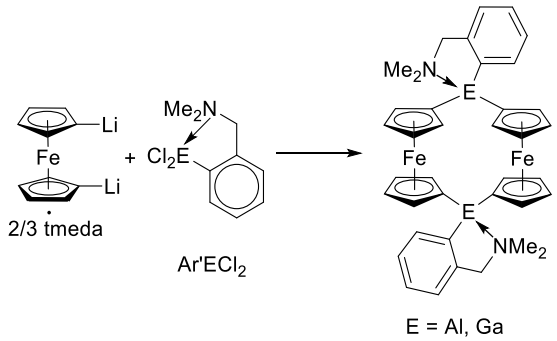

Inspection of structural data for [1]FCPs and [1.1]FCPs suggests that the space available for the bridging unit ER_x decreases from [1]FCPs to poly(ferrocene)s (PFs) to [1.1]FCPs (Figure 1-6).[21]

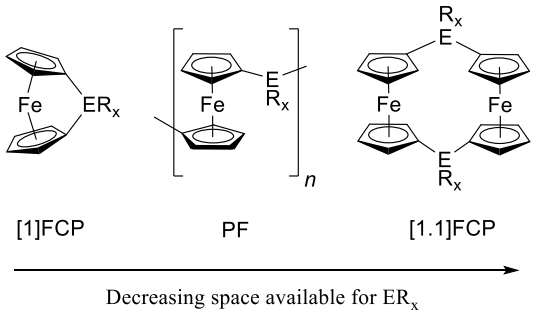

Figure 1-6. Illustration of space restrictions in [1]FCPs, PFs and [1.1]FCPs.

Hence, the required bulkiness of the ligands of the element dihalides should be moderate to be able to obtain [1]FCPs which are reactive toward ROP and block the formation of [1.1]FCPs.[22] As a consequence, the use of a ligand with the right bulkiness was the next attempt to obtain [1]FCPs that are reactive enough to undergo ROP. This led to the use of the Mamx ligand, which is a bulkier derivative of the Ar' ligand due to the presence of *t*Bu groups.[15, 16] The use of Mamx ligand resulted in highly reactive [1]FCPs, the *second generation* of strained aluminum- and gallium-bridged [1]metallocenophanes, which could not be isolated or purified (Scheme 1-4).[20]

Scheme 1-4. Reaction outcome with the Mamx ligand.

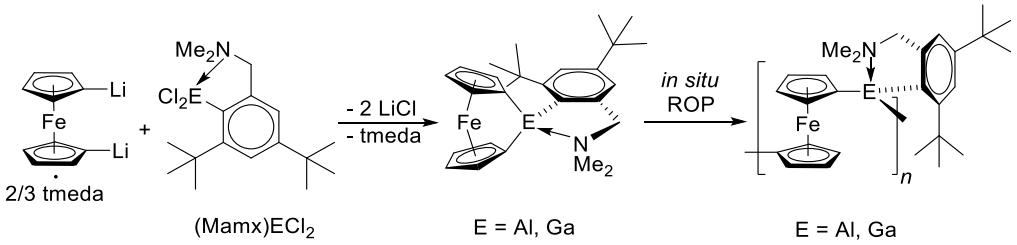

For the *third generation* of strained aluminum- and gallium-bridged [1]metallocenophanes instead of increasing the bulkiness of the ligand on the bridging element, the bulkiness of the ferrocene moiety was increased. This was achieved by replacing the H atoms in α positions with respect to the Br atoms on the Cp rings by bulky alkyl groups (**11**; Figure 1-7).[1, 20]

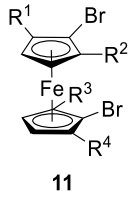

11

Figure 1-7. Proposed precursor for the preparation of α-substituted dilithioferrocene derivatives.

To do so, an approach developed by Ugi *et al.* was used.[23] The aim was to introduce an *ortho*-directing group, C*H(Me)NMe_2, on one or both Cp rings that leads to diastereoselective α lithiation. When reacting the dilithio derivative of S_p,S_p-**12** with element dichlorides, the targeted [1]FCPs S_p,S_p-**13** were formed (Scheme 1-5). This result provided evidence that isopropyl groups in α positions on Cp rings hinder the formation of [1.1]FCPs. This attempt resulted in isolable and reactive [1]FCPs, despite the low bulkiness of the ligand attached to the bridging element.[20]

Scheme 1-5. Synthesis of the chiral [1]FCPs S_p,S_p-**13**.

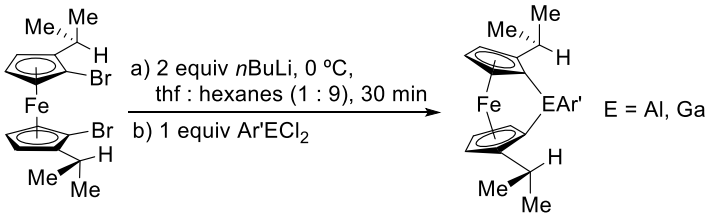

S_p,S_p-**12** S_p,S_p-**13**

1.1.2. Silicon-Bridged [1]Ferrocenophanes

Organometallic ferrocene-derivative polymers containing silicon in the bridging position, called poly(ferrocenylsilane)s (PFSs), are widely investigated because functionalized organosilanes have been shown to possess silicon-dependent electronic properties that operate over both short and long distances.[24]

As mentioned above, the first silicon-bridged [1]FCPs **9** and **10** (Figure 1-5) were synthesized in the 1970s by Osborne *et al.* Typical values of α angle for sila[1]ferrocenophanes lie between 16 and 21°.[25–27] As a result of their ring strain, they can readily undergo ROP reactions to give PFSs. These compounds are highly suitable for ROP as even sila[1]ferrocenophanes with an extremely bulky substituent, such as $Si(SiMe_3)_3$, attached to the silicon bridging element can undergo ROP.[28]

However, it was not until 1992 that Manners *et al.* reported the first ROP of silicon-bridged [1]FCPs (**14** and **9**; Scheme 1-6) using a thermal method, which afforded high-molecular-weight PFSs [$(\mathbf{14})_n$ and $(\mathbf{9})_n$].[26] The mechanism for this reaction is not understood yet, however, what is known is that it proceeds *via* a nonselective cleavage of Si−Cp bonds in the case of asymmetric [1]FCPs.

Scheme 1-6. First T-ROP of sila[1]ferrocenophanes.

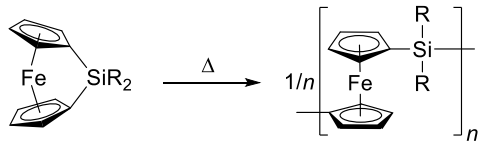

9 (R = Ph)
14 (R = Me)

$(\mathbf{9})_n$ (R = Ph)
$(\mathbf{14})_n$ (R = Me)

In 1995 it was found that ROP of sila[1]ferrocenophanes can be metal-catalyzed by some Rh^{I}, Pd^{II}, Pd^{0}, Pt^{II}, and Pt^{0} containing complexes.[29, 30] Transition-metal-catalyzed ROP (TMC-ROP) presents some advantages over anionic ROP and thermal ROP (T-ROP) as it does not require a high purity for the monomer or the solvent and it occurs at mild temperatures. On the other hand, the dispersity ($Đ$) is usually higher (> 1.4) than that expected for anionic ROP (≈1).[30]

1.2. Poly(ferrocene)s *via* Ring-Opening Polymerization of Strained [1]Ferrocenophanes

In 1955, the first metallopolymers with metal ions in the side-chains were prepared.[31] On the other hand, the preparation of metallopolymers containing metals in the main-chain was held back by synthetic difficulties. Main-chain ferrocene-containing polymers were first prepared by step-growth polycondensation reactions.[32] Polycondensation reactions of dilithioferrocene with dihaloorganosilanes (e.g. Me_2SiCl_2) afforded low-molecular-weight and highly dispersed polymers [(**14**)$_n$, Scheme 1-7] which correspond to 5 – 19 repeat units [M_n = 1700 – 3400].[32, 33] Moreover, the obtained low-molecular-weight polymers were impure.

Scheme 1-7. Polycondensation reactions to prepare poly(ferrocenylsilane)s.

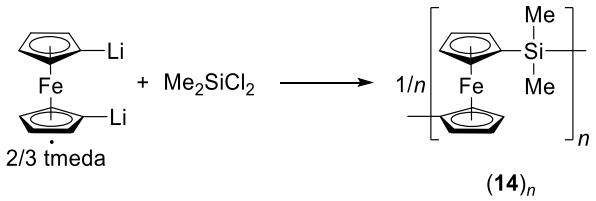

(**14**)$_n$

Since the early 1990s, many of the obstacles for the preparation of high-molecular-weight and soluble materials have been overcome through the development of new synthetic approaches that are compatible with the presence of metal centers. In 1992, the discovery of a ROP reaction afforded high-molecular-weight metallocene-containing polymers.[26] In order to undergo ROP, the monomers are required to present a cyclic structure and some strain. [1]FCPs bear some strain due

to the presence of the bridging element that tilts the Cp rings. Therefore, [1]FCPs are good candidates for ROP toward high-molecular-weight metallopolymers.

1.2.1. Thermal ROP

The first ROP of metallocenophanes was reported in 1992.[26] This ROP was thermally conducted and silicon-bridged [1]FCPs (**9** and **14**; Scheme 1-6) were employed. The required temperatures for sila[1]ferrocenophanes **9** and **14** were 230 °C and 130 °C, respectively. Polymer (**14**)$_n$ was successfully characterized, however, characterization of polymer (**9**)$_n$ was not possible due to its poor solubility.[26] The molecular weight for (**14**)$_n$ was determined to be in the range of $M_w = 10^5 – 10^6$ Da (rel. to PS).[26] The mechanism for the T-ROP is not understood yet, however, it is known that it proceeds with cleavage of the Cp–Si bond, which was reported by Manners *et al.* in 1995.[34] Despite being a convenient method to access metallopolymers from metallocenophanes, T-ROP affords no control over the molecular weight or the molecular-weight distribution of the polymers. In addition, obtained dispersities are large ($Đ = M_w / M_n \approx 1.5 – 2.5$).[35]

1.2.2. Anionic ROP

In 1994, Manners *et al.* reported the first anionic ROP reactions of metallocenophanes. Silicon-bridged [1]FCP **14** ring-opened in the presence of anionic initiators such as lithioferrocene, phenyllithium, or *n*BuLi (Scheme 1-8).[22]

Scheme 1-8. Anionic ROP of the silicon-bridged [1]FCP **14**.

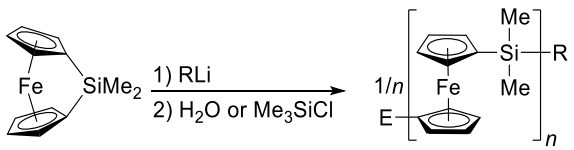

14 (**14**)$_n$

R = Fc, Ph, *n*Bu

E = H, Me_3Si

Anionic ROP of strained [1]FCPs can be conducted at room temperature, however, high purity of monomers and solvents are essential to avoid termination reactions and achieve living anionic ROP.[22, 36, 37] The mechanism for anionic ROP is widely accepted. For example, in the case of monomer **14**, the formation of an anionic growing chain is involved. This anionic chain has a living end that can either keep growing and continue the polymerization or be terminated with different capping agents to afford PFS (**14**)$_n$ (Scheme 1-8). As long as impurities are not present, chain transfer or uncontrolled termination reaction does not occur, resulting in low dispersities ($Đ$ < 1.10). An advantage for anionic ROP in comparison to T-ROP is the control over the molecular weight of the polymers. This is possible because the monomer-to-initiator ratio controls the number of chain propagating sites.[22, 36, 37] In addition to give access to well-defined homopolymers, anionic ROP also allows the synthesis of copolymers.[35, 37] This is achieved by adding a different monomer once the first monomer is consumed in the reaction mixture.[38]

1.2.3. Transition-Metal-Catalyzed ROP

In contrast to T-ROP or anionic ROP, TMC-ROP requires milder reaction conditions. For example, TMC-ROP is a methodology that allows the polymerization of the monomers at room temperature. Furthermore, it requires neither highly pure solvents nor pure monomers. This is a clear advantage over anionic ROP as it is often challenging to obtain pure solvents and monomers in high purity. The first TMC-ROP of strained [1]FCPs was reported in 1995.[29, 30] This type of ROP can be achieved by using late-transition-metal complexes, such as Karstedt's catalyst, $PtCl_2$, and $PdCl_2$.[29, 30] For example, silicon-bridged [1]FCP **14** underwent TMC-ROP resulting in polymer (**14**)$_n$ with $M_n \approx 10^5$ Da (Scheme 1-9).[29]

Scheme 1-9. TMC-ROP of the silicon-bridged [1]FCP **14**.

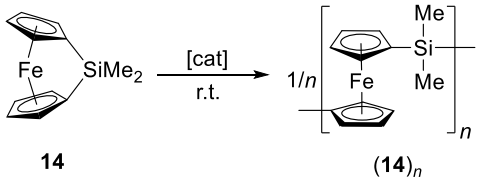

In addition to milder reaction conditions in terms of temperature and purity of monomers and solvents, TMC-ROP is also beneficial to obtain regioregular polymers of unsymmetrically substituted silicon-bridged [1]FCPs. For instance, TMC-ROP of monomer **15** gives a regioregular PFS (**15a**)$_n$ (Scheme 1-10), while T-ROP yields a regioirregular polymer (**15b**)$_n$ (Scheme 1-11).[34]

Scheme 1-10. TMC-ROP of the silicon-bridged [1]FCP **15**.

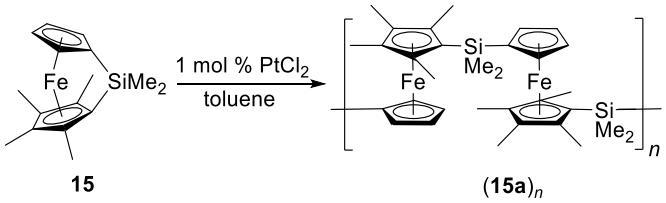

Scheme 1-11. T-ROP of the silicon-bridged [1]FCP **15**.

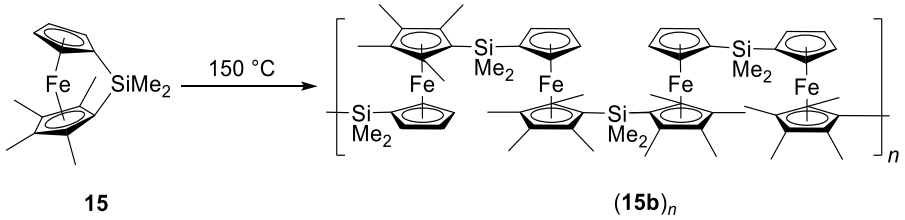

The mechanism for TMC-ROP is not completely understood, however, many proposals for the mechanism have been made. In 1997, a homogeneous reaction pathway[39] was considered, however, a heterogenic catalytic route has been proposed recently.[40] According to the heterogenic catalytic route, metallic colloids would act as the main active catalyst (Scheme 1-12). For example, if [Pt(1,5-cod)$_2$] is used as the pre-catalyst, insertion of the transition metal into the Cp-Si bond of

the monomer **14** to form platinasila[2]ferrocenophane **16** seems to be the first step (Scheme 1-12). Despite acting as a pre-catalyst, the dimethylsilylferrocenophane component within species **16** does not incorporate into the growing polymer. Incorporation of more monomer into the growing polymer leads to the formation of sila[1]ferrocenophanes and dimeric [1.1]FCPs. Employment of mercury, a well-known inhibitor for heterogeneous reactions, further supported the heterogeneous mechanism as significant retardation was observed.[40] Although mercury inhibited the ROP, polymer did slowly form in a significantly lower yield. This led to the conclusion that a minor homogeneous component is present.[40]

Scheme 1-12. Proposed mechanism for the TMC-ROP of silicon-bridged [1]FCP **14**.

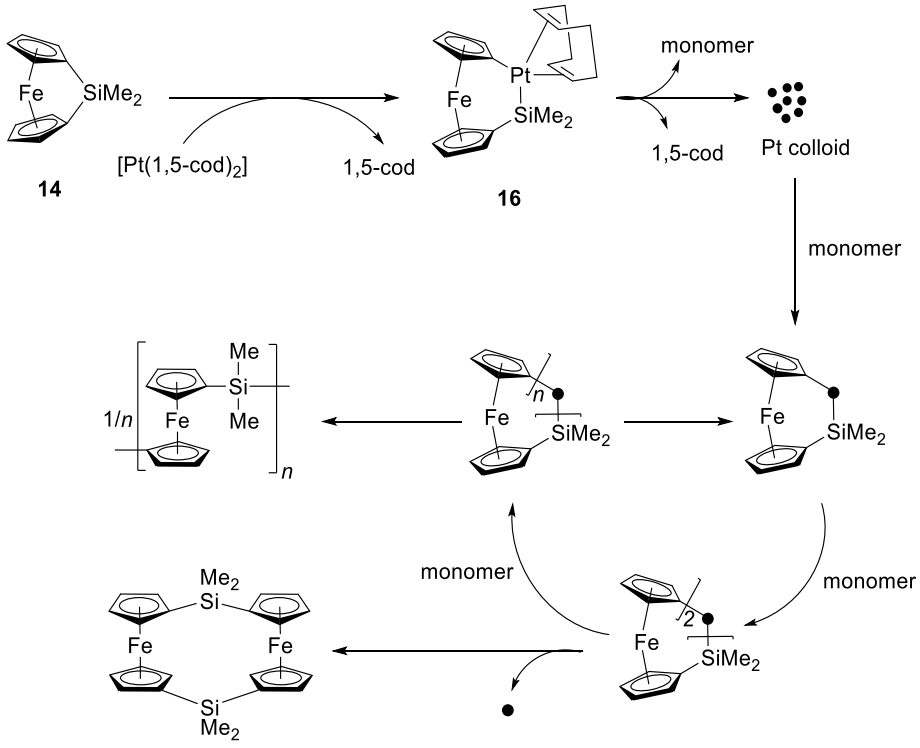

1.2.4. Photolytic ROP

In 2000 Mizuta *et al.* reported the first photolytic ROP reaction of a phosphorus-bridged [1]FCP.[41] However, it was not until 2007 that Manners *et al.* reported the first photolytic ROP for the silicon-bridged [1]FCP **14** (Scheme 1-13) and, in 2008, for the C_2H_4-bridged [2]FCP **21** (Scheme 1-14). Both monomers showed a η^5 to η^1 haptotropic shift, with irradiation and in the presence of donor ligands.[42, 43] The silicon-bridged [1]FCP **14** can be ring-opened photolytically in the presence of terpyridine **17** to give species **18**. Next, species **18** reacts with more monomer in order to propagate and form a growing PFS polymer chain **19**. After forming species **19**, backbiting and macrocondensation reactions may occur. Backbiting involves the formation of the cyclic dimer **20** due to the attack of the propagating Cp ring to the iron centre in the previous repeat unit. On the other hand, in the macrocondensation reaction the propagating Cp ring attacks the iron centre of the neighboring polymer chain to form a longer polymer.[43]

Scheme 1-13. Proposed mechanism for the photolytic ROP of silicon-bridged [1]FCP **14** using terpyridine **17** as initiator.

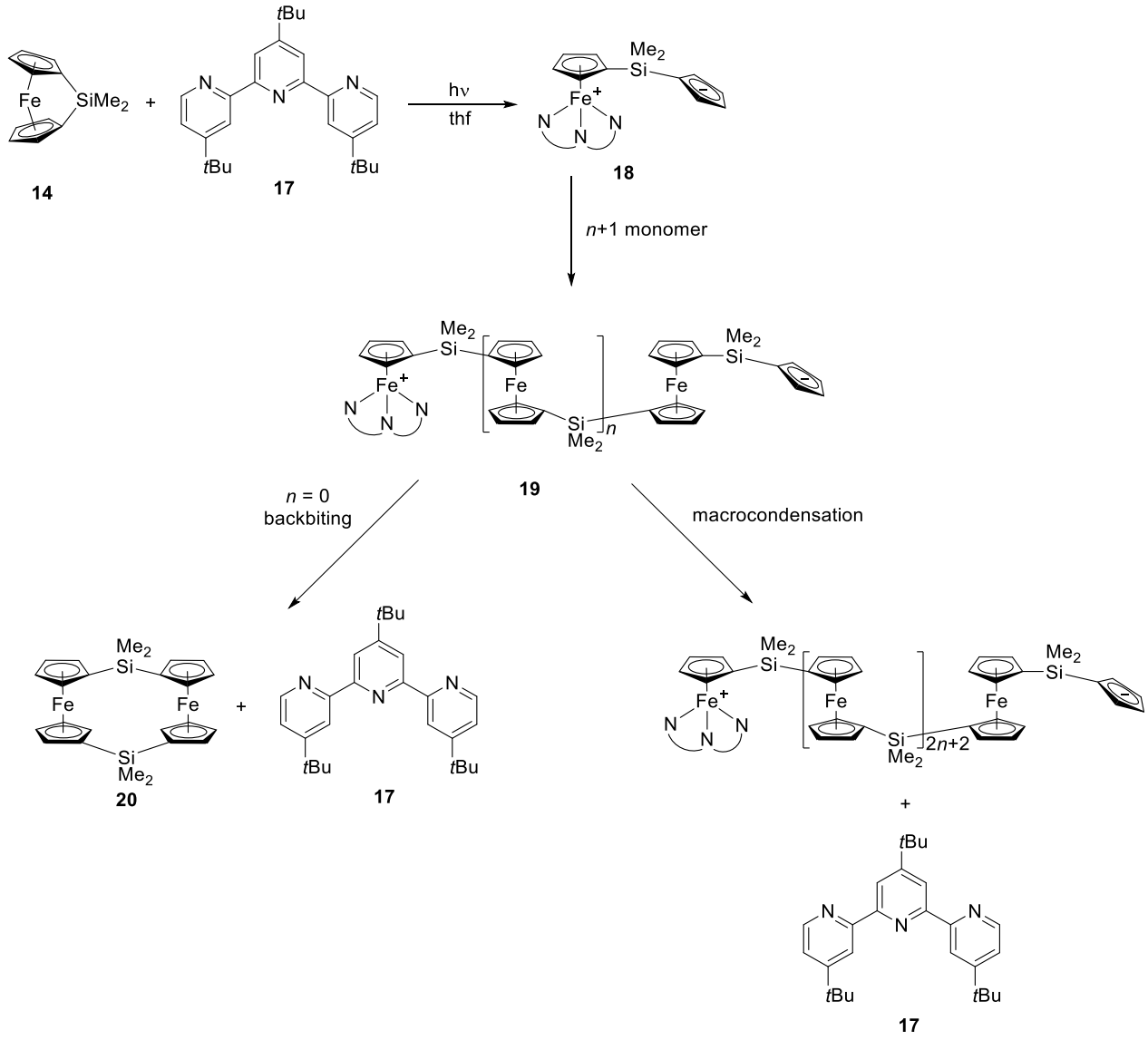

In the case of the photolytic ROP of monomer **21**, the solvent choice plays a crucial role in the outcome of the reaction (Scheme 1-14). The use of benzene as the solvent of the reaction afforded a yellow insoluble polymer (**21**)$_n$. By contrast, if the reaction is done in ethanol, ring-opened species **22a** and **22b** are obtained whose PMe_3 ligands can be replaced by a Cp ring *via* irradiation in the presence of NaCp to afford **23a** and **23b**.[42]

Scheme 1-14. Proposed mechanism for the photolytic ROP of ethane-bridged [2]FCP **21**.

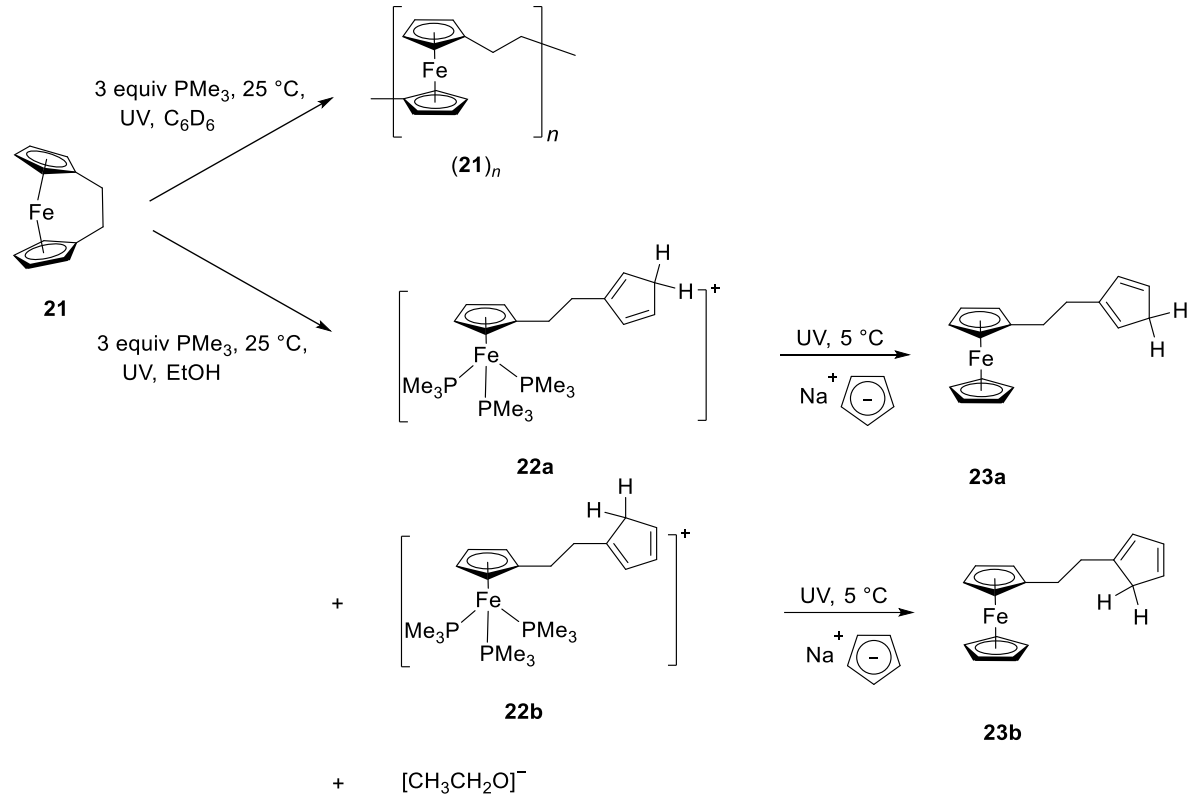

1.2.5. Applications of Metallopolymers

Synthetic organic polymers have played a revolutionary role in terms of the materials available to modern society. Adding metal centers to the polymer chain could lead to materials with advanced properties. Metal centers are of high importance in solids with extended two- or three-dimensional structures and in biological macromolecules. Some of the multiple examples include magnetic materials used in data storage, superconductors, electrochromic and luminescent materials, and homogeneous and biological catalysts including metalloenzymes.[44]

The incorporation of metals into the main chain of a polymer might be expected to enhance the conductivity of the system, due to the different oxidation states and unpaired electrons. However, matching the orbital energies of the metal center with those of the organic linkers is not usually efficient and, therefore, most metallopolymers behave like semiconductors. Unlike carbon,

transition metals can readily change coordination number or oxidation state. When these elements are incorporated into polymers, coordination number and oxidation-state changes can make the system alternate between states of relative high and low conductivity, which enables metallopolymers to act as both sensors and switches. For example, Swager and coworkers have developed conductive metallopolymers that can sense analytes by changes in resistivity.[45]

Metal-containing homopolymers that are sensitive to ultraviolet (UV) irradiation and resistant to plasmas have been synthesized. This makes them suitable for applications in surface patterning and decoration with functional metal-based nanostructures. For instance, PFSs (**9**)$_n$ and (**14**)$_n$ (Scheme 1-6), are extraordinary resists for reactive ion etching using oxygen plasmas, as the materials form an etch-resistant metal-containing surface layer of iron-silicon oxides.[46, 47]

Moreover, metal centers play a key role in the function of many important biological macromolecular materials, such as oxygen and electron transfer. The coordination of metal ions to DNA has been seen as a possible methodology for altering the electronic properties of DNA in a controlled manner.[48]

1.3. Planar-Chiral Ferrocenes

Preparation of ferrocene was reported at about the same time by two research groups, Pauson and Kealy in 1951[49] and Miller *et al.* in 1952.[50] Based on ferrocene's physical properties, a sandwich structure was proposed[51, 52] which was confirmed by X-ray diffraction (XRD) studies.[53] Since then, other metallocenes composed of other metals and other cyclic hydrocarbons, such as bisbenzenechromium and uranocene, have been prepared. Ferrocene was found to react like an electron-rich organic compound, similar to phenol.[54] Consequently, numerous known organic reactions were successfully tested on ferrocene. For example, Friedel-Crafts acylation produces ferrocenyl ketones that can be reduced to secondary ferrocenyl alcohols with a stereogenic carbon

atom. A derivative of ferrocene with two different substituents in the same Cp ring cannot be superposed with its mirror image, consequently, it is chiral. Based on Schlögl's systematic investigations, this isomerism is referred to as planar-chirality.[55] Planar-chirality is the chirality resulting from the arrangement of out-of-plane groups with respect to a plane called chiral plane.[56] In contrast to central-chirality, planar-chirality does not require a stereogenic center to be present. In order to assign the planar-chirality of a ferrocene derivative, one needs to base on the Cahn-Ingold-Prelog (CIP) rules. Similar to central chirality, if the shortest path from the substituent with higher priority to the one with lower priority is clockwise, the chirality descriptor is R_p, otherwise it is S_p (Figure 1-8).[57]

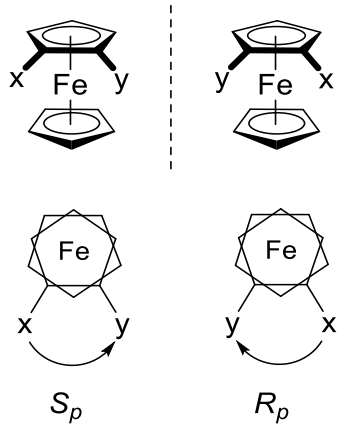

Figure 1-8. Assignment of planar-chirality for 1,2-heterodisubstituted ferrocenes, where x has a higher priority than y.

Due to the scientific interest in ferrocene, planar-chiral ferrocene derivatives have attracted a lot of attention. These compounds can be employed in asymmetric catalysis, such as asymmetric hydrogenation,[58] hydrosilylation,[45, 46] aldolization,[61, 62] cross coupling reactions,[63] Michael additions,[64] and asymmetric additions of diethyl zinc to aldehydes.[65] Planar-chiral ferrocene derivatives have also been used as chiral starting materials,[66] as chiral auxiliaries[66], and as modular

units in material science, such as in nonlinear optics and in ferroelectric liquid crystals.[67] In addition, chiral ferrocene derivatives could be of importance as structural units of products with biological and biochemical activities.[68]

1.3.1. Derivatization of Ferrocene

Planar-chiral ferrocene derivatives are important compounds in organometallic chemistry due to their various applications in asymmetric catalysis and industry. As a consequence of their importance, there are diverse synthetic ways to obtain these compounds. Different methodologies have been developed to access these molecules with a high degree of regio- and stereoselectivity.

Ferrocene is considered an aromatic compound and, as a consequence, acylation,[69] sulfonation,[70] metalation[71, 72] and arylation[70, 71] reactions can be performed. However, ferrocene has some resistance to alkylation.[70] Electrophilic aromatic substitutions of 1- or 1,1'-substituted ferrocenes (**24a-c**) leads to the formation of planar-chiral ferrocenes *rac*-**25a-c** and *rac*-**26a-c** (Scheme 1-15). For example, despite occurring with low regioselectivity, the formation of the 3-acetyl isomer is favored especially with diisopopylferrocene as the reactant.

Scheme 1-15. Friedel-Crafts monoacylation of 1- and 1,1'-alkylferrocenes.

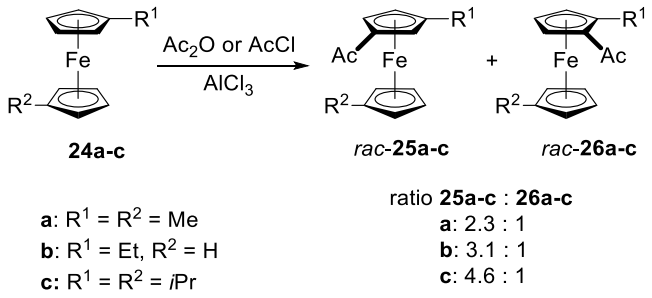

The preference for the 3-acetyl isomer can be related to the higher steric hindrance, although the inductive effect of the alkyl substituents favors the formation of the 2-acetyl isomer.[73]

Despite the electronic effects, it seems that steric hindrance is the predominant effect. The difference among the ratios for the different alkyl groups is not highly significant and this can be explained considering the bond angles. In a Cp ring, the bond angles are smaller than in benzene, hence the interaction among the substituents is weaker than in benzene (Figure 1-9).[74] That is the reason why in ferrocene the ratio difference should be smaller than in benzene.

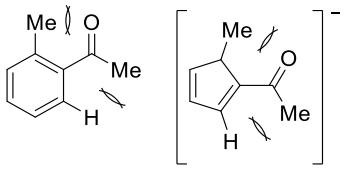

Figure 1-9. Interaction between substituents in benzene and in Cp.

The separation of isomers is usually a tedious task requiring several chromatographic columns and repeated recrystallization. Consequently, intermolecular electrophilic aromatic substitution is not the best method for the straightforward synthesis of planar-chiral ferrocene derivatives. Metalation, especially lithiation, is the most employed methodology for derivatization of ferrocene. Lithiation of ferrocene is possible using a strong lithium-containing base, such as *n*BuLi. The dilithiation of ferrocene was reported in 1967,[75] however, it was not until 1995 that exclusive monotlithiation of ferrocene was first performed.[76, 77]

1.3.2. *ortho*-Directed Metalation of Ferrocene

ortho-Directed metalation of ferrocene was first reported in 1961, whereby an alcohol group played the role of the *ortho*-directing group (ODG).[71] The reaction of **27** with *n*BuLi in diethyl ether at room temperature followed by addition of dry ice or methyl iodide results in the formation of 1,2-disubstituted ferrocene derivatives *rac*-**28a**,**b** (Scheme 1-16). Lithiation at the position 3, non-substituted Cp ring or at one of the phenyl rings did not occur.

Scheme 1-16. *Ortho*-directed lithiation of ferrocene derivative **27** containing an alcohol.

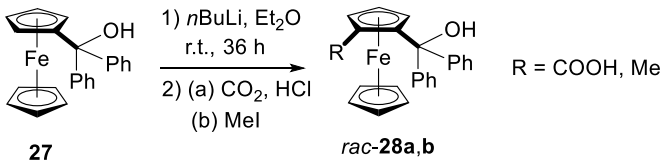

27 *rac*-**28a**,**b**

ortho-Directed metalation has become one of the most popular methods to synthesize planar-chiral ferrocene derivatives, due to its versatility and high regioselectivity. The most popular metalations are lithiation and mercuration.[78] Treating ferrocene with strong bases, such as *n*BuLi, leads to deprotonation of the Cp ring followed by metalation. This method involves the use of a ferrocene derivative with an ODG which facilitates the metalation of an *ortho*-position to that substituent.

In 1965, Slocum *et al.* reported the ferrocene derivative **29** containing an aminic ODG.[79] Lithiation of species **29** and subsequent addition of Ph_2CO led to the exclusive formation of compound *rac*-**30** (Scheme 1-17). This suggested that lithiation only took place in *ortho* position to the aminic ODG. Product *rac*-**30** was obtained as long as a diethyl ether / hexanes mixture was used as the reaction solvent. By contrast, thf / hexanes mixture resulted in a mixture of substituted ferrocene derivatives.

Scheme 1-17. *Ortho*-directed lithiation of ferrocene derivative **29** containing an amine.

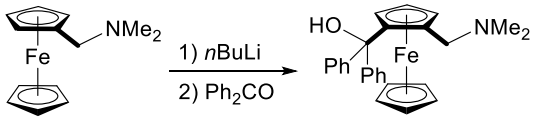

29 *rac*-**30**

1.3.3. Diastereoselective *ortho*-Directed Metalation of Ferrocene

ortho-Directed metalation of achiral ferrocene derivatives yields a racemate, in which both α positions to the ODG are equally lithiated. Consequently, two enantiomers are formed, which can be challenging to separate. On the other hand, if the ferrocene derivative bears a chiral ODG, instead of enantiomers, diastereomers will form. If one of the diastereomers forms selectively, the phenomenon is known as diastereoselective *ortho*-directed metalation, which involves a specific conformation of the ODG. In this conformation, the functional group that facilitates lithiation tipically orients to the *ortho* position in which the rest of substituents of the ODG are oriented away from the ferrocene moiety (Scheme 1-18).

The main ODGs are amines, phoshines, sulfoxides, acetals, and oxazolines. All these functional groups have in common, at least, the presence of a lone pair of electrons that can coordinate to electron-deficient metals with empty orbitals to stabilize them. One of the most well-known diastereoselective *ortho*-directed metalations is Ugi's method, which was introduced in the 1970s.[23]

The monolithiation of the R enantiomer of Ugi's amine (*R*-**31**; Scheme 1-18) proceeds stereoselectively at the 2 or 5 position in a ratio of 96 to 4.[23, 80] The lithium-containing ferrocene derivative is stabilized due to coordination of the nitrogen to lithium. The conformation with the methyl group away from the ferrocene moiety and $-NMe_2$ group in the same plane as the Cp ring is favoured. [23, 81] In other words, the diastereomer with the hydrogen atom at the *endo*-side will be the major product (*R*,S_p-**32**). The product with the methyl group at the *endo*-side will be the minor product (*R*,R_p-**32**) because of repulsing interactions with the ferrocene moiety. [23, 80, 81, 82]

Scheme 1-18. Diastereoselective *ortho*-lithiation of Ugi's amine **31**.

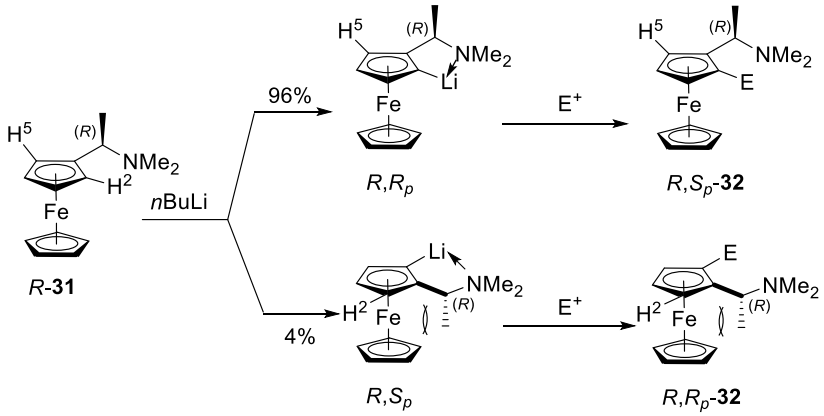

In 1998, Knochel *et al*. reported the double Ugi's amine with two aminic groups as ODGs.[81] Dilithiation of the double Ugi's amine (*R*,*R*-**33**; Scheme 1-19) followed by electrophilic substitution with Ph_2PCl leads to the formation of species (*R*,*R*,*S*$_p$,*S*$_p$-**34**), which has C_2-symmetry.[81]

Scheme 1-19. Diastereoselective lithiation of *R*,*R*-**33** followed by electrophilic substitution reaction with Ph_2PCl.

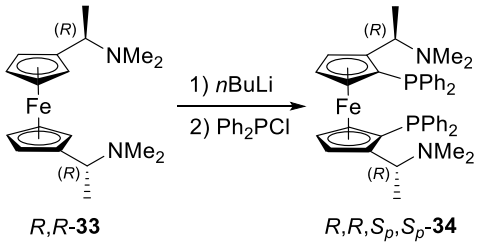

What makes Ugi's amine very suitable to prepare planar-chiral ferrocene derivatives is not only its ability to diastereoselectively *ortho*-direct metals, but also the ease with which the amine group can be displaced by nucleophiles (Scheme 1-20).[79, 83, 84] Substitution of the $-NMe_2$ group occurs according to an S_N1 mechanism, which leads to retention of configuration, as nucleophiles

preferentially attack from the top of the Cp ring and away from iron. The top-oriented attack is a consequence of the carbocation-iron interaction, which in turn stabilizes the carbocation.[82, 23]

Scheme 1-20. S_N1 reaction of *R*-**31** with retention of configuration.

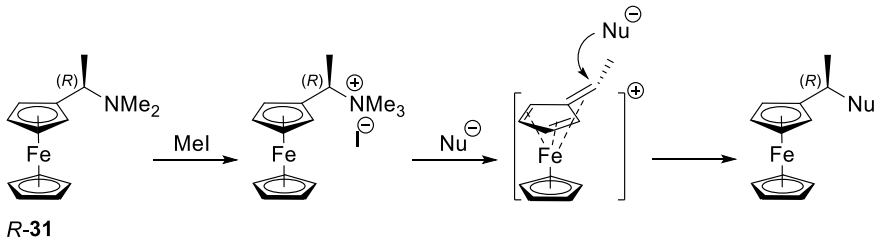

R-**31**

1.4. Research Objectives

My work involves investigating how the bulkiness of alkyl groups in sila[1]ferrocenophanes (the monomers) affects the polymer formation through T-ROP and TMC-ROP. At the same time, for certain polymers, the effect of altering alkyl groups to improve the solubility was explored. This would allow the characterization of the metallopolymers by standard methods, including NMR spectroscopy and GPC analysis. Because of the built-in chirality of the repeating units, it is hoped that these macromolecules will exhibit a chiral secondary structure. If successful, this would open a new area of polyferrocenes as chiral polymers of this type are unknown to date. Consequently, my work consists of two different parts.

The aim of the first part was the synthesis of mono- and disubstituted sila[1]ferrocenophanes of type **A** (Figure 1-10) with various alkyl groups on the ferrocene moiety and on the bridging silicon atom.

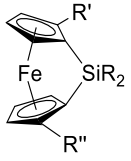

A

Figure 1-10. Proposed sila[1]ferrocenophanes with C_2 and C_1 symmetry.

In order to synthesize these silicon-bridged [1]FCPs, dibromoferrocene derivatives of types **B** and **C** (Figure 1-11) needed to be prepared first and be used as precursors in salt-metathesis reactions. The preparation and characterization of these types of mono- and disubstituted dibromoferrocene precursors are described in Section 2.1.

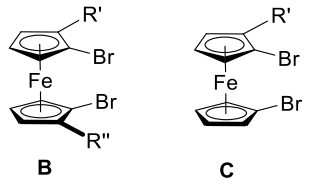

Figure 1-11. Proposed dibromoferrocene derivatives with C_2 and C_1 symmetry.

As the ultimate goal of preparing new strained [1]FCPs is to obtain new metallopolymers, new sila[1]ferrocenophanes (*rac*-**35**, *rac*-**36**, S_p,S_p-**37**) and known sila[1]ferrocenophanes (*rac*-**38**, S_p,S_p-**39**) have been synthesized and polymerized using different ROP methodologies, such as TMC-ROP and T-ROP. The synthesis and characterization of the new monomers are described in Section 2.1.

In order to compare how the bulkiness of the alkyl groups can affect the outcome of T-ROP, either *i*Pr groups in the known species *rac*-**38** and S_p,S_p-**39** (Figure 1-12) have been replaced by Et groups, giving rise to new species *rac*-**36** and S_p,S_p-**37** (Figure 1-12), or Me groups have been replaced in the known species *rac*-**38** (Figure 1-12) by Et groups, leading to the new species *rac*-**35** (Figure 1- 12). The aim behind the use of TMC-ROP for species S_p,S_p-**39** and *rac*-**38** (Figure 1-12) was to solve polymer-solubility problems and study the regularity of the resulting polymers, respectively. In addition to homopolymers, copolymers with different ratios of species S_p,S_p-**39** and *rac*-**38** have also been prepared *via* T-ROP. The outcome of these explorations is summarized in Sections 2.2. and 2.3.

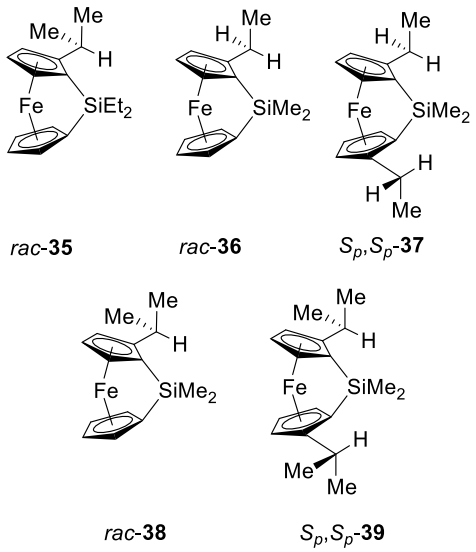

Figure 1-12. Proposed and known sila[1]ferrocenophanes.

CHAPTER 2

RESULTS AND DISCUSSION

This chapter consists of three main parts. In Section 2.1., the preparation of different dibromoferrocene derivatives and sila[1]ferrocenophanes, following an established methodology, is discussed. The results of T-ROP of the newly obtained and of known silicon-bridged [1]FCPs are presented in Section 2.2. In Section 2.3., the results of TMC-ROP of known silicon-bridged [1]FCPs are discussed.

2.1. Dibromoferrocene Derivatives and Sila[1]ferrocenophanes

Following a similar approach that was used for the preparation of known species *rac*-**40** and S_p,S_p-**12** (Figure 2-1), a series of new dibromoferrocene derivatives bearing one or two alkyl groups, respectively, in α position to bromine (*rac*-**41** and S_p,S_p-**42**; Figure 2-1) were synthesized. Following this, the preparation of new sila[1]ferrocenophanes are described using these new dibromoferrocene derivatives. These results are described in the following sections.

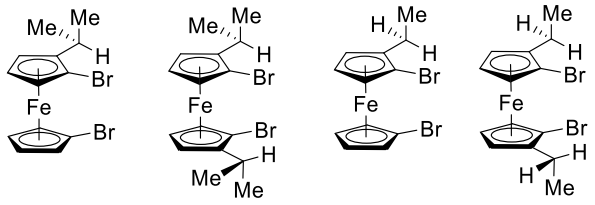

rac-**40** S_p,S_p-**12** *rac*-**41** S_p,S_p-**42**

Figure 2-1. Illustration of new and known dibromoferrocene derivatives with C_1 and C_2 symmetry.

2.1.1. Synthesis and Characterization of C_1-Symmetric Dibromoferrocene Derivatives

2.1.1.1. Synthesis and Characterization of *rac*-1,1'-Dibromo-2-ethylferrocene

Alkyl groups are usually incorporated into the ferrocene moiety in order to increase the solubility of the resulting polymers. The Müller group recently worked with dibromoferrocene derivatives equipped with one *i*Pr group to prepare sila[1]ferrocenophanes. The idea behind replacing the *i*Pr with an ethyl group was that it might influence the selectivity of the T-ROP and the M_w of the resulting polymer (see Section 2.2.).

Compound *rac*-**41**, equipped with just one ethyl group on one Cp ring, was synthesized following a published multistep procedure.[85] The known species *rac*-2-[1-(dimethylamino)ethyl)-1,1'-dibromoferrocene (*rac*-**43**) was prepared first (Scheme 2-1). It should be noted that species *rac*-**43** is a 1 : 1 mixture of the (R,S_p) and (S,R_p) isomers, and, for reasons of simplification, only one enantiomer of this racemate is shown in Schemes 2-1, 2-2, and 2-3.

Scheme 2-1. Multistep synthesis of the known species *rac*-2-[1-(dimethylamino)ethyl)-1,1'-dibromoferrocene (*rac*-**43**).

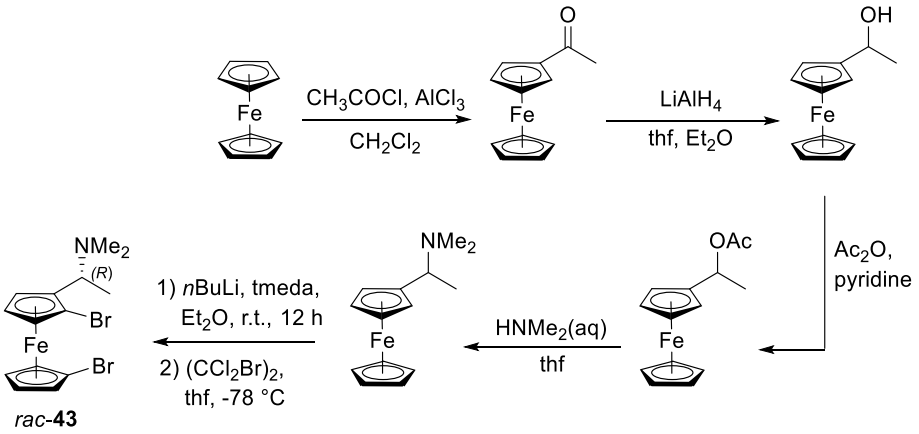

Treatment of *rac*-**43** with methyl iodide in CH_3CN led to the formation of *rac*-2-[1-(trimethylamino)ethyl)-1,1'-dibromoferrocene iodide (*rac*-**44**) as a yellow solid (95%; Scheme 2-2). The new species *rac*-**44** could not be further purified due to its insolubility in many common

organic solvents; crystallization or flash column chromatography could not be performed. However, *rac*-**44** was found to be soluble in CH_2Cl_2, $CDCl_3$, MeOH, and D_2O. ^{1}H NMR spectroscopy revealed that the crude compound was of sufficient purity so the next step was executed. Reduction of the quaternary ammonium salt *rac*-**44** with $NaBH_4$ resulted in the new species *rac*-**41**, which was obtained as a dark yellow oil after flash column chromatography. Crystallization resulted in a brown solid that melted at r.t. (62%; Scheme 2-2). These two last steps are based on a published procedure toward (S_p)-1-bromo-2-ethylferrocene.[86]

Scheme 2-2. Synthesis of *rac*-1,1'-dibromo-2-ethylferrocene (*rac*-**41**).

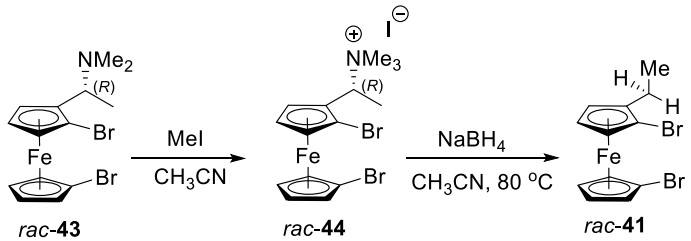

rac-**43** *rac*-**44** *rac*-**41**

^{1}H NMR spectroscopy of *rac*-**44** and *rac*-**41** confirmed the formation of the targeted species. The ^{1}H NMR spectrum of *rac*-**44** shows the expected seven signals for the Cp protons, as well as a singlet for the 9 H atoms of the $–NMe_3^+$ group at δ = 3.29 ppm, confirming the formation of the quaternary ammonium salt. However, instead of the expected seven signals for the Cp protons of *rac*-**41**, only four apparent signals with intensity ratios of 4 : 1 : 1 : 1 were found, as the signals for α and β protons overlap. Methylene protons are not chemically equivalent; therefore, they should give two doublets of quartets in the ^{1}H NMR spectrum. However, the signal for the methylene protons is an apparent nonet. This apparent nonet could come from the overlap of two apparent sextets that have similar chemical shifts. Each of these apparent sextets may come from a doublet of quartets, with the *J* value for the doublet being twice that of the quartet (Figure 2-2). The close chemical shifts and *J* coupling constant values give rise to an ABX_3 second order system.

The chemical shifts (δ = 2.43, 2.46 ppm) and *J* coupling constant values (J_{AB} = 15.0, J_{AX} = 7.5, J_{BX} = 7.5 Hz) were determined from computer simulation.[87] Lastly, the methyl group appears as a triplet at δ = 1.18 ppm with a coupling constant of 7.5 Hz.

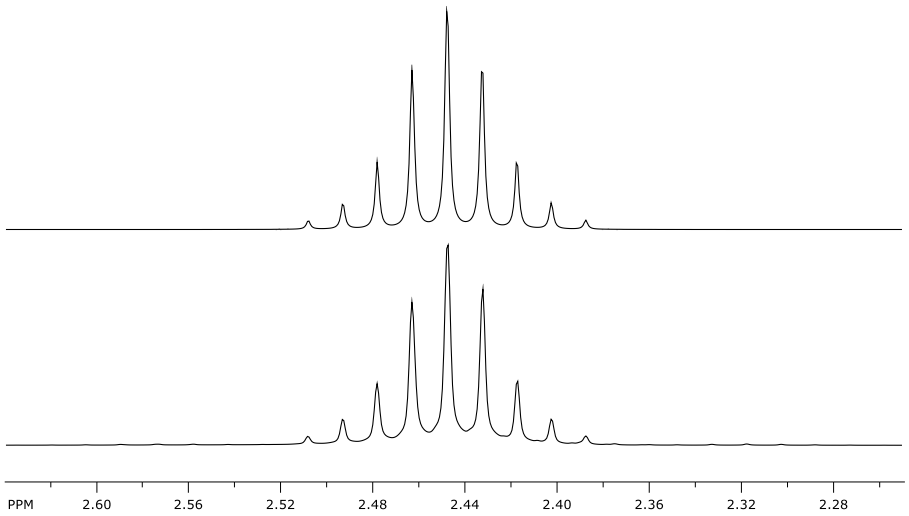

Figure 2-2. Simulated (top) and experimental (bottom) ^{1}H NMR signal for methylene protons in *rac*-**41**.

2.1.1.2. Synthesis and Characterization of *rac*-1,1'-Dibromo-2-(hydroxyethyl)ferrocene

The synthesis of *rac*-1,1'-dibromo-2-(hydroxyethyl)ferrocene (*rac*-**46**) was performed with the purpose of accessing new vinyl-containing silicon-bridged [1]FCPs (Scheme 2-3). Species *rac*-**46** bears a hydroxyl group that can react with different vinyl bromides [$Br(CH_2)_n(CHCH_2)$], for example with allyl bromide in the presence of NaH, to form ether-functionalized ferrocene derivatives *via* Williamson ether synthesis. The aim was to prepare PFSs, whose vinyl groups can be further functionalized. Stirring *rac*-**43** and acetic anhydride in the absence of any proton source led to the substitution of the amine by an acetoxy group.[85] However, if the reaction is done in the presence of a proton source, such as acetic acid, an elimination reaction affords compound *rac*-**45**. Synthesis of the new species *rac*-**45** is based on a published procedure toward (S_p)-1-bromo-2-

vinylferrocene.[88] Although no use of any proton source was reported in this reference, some traces of acetic acid might have been present in the acetic anhydride, as it is a common impurity. After flash column chromatography, compound *rac*-**45** was obtained as a dark red oil (71%; Scheme 2-3). The ^{1}H NMR spectrum of *rac*-**45** showed the expected signals for the various groups and the presence of ca. 3% of the mono-brominated species *rac*-1-bromo-2-vinylferrocene as an impurity. The most distinctive signals for *rac*-**45** are the three doublets of doublets due to the vinyl group.

Scheme 2-3. Synthesis of *rac*-1,1'-dibromo-2-(hydroxyethyl)ferrocene (*rac*-**46**).

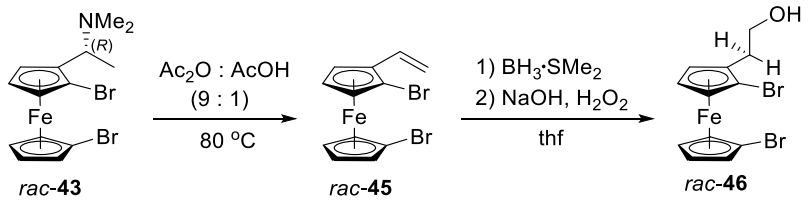

The next step involves the hydroboration of the vinyl group in order to obtain 1,1'-dibromo-2-(hydroxyethyl)ferrocene (*rac*-**46**). The synthesis of the new species *rac*-**46** is based on a procedure from the literature to synthesize 3-(ferrocenylmethoxy)propanol.[89] As expected, the hydroxyl group adds onto the less-hindered side of the vinyl group, in other words, the *anti*-Markovnikov alcohol was prepared. Treatment of *rac*-**45** with $BH_3{\cdot}SMe_2$ to form the organoborane and subsequent oxidation with hydrogen peroxide in the presence of NaOH led to the replacement of C−B with C−OH. Compound *rac*-**46** was obtained as an orange oil after column chromatography (54%; Scheme 2-3). Seven signals are expected for the Cp protons of *rac*-**46** in the ^{1}H NMR spectrum. Because of signal overlap, only five signals were found, with two signals having twice the intensity relative to the other three signals. The hydroxyl-containing aliphatic chain shows a second order pattern of ABCDE system. The –OH group appears as a triplet at δ =

1.40 ppm as its H atom couples with the methylene protons of the neighbouring carbon. The methylene protons close to the ferrocene moiety should give two doublets of doublets of doublets, however, it results in a second order system [(1); Figure 2-3]. Similarly, the methylene protons close to the hydroxyl group give rise to an even more complicated second order system, even though, they should give rise to two doublets of doublets of doublets of doublets, [(2); Figure 2-3]. The chemical shifts and *J* coupling constant values for this ABCDE second order system were calculated *via* computer simulation.[87] Multiplet (1) (Figure 2-3) shows chemical shifts δ = 2.71 and 2.80 ppm, while the chemical shifts for multiplet (2) (Figure 2-3) are δ = 3.77 and 3.83 ppm. *J* coupling constant values are J_{AB}= 14.5, J_{AC} = 6.0, J_{AD} = 6.0, J_{BC} = 6.0, J_{BD} = 7.0, J_{CD} = 11.5, J_{CE} = 6.0, and J_{DE} = 6.0 Hz.

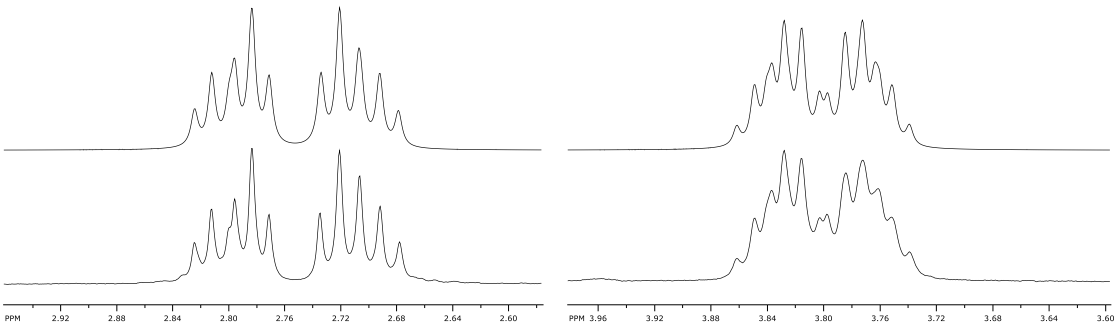

(1) (2)

Figure 2-3. Simulated (top) and experimental (bottom) ^{1}H NMR signals for (1) close-to-ferrocene and (2) close-to-OH methylene protons in *rac*-**46**.

2.1.2. Synthesis of C_2-Symmetric Dibromoferrocene Derivatives

2.1.2.1. Synthesis and Characterization of (S_p,S_p)-1,1'-Dibromo-2,2'-diethylferrocene

The T-ROP of the known sila[1]ferrocenophane S_p,S_p-**39** equipped with two *i*Pr groups on the Cp rings afforded an insoluble material in common organic solvents, such as CH_2Cl_2, thf, $CDCl_3$, and benzene.[90] It is speculated that the sterically demanding *i*Pr groups do not have enough conformational freedom to make the polymer soluble.[90] For this reason, replacing the *i*Pr groups by ones possessing a higher conformational freedom, such as Et groups, may improve the solubility of the resulting polymer.

Enantiopure dibromoferrocene derivative S_p,S_p-**12** equipped with two *i*Pr substituents was first synthesized in the Müller group and the corresponding sila[1]ferrocenophane S_p,S_p-**39** was prepared.[1] The synthesis of S_p,S_p-**42** equipped with two Et groups was based on a procedure[1] that, due to its versatility, allows the incorporation of different alkyl groups. The procedure involves the synthesis of the known species (R,R,S_p,S_p),-2,2'-bis[1-(dimethylamino)ethyl]-1,1'-dibromoferrocene (R,R,S_p,S_p-**47**) (Scheme 2-4), which was prepared first. Flash column chromatography of R,R,S_p,S_p-**47** afforded a brown solid (52% for last step; Scheme 2-4).

Scheme 2-4. Multistep synthesis of (*R*,*R*,S_p,S_p)-2,2'-bis[1-(dimethylamino)ethyl]-1,1'-dibromoferrocene (*R*,*R*,S_p,S_p-**47**).

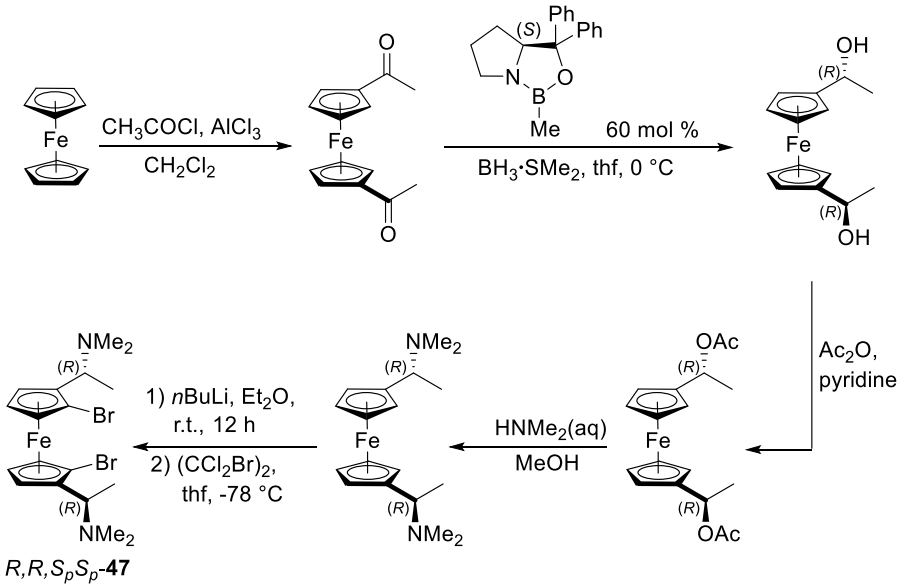

R,*R*,$S_p$$S_p$-**47**

Formation of the new species *R*,*R*,S_p,S_p-**48** was accomplished by adding methyl iodide into a solution of *R*,*R*,S_p,S_p-**47** in CH_3CN. The crude compound was obtained as a yellow powder (80%; Scheme 2-5) that could not be further purified as it was not soluble in many common organic solvents. However, *R*,*R*,S_p,S_p-**48** was found to be soluble in MeOH and D_2O. The crude material was used in the next step, which led to the enantiopure dibromoferrocene derivative S_p,S_p-**42** *via* reduction with $NaBH_4$. The new compound S_p,S_p-**42** was purified by flash column chromatography, which afforded a dark yellow oil (86%; Scheme 2-5). These two last steps are based on a published procedure toward *(*S_p*)*-1-bromo-2-ethylferrocene.[86]

Scheme 2-5. Synthesis of (S_p,S_p)-1,1'-dibromo-2,2'-diethylferrocene (S_p,S_p-**42**).

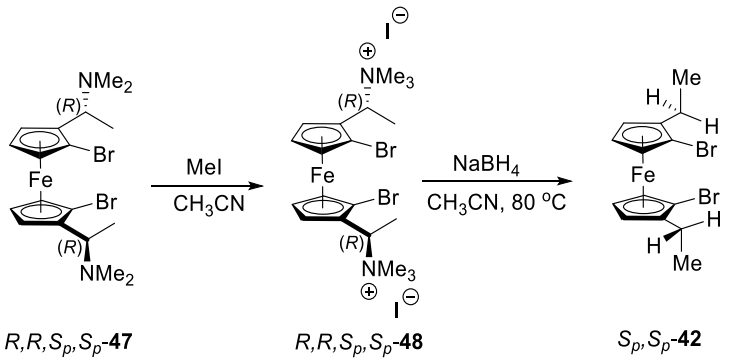

R,*R*,S_p,S_p-**47** *R*,*R*,S_p,S_p-**48** S_p,S_p-**42**

^{1}H NMR spectroscopy of *R*,*R*,S_p,S_p-**48** and S_p,S_p-**42** revealed the formation of the targeted species. ^{1}H NMR data of *R*,*R*,S_p,S_p-**48** could just be collected in D_2O, whose residual peak appears at δ = 4.79 ppm. As the protons for the Cp ring are expected in the 4 – 5 ppm range, the Cp protons could not be analyzed correctly due to signal overlap with the solvent signal. However, the singlet resonance at δ = 2.93 ppm for 18 H atoms confirms the presence of the $-NMe_3^+$ groups. The methine protons appear as a multiplet at δ = 4.66 ppm, and the methyl groups give rise to a doublet at δ = 1.95 ppm. Three signals are expected for the Cp protons of S_p,S_p-**42**. However, just two apparent signals with intensity ratios of 4 : 2 are present due to overlap between two signals. The methyl groups appear as a triplet at δ = 1.13 ppm. Methylene protons are not chemically equivalent; therefore, they should give two doublets of quartets in the ^{1}H NMR spectrum. However, the signal for the methylene protons appears as a ABX_3 system (Figure 2-4). The chemical shifts (δ = 2.36, 2.38 ppm) and *J* coupling constant values (J_{AB} = 15.0, J_{AX} = 7.5, J_{BX} = 7.5 Hz) for the ABX_3 second order system were determined from computer simulation.[87]

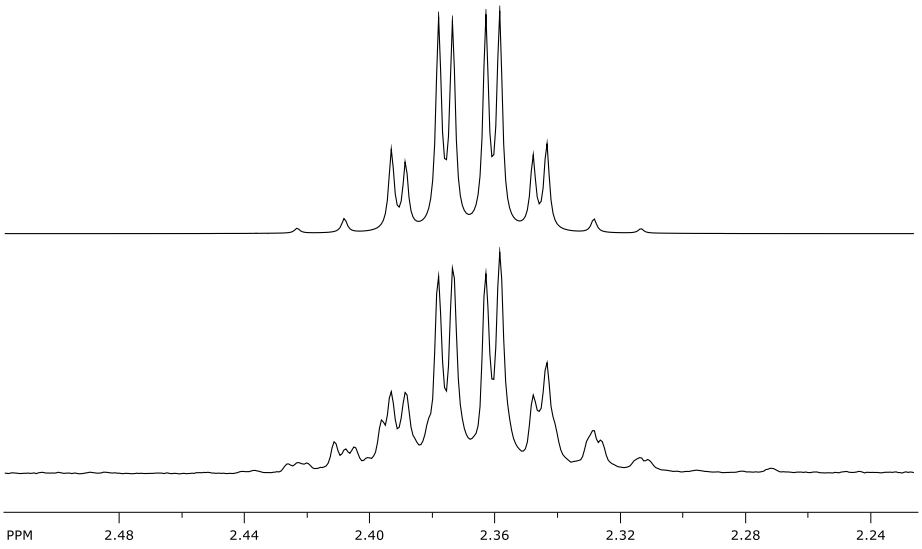

Figure 2-4. Simulated (top) and experimental (bottom) ^{1}H NMR signal for methylene protons in S_p,S_p-**42**.

2.1.3. Synthesis and Characterization of C_1-Symmetric Sila[1]ferrocenophanes

2.1.3.1. Synthesis and Characterization of the Racemic Sila[1]ferrocenophane *rac*-35

Comparison of the six closely related silicon-bridged [1]FCPs **14**,[91] *rac*-**35**, *rac*-**36**, S_p,S_p-**37**, *rac*-**38**,[90] and S_p,S_p-**39**[1] (Figure 2-5) could help to test the effect of ethyl groups in α positions to silicon and directly bound to silicon. Species **14**, *rac*-**38**, and S_p,S_p-**39** are known, whereas silicon-bridged [1]FCPs *rac*-**35**, *rac*-**36,** and S_p,S_p-**37** are new.

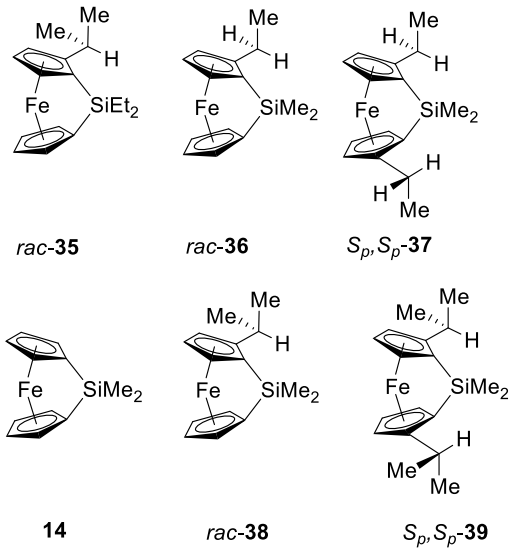

Figure 2-5. Family of closely related silicon-bridged [1]FCPs *rac*-**35**, *rac*-**36**, S_p,S_p-**37**, **14**, *rac*-**38**, and S_p,S_p-**39**.

As illustrated in Scheme 2-6, the known dibromoferrocene species *rac*-**40** was lithiated using *n*BuLi and reacted with dichlorodiethylsilane to give the new silicon-bridged [1]FCP *rac*-**35**. The *in situ* preparation of dilithio derivative of *rac*-**40** and the respective salt-metathesis reaction is based on the published procedure for the similar compound *rac*-**38**.[90] After all volatiles were removed, the product was dissolved in hexanes and LiCl was filtered out. Flash column chromatography and crystallization yielded *rac*-**35** as a red solid in a yield of 75%. The identity of *rac*-**35** was confirmed with ^{1}H, ^{13}C and ^{29}Si NMR spectroscopy, mass spectrometry, elemental analysis, and single-crystal X-ray analysis. The elemental analysis of this compound was obtained by Elaheh Khozeimeh Sarbisheh and the suitable crystals for X-ray analysis were obtained by Brady J. Anderson.

Scheme 2-6. Synthesis of the racemic silicon-bridged [1]FCP *rac*-**35**.

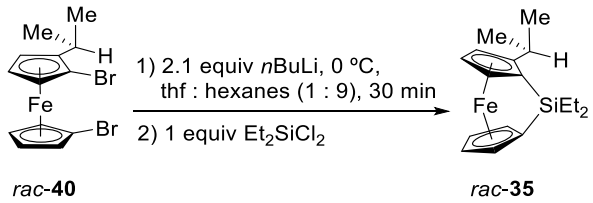

rac-**40** *rac*-**35**

The ^{1}H NMR spectrum of *rac*-**35** shows the expected seven signals for the seven Cp protons of this compound with C_1 symmetry. These seven signals for the Cp protons [δ = 3.65 (1H, H-α), 3.86 (1H, H-α), 3.93 (1H, H-α), 4.33 (1H, H-β), 4.36 (1H, H-β), 4.40 (1H, H-β), 4.52 (1H, H-β) ppm] have similar chemical shifts to those of the closely related compounds *rac*-**38** (Figure 2-5) [δ = 3.61 (1H, H-α), 3.84 (1H, H-α), 3.90 (1H, H-α), 4.34 (1H, H-β), 4.35 (1H, H-β), 4.39 (1H, H-β), 4.54 (1H, H-β) and *rac*-**36** (Figure 2-5) [δ = 3.60 (1H, H-α), 3.84 (1H, H-α), 3.90 (1H, H-α), 4.32 (1H, H-β), 4.35 (1H, H-β), 4.39 (1H, H-β), 4.56 (1H, H-β) ppm]. This suggests that neither the replacement of Me groups with Et groups on the Si atom nor replacement of *i*Pr with Et groups on the ferrocene moiety affects the shielding for the Cp protons significantly. The observed shielding for α protons of S_p,S_p-**39** relative to β protons was presumably due to the proximity of the α proton to the alkyl group in the neighbouring Cp ring.[1] This hypotheses has been recently confirmed by further investigation with *rac*-**38**.[90] The same shielding effect has been found for *rac*-**35** and *rac*-**36**. The alkyl region for *rac*-**35** shows different overlapping resonances, which were identified considering their relative intensities. Two overlapping quartets and a multiplet at δ = 0.92 and 1.08 ppm, respectively, correspond to the methylene protons on the bridging silicon atom. The methyl groups attached to the silicon give rise to two triplets at δ = 1.16 and 1.19 ppm. The *i*Pr group on the Cp ring appears as two doublets for the methyl groups at δ = 1.10 and 1.19 ppm and a septet for the methine proton at δ = 2.60 ppm. ^{13}C NMR spectroscopy showed upfield signals at δ = 30.4 and 33.2 ppm for the Cp carbon atoms bound to silicon (*ipso*-

Cp^{Si}), which is characteristic of sila[1]ferrocenophanes.[26, 92] In the ^{29}Si NMR spectrum, there is a signal at 1.0 ppm which differs from the signal at -5.7 ppm for species *rac*-**38** and *rac*-**36**. However, if one considers the width of known chemical shifts in ^{29}Si NMR spectroscopy (-392 to 567 ppm), the detected differences of a few ppm is probably insignificant.

The molecular structure of species *rac*-**35** was determined by single-crystal X-ray analysis. The compound shows the typical orientation of an *i*Pr group on a ferrocene skeleton where one methyl group (C13) points away from the ferrocene moiety, whereas the other methyl group (C12) is approximately in the same plane as the Cp ring (Figure 2-6; Table 2-1; Table 2-2).[90] The common set of distortion angles α, δ, β, and θ (Figure 1-3) to describe [1]FCPs are compiled in Table 2-1. The tilt angle α between the two Cp rings is 19.74(12)°, which is in the range of the α angle for strained silicon-bridged [1]FCPs (16 – 21°).[1, 93]

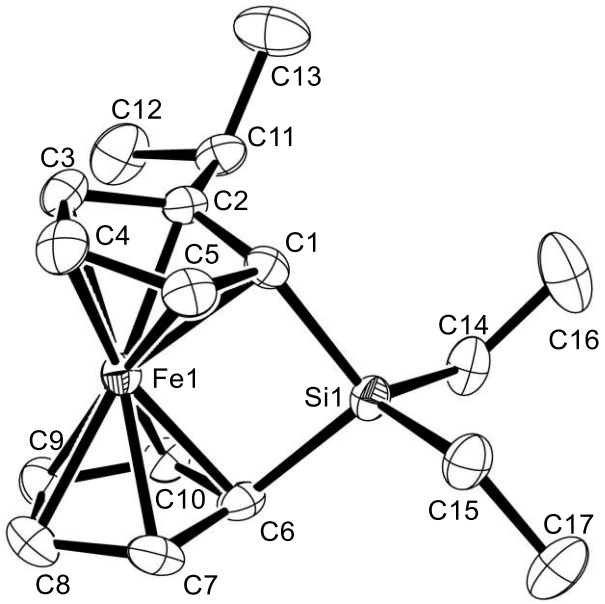

Figure 2-6. Molecular structure of *rac*-**35** with thermal ellipsoids at 50% probability level. Hydrogen atoms are omitted for clarity.

Table 2-1. Experimental distortion angles [°] in *rac*-**35**.

	rac-**35**
α	19.74(12)
δ	165.34(2)
β/β'	37.92(14)/38.23(13)
θ	96.13(8)
γ	86.29(8)

Table 2-2. Crystal and structural refinement data for compound *rac*-**35**.

	rac-**35**
empirical formula	$C_{17}H_{24}FeSi$
fw	312.30
cryst. Size / mm^3	0.230 × 0.150 × 0.070
cryst. system,	monoclinic
space group	$P2_1/n$
Z	4
a / Å	13.4712(10)
b / Å	7.2681(5)
c / Å	16.4034(11)
α / °	90
β / °	95.905(3)
γ / °	90
volume / $Å^3$	1597.54(19)
ρ_{calc} / mg m^{-3}	1.298
temperature / K	173(2)
μ_{calc}./ mm^{-1}	1.004
θ range / °	2.497 to 27.497
completeness to theta = 25.242°/ %	99.9
collected reflections	24981
independent reflections	3685 [R(int) = 0.0437]
absorption correction	multi-scan
data / restraints / params	3685 / 0 / 176
goodness-of-fit	1.024
R_1 [I > 2 σ(I)][a]	0.0326
wR_2 (all data)[a]	0.0788
largest diff. peak and hole, $\Delta\rho_{elect}$ / e $Å^{-3}$	0.298 and -0.291

[a] $R_1 = [\Sigma||F_o|-|F_c||]/[\Sigma|F_o|]$ for $[F_o^2 > 2\sigma(F_o^2)]$, $wR_2 = \{[\Sigma w(F_o^2-F_c^2)^2]/[\Sigma w(F_o^2)^2]\}^{1/2}$ [all data].

2.1.3.2. Synthesis and Characterization of the Racemic Sila[1]ferrocenophane *rac*-36

Salt-metathesis reaction of the dilithio derivative of *rac*-**41** with Me_2SiCl_2 afforded the strained sila[1]ferrocenophane *rac*-**36**. Flash column chromatography of species *rac*-**36** yielded a red oil in a yield of 65% (Scheme 2-7). This new species is similar to its closely related compound *rac*-**38** (Figure 2-5) that is equipped with an *i*Pr instead of an Et group. Compound *rac*-**36** was obtained pure and has been characterized by ^{1}H, ^{13}C, and ^{29}Si NMR spectroscopy and mass spectrometry. However, all the attempts to crystallize *rac*-**36** were unsuccessful, as presumably the Et group causes it to be a highly soluble species due to its conformational freedom.

Scheme 2-7. Synthesis of the racemic silicon-bridged [1]FCP *rac*-**36**.

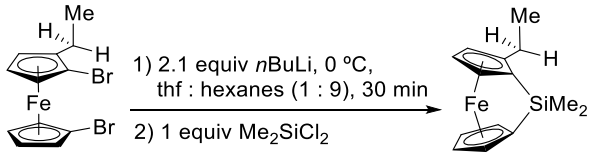

rac-**41** *rac*-**36**

The ^{1}H NMR spectrum of *rac*-**36** shows the expected seven signals for the seven Cp protons of this C_1-symmetric compound. The chemical shifts for the signals of the Cp protons δ = 3.60 (1H, H-α), 3.84 (1H, H-α), 3.90 (1H, H-α), 4.32 (1H, H-β), 4.35 (1H, H-β), 4.39 (1H, H-β), 4.56 (1H, H-β) ppm are similar to those of *rac*-**38**. The methylene protons are diastereotopic, so they give rise to two doublets of quartets. The quartets of each doublet of quartets and two quartets of different doublets of quartets have a very similar chemical shift. The similar chemical shifts and the *J* coupling constant values lead to an ABX_3 second order system (Figure 2-7). The chemical shifts (δ = 2.21, 2.28 ppm) and *J* values (J_{AB} = 15.0, J_{AX} = 7.5, J_{BX} = 7.5 Hz) were determined from computer simulation.[87]

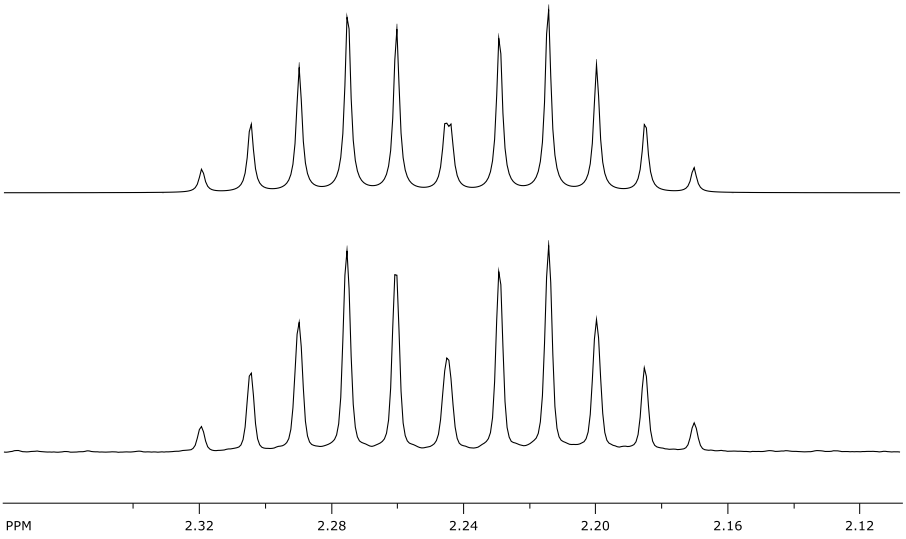

Figure 2-7. Simulated (top) and experimental (bottom) ^{1}H NMR signal for methylene protons in S_p,S_p-**42**.

For ^{13}C NMR spectroscopy, two expected signals appeared at δ = 31.3 and 33.9 ppm for the Cp carbons bound to the bridging silicon atom. Similarly to *rac*-**38**, the chemical shift at δ = 31.3 ppm is comparable to that of S_p,S_p-**39** (δ = 32.2 ppm),[1] whereas the other one at δ = 33.9 ppm is very similar to that of **14** (δ = 33.5 ppm).[94] Therefore, one can assign the signal at δ = 31.3 ppm to the silicon-bound *ipso* carbon atom of the alkylated Cp ring and the signal at δ = 33.9 ppm to the silicon-bound *ipso* carbon atom of the non-alkylated Cp ring. In contrast to *rac*-**35**, the ^{29}Si NMR spectrum of *rac*-**36** shows a signal at δ = -5.7 ppm, which is identical to that of *rac*-**38**.

2.1.4. Synthesis and Characterization of C_2-Symmetric Sila[1]ferrocenophanes

2.1.4.1. Synthesis and Characterization of the Chiral Sila[1]ferrocenophane S_p,S_p-37

Compound S_p,S_p-**37** has been prepared from the reaction between the dilithio derivative of S_p,S_p-**42** and Me_2SiCl_2. After all volatiles were removed, the product was dissolved in hexanes and LiCl was filtered out. Flash column chromatography yielded S_p,S_p-**37** as a red oil in a yield of 76% (Scheme 2-8).

Scheme 2-8. Synthesis of the enantiopure silicon-bridged [1]FCP S_p,S_p-**37**.

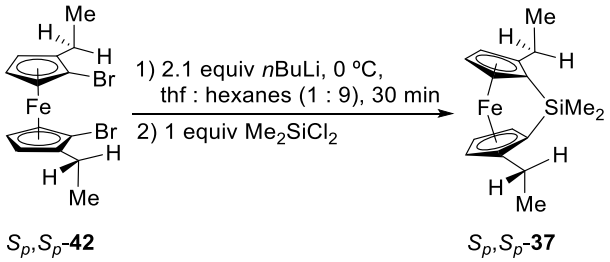

S_p,S_p-**42** S_p,S_p-**37**

All attempts to crystallize S_p,S_p-**37** were unsuccessful. Similarly to *rac*-**36**, the replacement of the *i*Pr groups by Et groups on the ferrocene moiety gives a highly soluble species. Also, according to ^{1}H NMR spectroscopy small impurities are present, which might prevent the crystallization of the compound. The identity of S_p,S_p-**37** was confirmed with ^{1}H, ^{13}C, and ^{29}Si NMR spectroscopy and mass spectrometry. As S_p,S_p-**37** is a C_2-symmetric compound, just three signals for the Cp protons with intensity ratios of 2 : 2 : 2 are expected. The ^{1}H NMR spectroscopy showed three signals for the Cp protons at δ = 3.50, 4.30, and 4.50 ppm, which are similar to the ones from the closely related species S_p,S_p-**39** (δ = 3.53, 4.31 and 4.46 ppm).[1] Similarly to *rac*-**36**, the methylene protons should appear as two doublets of quartets that, due to overlap between the signals and the *J* coupling constant values, give rise to an ABX_3 second order system (Figure 2-8).

The chemical shifts (δ = 2.21, 2.28 ppm) and *J* values (J_{AB} = 15.0, J_{AX} = 7.5, J_{BX} = 7.5 Hz) were determined from computer simulation.[87]

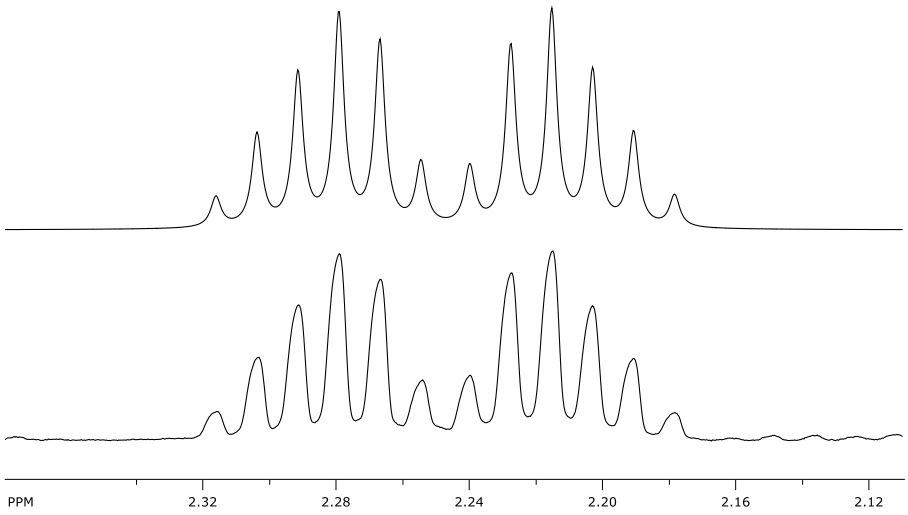

Figure 2-8. Simulated (top) and experimental (bottom) ^{1}H NMR signal for methylene protons in S_p,S_p-**37**.

The ^{13}C NMR spectroscopy showed just one upfield signal at δ = 32.2 ppm for the Cp carbon atom bound to silicon (*ipso*-Cp, Si), which is very similar to that of S_p,S_p-**39** (δ = 31.7 ppm).[1] The ^{29}Si NMR spectrum showed a signal at δ = -5.9 ppm which is similar to that of *rac*-**36** and *rac*-**38** (δ = -5.7 ppm). However, it slightly differs from that of **14** at δ = -4.6 ppm.[26]

2.2. Thermal ROP of Sila[1]ferrocenophanes

The results from the T-ROP of known species **14**,[91] *rac*-**38**,[90] and S_p,S_p-**39**[1] (Figure 2-5) were compared with the results from the T-ROPs of new species *rac*-**35**, *rac*-**36**, S_p,S_p-**37**, as well as with the resulting copolymers from combining *rac*-**38** and S_p,S_p-**39** in different ratios (Figure 2-5). It was expected that replacing the *i*Pr groups (S_p,S_p-**39**) with Et groups (S_p,S_p-**37**) on the Cp rings would afford a soluble polymer. Moreover, T-ROP of *rac*-**35** and *rac*-**36**, has been explored to

investigate the influence of the Et groups, either on the ferrocene moiety or on the silicon atom, on the M_w of the resulting polymers.

2.2.1. Thermal ROP of C_1-Symmetric Sila[1]ferrocenophanes

2.2.1.1. Thermal ROP of the Racemic Sila[1]ferrocenophane *rac*-35

Heating of the monomer *rac*-**35** at 160 ºC led to the formation of the PFS (*rac*-**35**)$_n$ which was soluble in thf. Repeated precipitations into MeOH afforded the polymer as an orange, powdery material in a 90% yield (Scheme 2-9). Polymer (*rac*-**35**)$_n$ was characterized by ^{1}H, ^{13}C, and ^{29}Si NMR spectroscopy and GPC analysis.

Scheme 2-9. T-ROP of the racemic silicon-bridged [1]FCP *rac*-**35**.

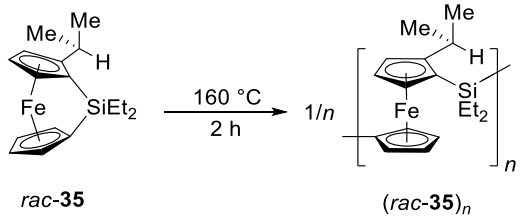

rac-**35** (*rac*-**35**)$_n$

T-ROP reaction mechanism is expected to proceed through the cleavage of Si−Cp^H and Si−Cp^{iPr} bonds.[90] As the asymmetric monomer *rac*-**35** has two different Si−C^{ipso} bonds (Si−Cp^H and Si−Cp^{iPr}), cleavage and reformation of these bonds in the polymer could result in six possible arrangements. However, repeating units with the opposite stereochemical configuration will give rise to enantiomers (S_p−Si−Cp and R_p−Si−Cp; S_p−Si−S_p and R_p−Si−R_p; Figure 2-9), and therefore, the same ^{29}Si chemical shift. Consequently, six different chemical environments around the silicon atom are possible (Figure 2-9), and four signals are expected in the ^{29}Si NMR spectrum. However, the quality of the spectrum in terms of signal to noise ratio and signal overlap is not sufficient. Consequently, the signals could not be analyzed correctly (Figure 2-10).

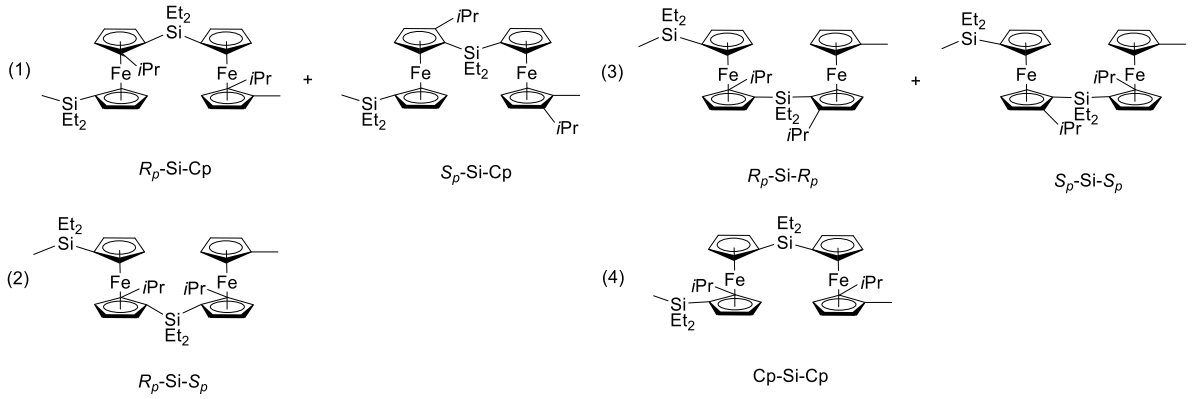

Figure 2-9. Illustration of the possible environments for silicon atom *via* cleavage of Si−Cp^H and Si−Cp^{iPr} bonds in the T-ROP of *rac*-**35**.

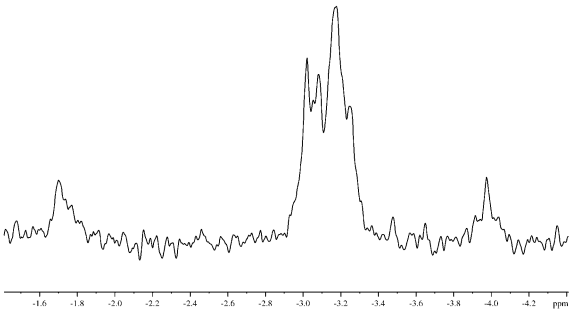

Figure 2-10. ^{29}Si NMR spectrum of polymer (*rac*-**35**)$_n$.

GPC analysis with a triple detection system revealed an absolute molecular weight of M_w = 4.96 × 10^4 Da and $Đ$ = 2.32 for polymer (*rac*-**35**)$_n$ (Figure 2-11; Table 2-3). The obtained M_w for polymer (*rac*-**35**)$_n$ is considerably smaller than that of the closely related polymer (*rac*-**38**)$_n$ obtained from T-ROP of species *rac*-**38** (M_w = 2.50 × 10^6 Da).[90] In addition, dispersities are also noticeably different, being $Đ$ = 2.32 for (*rac*-**35**)$_n$ and $Đ$ = 1.77 for (*rac*-**38**)$_n$.[90] As the only difference between these two compounds is the replacement of the Me groups on the silicon bridging atom by Et groups, the increase of the steric bulkiness on the silicon atom may prevent the propagation step and, therefore, the formation of longer polymer chains. Another hypothesis could be that the Et groups may open up chain terminations so that M_w is lower and $Đ$ is larger.

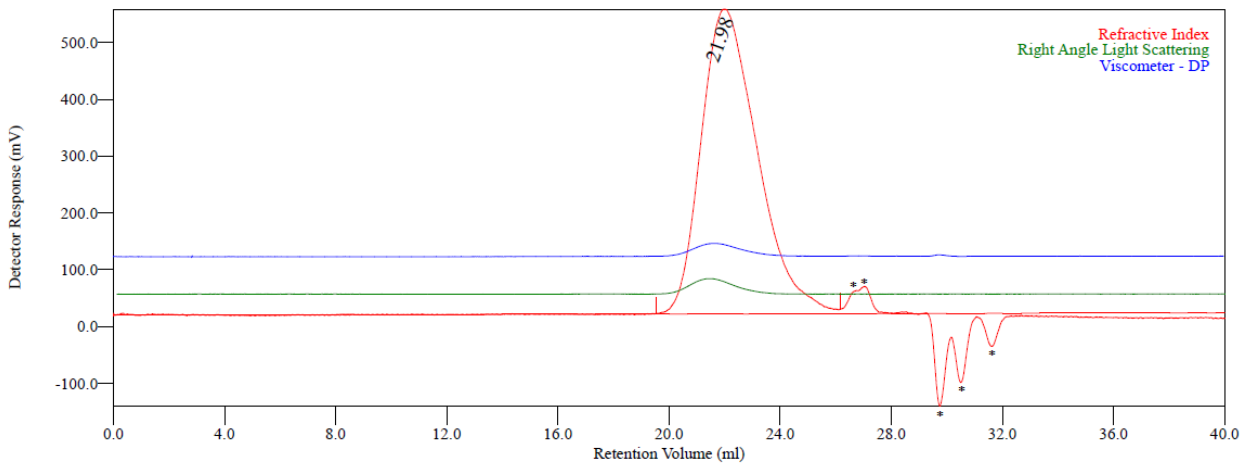

Figure 2-11. GPC trace of polymer (*rac*-**35**)$_n$ (c = 13.0 mg / 6.5 mL thf). System peaks are indicated with *.

Table 2-3. GPC analysis of polymer (*rac*-**35**)$_n$.

	(*rac*-**35**)$_n$
M_n (Da)	2.13 x 10^4
M_w (Da)	4.96 x 10^4
M_w / M_n	2.32

2.2.1.2. Thermal ROP of the Racemic Sila[1]ferrocenophane *rac*-36

T-ROP of *rac*-**36** resulted in a glassy red solid which was completely soluble in thf. Repeated precipitations into MeOH afforded polymer (*rac*-**36**)$_n$ as a yellow, powdery material in an 87% yield (Scheme 2-10). The polymer was characterized by ^{1}H, ^{13}C, and ^{29}Si NMR spectroscopy and GPC analysis.

Scheme 2-10. T-ROP of the racemic silicon-bridged [1]FCP *rac*-**36**.

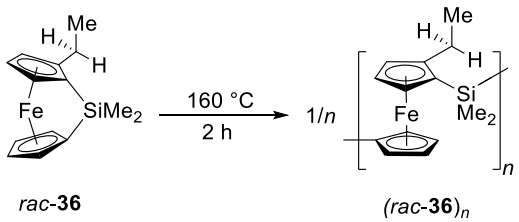

rac-**36** (*rac*-**36**)$_n$

The ^{29}Si NMR spectroscopy showed four signals at δ = -7.3, -7.1, -6.8 and -6.1 ppm with intensity ratios of 0.19 : 1.0 : 0.63 : 0.25 (Figure 2-12).

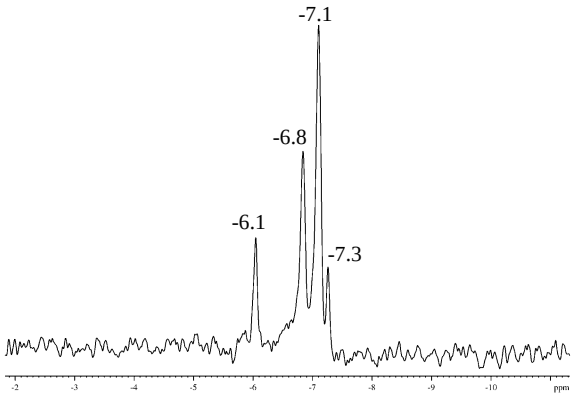

Figure 2-12. ^{29}Si NMR spectrum of polymer (*rac*-**36**)$_n$

Having four signals in the ^{29}Si NMR spectrum matches the expectations for a T-ROP reaction mechanism proceeding through the cleavage of Si−Cp^{H} and Si−Cp^{Et} bonds,[90] as it was stated in Section 2.2.1.1. Similar to (*rac*-**35**)$_n$, six different chemical environments around the silicon atom are possible (Figure 2-13) and, consequently, four signals in the ^{29}Si NMR spectrum are expected (Figure 2-12). The assignment of the signals has been performed considering the assignment of the signals of the PFS (*rac*-**38**)$_n$ from the thermally ring-opened monomer *rac*-**38** (δ = -8.2, -7.4, -6.7, -5.8 ppm).[90] The assignment was done considering a similar trend for the integrals of the signals. That means, the peak at δ = -6.1 ppm is caused by S_p−Si−R_p moieties, the resonance at δ = -6.8 ppm was assigned to the Cp−Si−Cp environment, the peak at δ = -7.1 ppm was assigned to S_p−Si−Cp / R_p−Si−Cp moieties, and the resonance at δ = -7.3 ppm was assigned to S_p−Si−S_p / R_p−Si−R_p moieties (Figure 2-13). The intensities for (*rac*-**36**)$_n$ are more evenly distributed (0.19 : 1.0 : 0.63 : 0.25) than those of (*rac*-**38**)$_n$ (0.21 : 1.0 : 0.36 : 0.21). This led to the conclusion that

the sterics on the ferrocene moiety of the monomer plays a crucial role in the selectivity of the addition of new monomers to the propagating chain end.

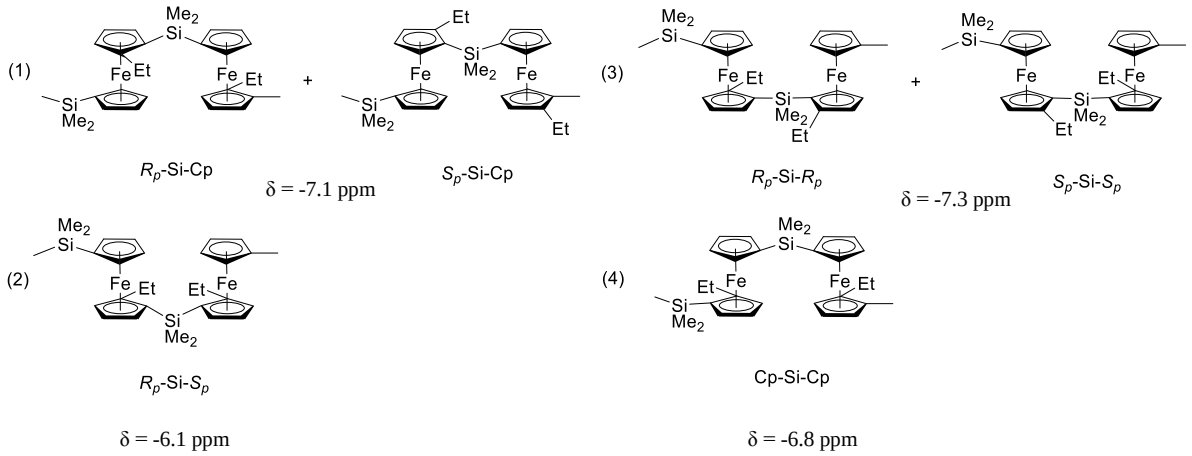

Figure 2-13. Illustration of the possible environments for silicon atom *via* cleavage of Si–Cp^H and Si–Cp^{Et} bonds in the T-ROP of *rac*-**36**.

In addition, GPC analysis with a triple detection system revealed an absolute molecular weight of M_w = 4.02 × 10^5 Da with $Đ$ = 1.83 for polymer (*rac*-**36**)$_n$ (Figure 2-14; Table 2-4). The M_w and dispersity values are similar to that of polymer (*rac*-**38**)$_n$ (M_w = 2.50 × 10^6 Da; $Đ$ = 1.77).

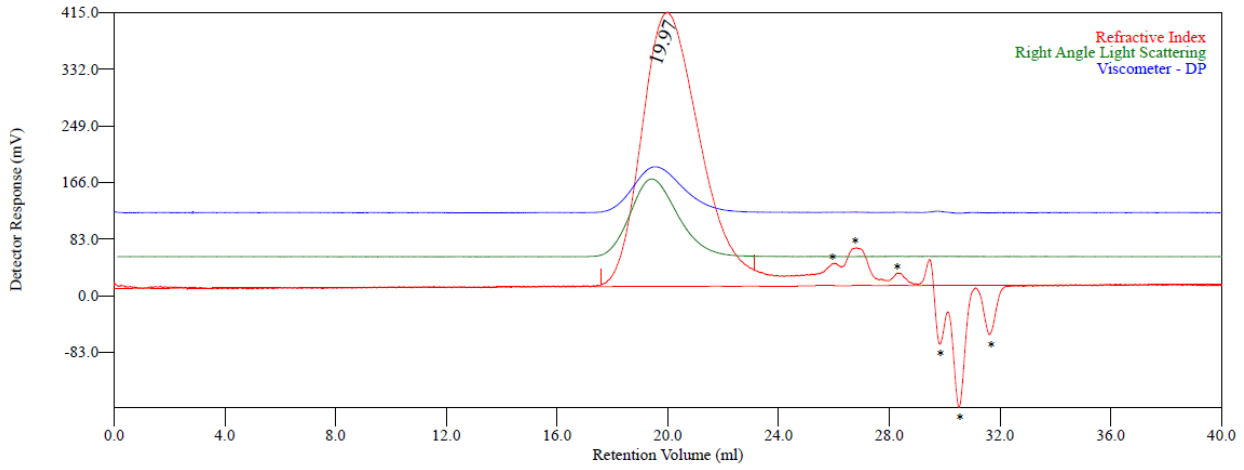

Figure 2-14. GPC trace of polymer (*rac*-**36**)$_n$ (c = 11.4 mg / 5.5 mL thf). System peaks are indicated with *.

Table 2-4. GPC analysis of polymer (*rac*-**36**)$_n$.

	(*rac*-**36**)$_n$
M_n (Da)	2.20 x 10^5
M_w (Da)	4.02 x 10^5
M_w / M_n	1.83

2.2.2. Thermal ROP of C_2-Symmetric Sila[1]ferrocenophanes

2.2.2.1. Thermal ROP of the Chiral Sila[1]ferrocenophane S_p,S_p-37

T-ROP of S_p,S_p-**37** resulted in a glassy dark-red solid which was not soluble in thf, CH_2Cl_2, $CDCl_3$, or benzene. This solid was partially dissolved in 1,2,4-trichlorobenzene (TCB) at 150 °C and repeated precipitations into MeOH afforded polymer (S_p,S_p-**37**)$_n$ as a dark brown solid in a 54% yield (Scheme 2-11).

Scheme 2-11. T-ROP of the enantiopure silicon-bridged [1]FCP S_p,S_p-**37**.

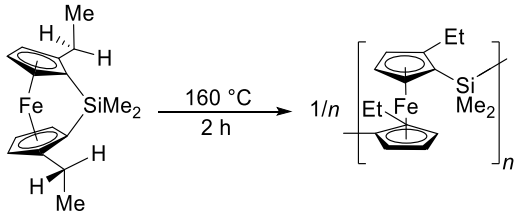

S_p,S_p-**37** (S_p,S_p-**37**)$_n$

Of the solvents tested, polymer (S_p,S_p-**37**)$_n$ is only soluble in TCB at high temperature and, after reaching room temperature, it results in a dark brown solution with solid particles in form of platelets. As there is just one possible chemical environment for silicon (Scheme 2-11), only one signal is expected in the ^{29}Si NMR spectrum. However, similar to its closely related polymer (S_p,S_p-**39**)$_n$, its poor solubility in common organic solvents prevented its characterization with multi-nuclear solution NMR spectroscopy or GPC analysis.

2.2.3. Synthesis and Characterization of Copolymers

T-ROP of S_p,S_p-**39** resulted in an insoluble material (S_p,S_p-**39**)$_n$ and its characterization was not possible. In order to get some insight into the properties of this insoluble polymer, soluble copolymers **49** and **50** respectively, from two different monomers *rac*-**38** and S_p,S_p-**39** in ratios of 9 : 1 and 7 : 3 were prepared.

Thermal ROP toward Copolymer 49

Heating of the monomers *rac*-**38** and S_p,S_p-**39** in a 90 : 10 ratio at 160 ºC led to the formation of a PFS which was soluble in thf. Repeated precipitations into MeOH afforded copolymer **49** an orange, powdery material in an 83% yield (Scheme 2-12). The copolymer **49** was characterized by ^{1}H, ^{13}C, and ^{29}Si NMR spectroscopy and GPC analysis.

Scheme 2-12. T-ROP toward copolymer **49**.

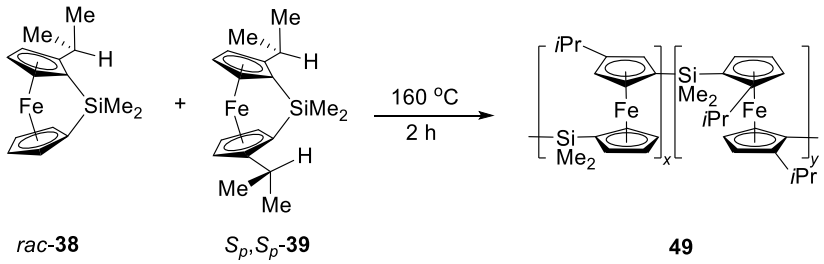

rac-**38** S_p,S_p-**39** **49**

As discussed in Section 2.2.1., six different chemical environments around the silicon atom are possible (Figure 2-15).

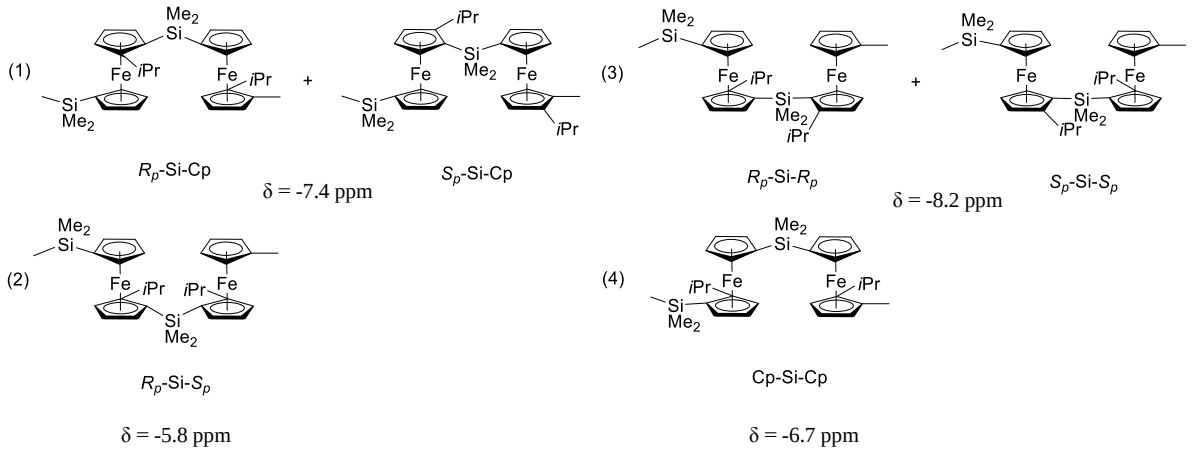

Figure 2-15. Illustration of the possible environments for silicon atom *via* cleavage of Si−Cp^H and Si−Cp^{iPr} bonds in the T-ROP toward **49**, **50**, and (*rac*-**38**)$_n$.

Four different signals with identical chemical shift as those of (*rac*-**38**)$_n$ are expected in the ^{29}Si NMR spectrum (δ = -8.2, -7.4, -6.7, and -5.8 ppm). However, the relative intensities of the signals are not expected to be the same. A statistical distribution of all possible types of silicon atoms for polymer (*rac*-**38**)$_n$ (Figure 2-15) obtained from T-ROP would result in a 0.25 : 1.0 : 0.50 : 0.25 intensity ratio, respectively. Even though the measured intensity ratio of 0.21 : 1.0 : 0.36 :0.21 does not match a statistical distribution, its pattern is similar. Therefore, there is some selectivity in the T-ROP.[90] As 10% of the monomer *rac*-**38** has been replaced by the enantiopure monomer S_p,S_p-**39** in copolymer **49**, the expected relative intensities for a statistical distribution for the signals at δ = -8.2, -7.4, -6.7, and -5.8 ppm would result in 0.32 : 1.0 : 0.41: 0.30, respectively. ^{29}Si NMR spectroscopy for copolymer **49** showed the expected four signals at the expected four chemical shifts with relative intensities of 0.15 : 1.0 : 0.48 : 0.24 (Figure 2-16). If the pattern for **49** followed that of (*rac*-**38**)$_n$, it would result in a 0.27 : 1.0 : 0.30 : 0.25 intensity

ratio. Comparison of the relative intensities for **49** with those of (*rac*-**38**)$_n$, led to the conclusion that there is no evidence that copolymer **49** formed, as the pattern for the signals is not similar.

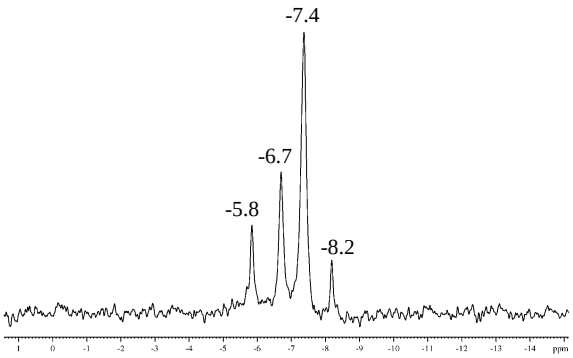

Figure 2-16. ^{29}Si NMR spectrum for copolymer **49**.

In addition, GPC analysis with a triple detection system revealed an absolute molecular weight of M_w = 1.70 × 10^6 Da and $Đ$ = 2.09 for copolymer **49** (Figure 2-17; Table 2-5). The M_w value is similar to that of homopolymer (*rac*-**38**)$_n$ (M_w = 2.50 × 10^6 Da), however, the dispersity is higher ($Đ$ = 1.77).

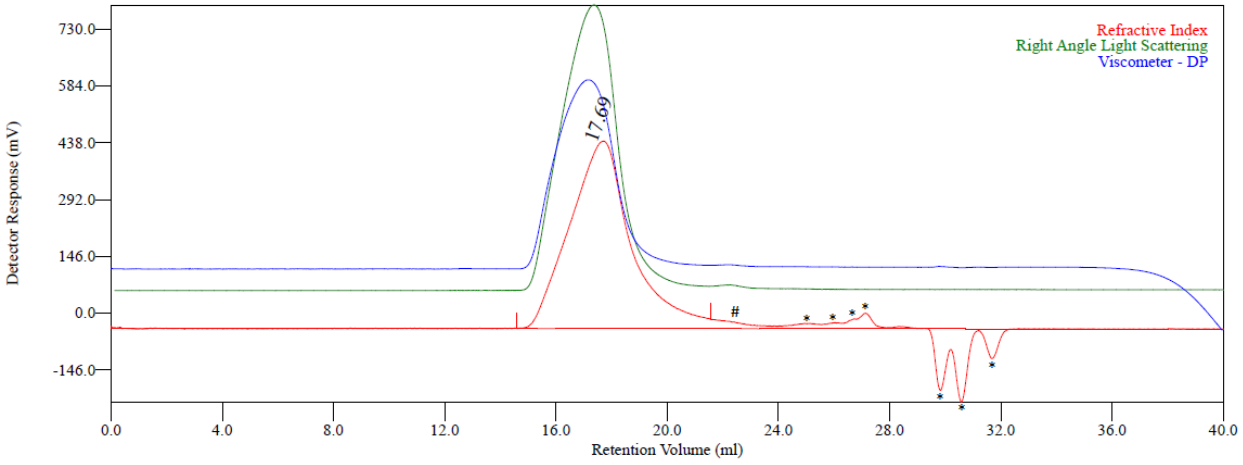

Figure 2-17. GPC trace of polymer **49** (c = 11.4 mg / 6.0 mL thf). While a lower molecular weight fraction is indicated with #, system peaks are indicated with *.

Table 2-5. GPC analysis of copolymer **49**.

	49
M_n (Da)	1.70 x 10^6
M_w (Da)	3.56 x 10^6
M_w / M_n	2.09

Thermal ROP toward Copolymer 50

Heating of the monomers *rac*-**38** and S_p,S_p-**39** in a 70 : 30 ratio at 160 ºC led to the formation of a PFS which was soluble in thf. Precipitation into MeOH afforded copolymer **50** an orange, powdery material in an 81% yield (Scheme 2-13). The copolymer was characterized by ^{1}H, ^{13}C, and ^{29}Si NMR spectroscopy and GPC analysis.

Scheme 2-13. T-ROP toward copolymer **50**.

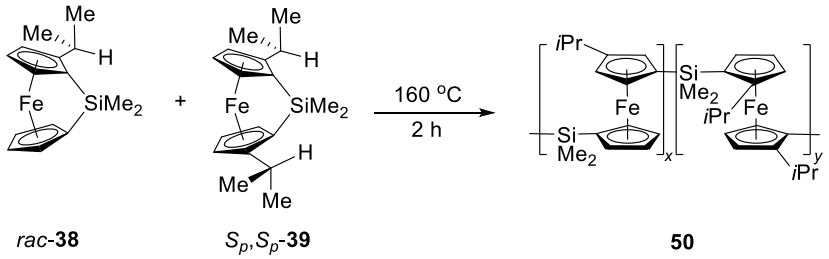

rac-**38** S_p,S_p-**39** **50**

Analogous to copolymer **49**, six chemical environments are expected for the silicon atom (Figure 2-15), which will give rise to four signals in the ^{29}Si NMR spectrum.

In the same way as copolymer **49**, four different signals with identical chemical shifts of those of (*rac*-**38**)$_n$ but different relative intensities are expected in the ^{29}Si NMR spectrum. The enantiopure monomer S_p,S_p-**39** replaced 30% of the monomer *rac*-**38**; therefore, the expected relative intensities for the signals at δ = -8.2, -7.4, -6.7, and -5.8 ppm would be 0.56 : 1.0 : 0.27 : 0.37, respectively, for a statistical distribution. ^{29}Si NMR spectroscopy for copolymer **50** showed the expected four signals at the expected four chemical shifts. The relative intensities for the signals

are 0.22 : 1.0 : 0.47 : 0.25 (Figure 2-18). If the pattern for **50** followed that of (*rac*-**38**)$_n$, it would result in a 0.47 : 1.0 : 0.19 : 0.31 intensity ratio. Comparison of the relative intensities for **50** with those of (*rac*-**38**)$_n$, resulted in no similar pattern. Consequently, the formation of the targeted copolymer **50** cannot be confirmed.

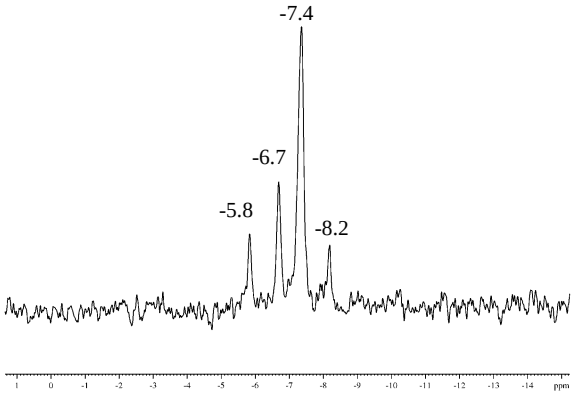

Figure 2-18. ^{29}Si NMR spectrum of copolymer **50**.

In addition, GPC analysis with a triple detection system revealed an absolute molecular weight of M_w = 1.06 × 10^6 Da and $Đ$ = 2.08 for copolymer **50** (Figure 2-19; Table 2-6). The M_w value is close to that of homopolymer (*rac*-**38**)$_n$, (M_w = 2.50 × 10^6 Da), however, the dispersity is higher ($Đ$ = 1.77).

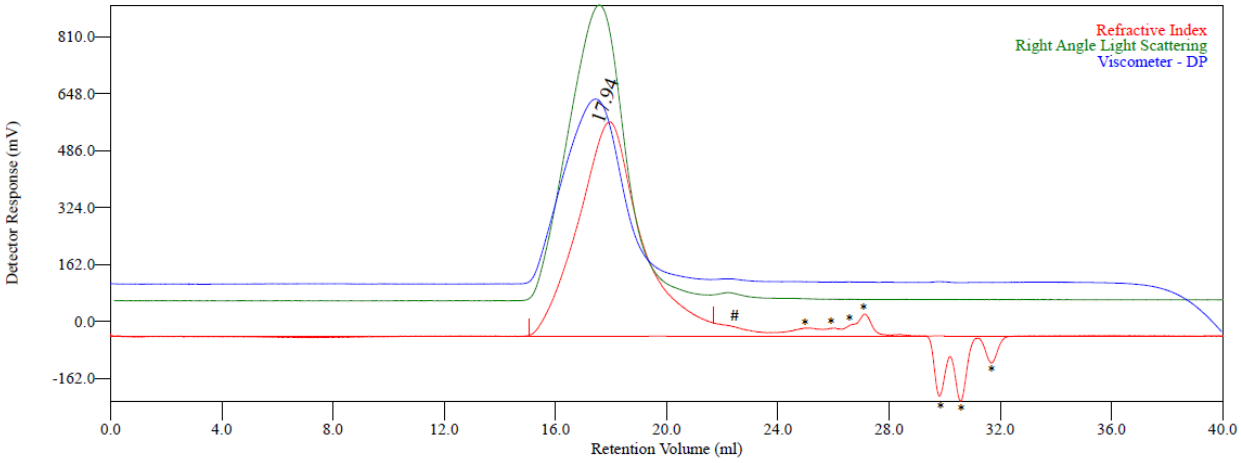

Figure 2-19. GPC trace of polymer **50** (c = 11.4 mg / 6.0 mL thf). While a lower molecular weight fraction is indicated with #, system peaks are indicated with *.

Table 2-6. GPC analysis of copolymer **50**.

	50
M_n (Da)	1.06 x 10^6
M_w (Da)	2.20 x 10^6
M_w / M_n	2.08

2.3. Transition-Metal-Catalyzed ROP of Sila[1]ferrocenophanes

2.3.1. Transition-Metal-Catalyzed ROP of the Racemic Sila[1]ferrocenophane *rac*-38

As stated in Section 2.2.1.1., monomer *rac*-**38** has two different Si−C^{ipso} bonds (Si−Cp^H and Si−Cp^{iPr}) and cleveage and reformation of these bonds in the course of the formation of the polymer could result in six different chemical environments for silicon (Figure 2-15). Due to two pairs of enantiomers, just four signals in the ^{29}Si NMR spectrum are expected.

As discussed in previous sections, monomer *rac*-**38** has recently been thermally ring-opened and four signals in the ^{29}Si NMR spectrum have been seen.[90] The four signals were assigned to the different environments (Figure 2-15).[90]

In order to study the selectivity of the cleavage of the Si−Cp bond *via* TMC-ROP, *rac*-**38** has been ring-opened using $PtCl_2$ as a known transition-metal pre-catalyst. Stirring of monomer *rac*-**38** in toluene in the presence of $PtCl_2$ resulted in PFS (*rac*-**38**)$_n$. Repeated precipitations into MeOH afforded the polymer as a yellow, powdery material in a 79% yield (Scheme 2-14).

Scheme 2-14. TMC-ROP of the racemic silicon-bridged [1]FCP *rac*-**38**.

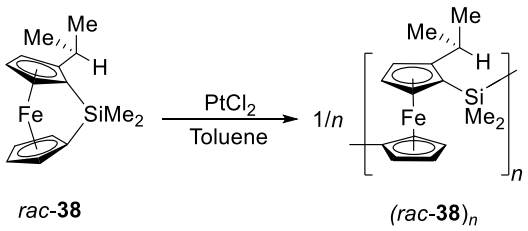

rac-**38** (*rac*-**38**)$_n$

The polymer was characterized by ^{1}H, ^{13}C, and ^{29}Si NMR spectroscopy and GPC analysis. ^{1}H NMR spectroscopy shows broad signals, but narrower in comparison to the polymer obtained from T-ROP.[90] The narrowing of the signals is a consequence of the lower M_w, which was determined by GPC analysis (discussed below). ^{29}Si NMR spectroscopy revealed the presence of the expected four signals at δ = -8.2, -7.4, -6.7, and -5.8 ppm with intensity ratios of 0.09 : 1.0 : 0.23 : 0.14 (Figure 2-20). ^{29}Si NMR spectroscopy data shows that the chemical shifts for the signals of the polymer obtained through T-ROP and TMC-ROP are identical, however, the relative intensities for the signals are different. The intensity ratios for the polymer obtained from T-ROP are 0.21 : 1.0 : 0.36 : 0.21 (Figure 2-20).[90] The significantly more intense peak at δ = -7.4 suggests that the S_p-Si-Cp / R_p-Si-Cp environments are the most abundant silicon environment in the polymer. Whereas in T-ROP 56% of the repeating units in the polymer are S_p-Si-Cp / R_p-Si-Cp units, in TMC-ROP 69% of the repeating units are S_p-Si-Cp / R_p-Si-Cp. Consequently, this comparison clearly shows that TMC-ROP is a more selective process so that a more uniform polymer results.

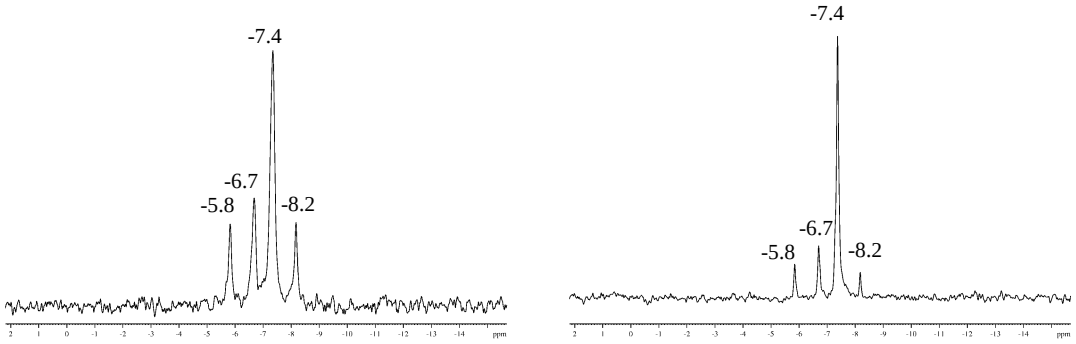

Figure 2-20. ^{29}Si NMR spectra of PFSs (*rac*-**38**)$_n$ obtained from T-ROP[90] (left) and TMC-ROP (right).

In addition, GPC analysis with a triple detection system revealed a trimodal distribution. The molecular weight for each distribution are estimates as overlap between the signals occurs $M_w \sim 5.8 \times 10^6$, 3.9 x 10^5, 6.7 x 10^4 Da (Figure 2-21). The trimodal distribution indicates that different polymerization mechanisms are occurring simultaneously. As stated in Section 1.2.3. Manners *et al.* reported that the metal nanoparticles are the main active catalysts. However, even with mercury poisoning, polymerization occurred to some extent which revealed that homogeneous catalysis caused by transition-metal complexes was happening.[40] Based on these results one can speculate that, at least, both mechanisms are in effect in the TMC-ROP of *rac*-**38** leading to a multimodal distribution.

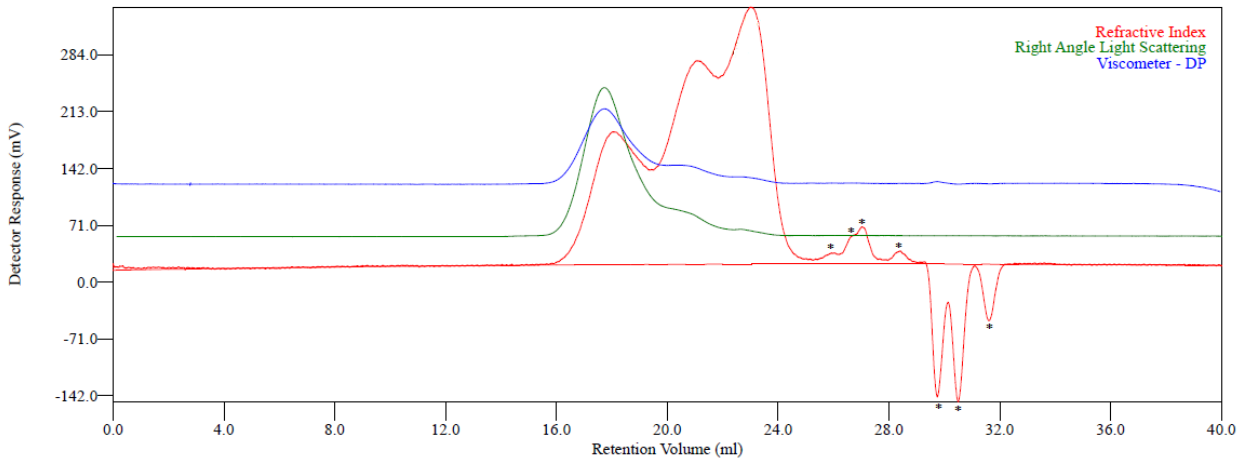

Figure 2-21. GPC trace of polymer (*rac*-**38**)$_n$ (c = 15.8 mg / 7.9 mL thf). System peaks are indicated with *.

2.3.2. Transition-Metal-Catalyzed ROP of the Chiral Silicon-Bridged [1]Ferrocenophane *S*$_p$,*S*$_p$-39

T-ROP of the planar-chiral sila[1]ferrocenophane *S*$_p$,*S*$_p$-**39** resulted in PFS (*S*$_p$,*S*$_p$-**39**)$_n$. This polymer was insoluble in thf, CH_2Cl_2, or benzene, and only swelling and partial solubility were observed in heated TCB. However, the lack of solubility of the polymer prevented its characterization. In order to obtain a soluble polymer, TMC-ROP of monomer *S*$_p$,*S*$_p$-**39** was executed, as a polymer with a lower M_w was expected.

TMC-ROP of monomer *S*$_p$,*S*$_p$-**39** in the presence of $PtCl_2$ or Karstedt's catalyst resulted in PFS (*S*$_p$,*S*$_p$-**39**)$_n$ (Scheme 2-15). Unfortunately, polymer (*S*$_p$,*S*$_p$-**39**)$_n$ was not soluble in thf, CH_2Cl_2, or benzene and only swelling and partial solubility were observed in heated TCB. The lack of solubility of the polymer did not allow the use of multi-nuclear solution NMR spectroscopy or GPC analysis for its characterization.

Scheme 2-15. TMC-ROP of the enantiopure silicon-bridged [1]FCP S_p,S_p-**39**.

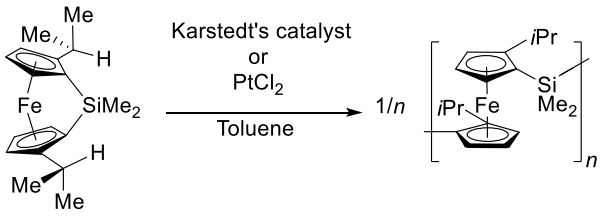

S_p,S_p-**39** $(S_p,S_p\text{-}\mathbf{39})_n$

CHAPTER 3

SUMMARY AND CONCLUSIONS

3.1. Dibromoferrocene Derivatives

Using the well-known "Ugi's amine" chemistry and subsequent treatment with methyl iodide led to the formation of quaternary ammonium salts (*rac*-**44** and *R*,*R*,S_p,S_p-**48**). The use of $NaBH_4$ as a reducing reagent gave rise to racemic and enantiopure dibromoferrocene derivatives (*rac*-**41** and S_p,S_p-**42**; Scheme 3-1) with C_1 and C_2 symmetry, respectively.

Scheme 3-1. Multistep synthesis of enantiopure dibromoferrocene S_p,S_p-**42**.

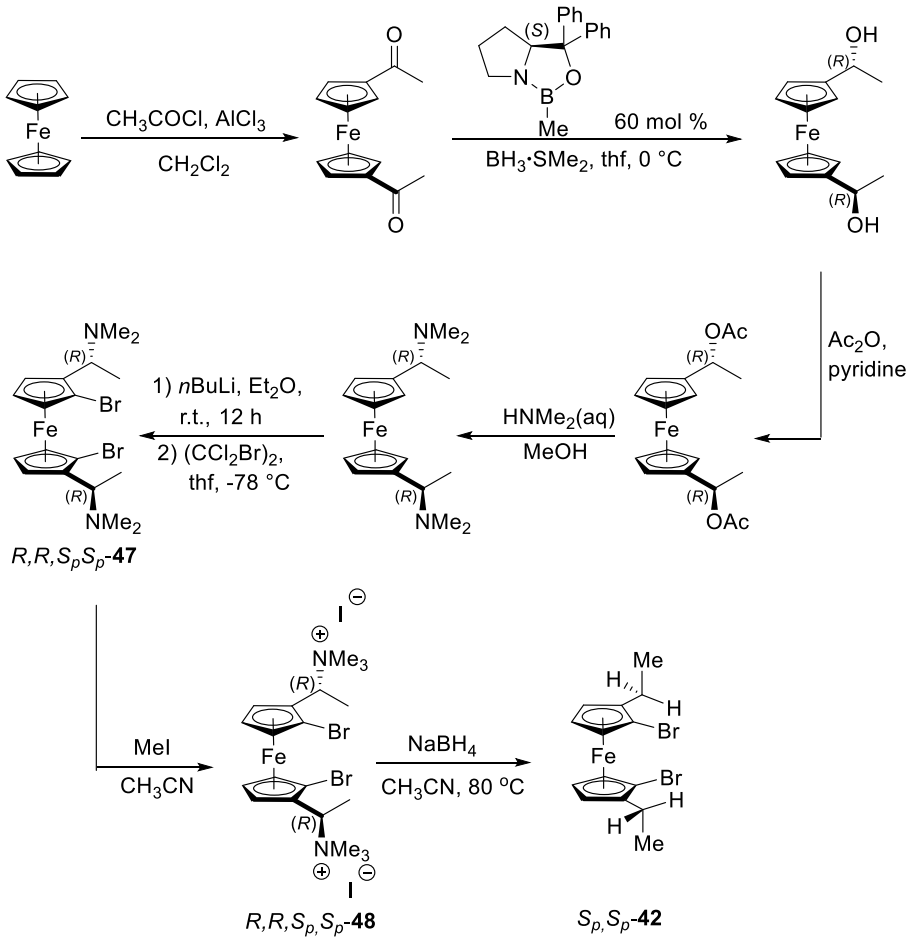

Species *rac*-**45** can be prepared through an elimination reaction of *rac*-**43** (Scheme 3-2). The vinyl-containing compound was aimed to be synthesized in order to introduce a hydroxyl group (*rac*-**46**). This hydroxyl group can probably be deprotonated and act as a nucleophile to obtain different dibromoferrocenes. For example, *rac*-**46** could be used in the future to prepare ethers with different groups, such as vinyl, that can be further functionalized.

Scheme 3-2. Synthesis of 1,1'-dibromo-2-(hydroxyethyl)ferrocene (*rac*-**46**).

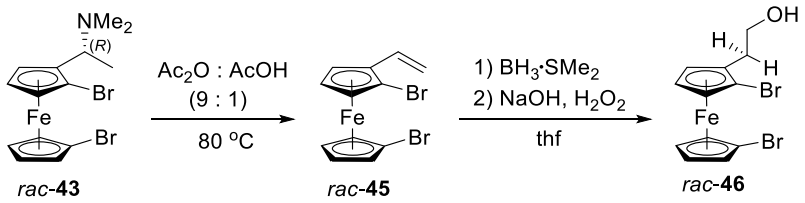

3.2. [1]Ferrocenophanes

Species *rac*-**41** and S_p,S_p-**42** allowed access to the new [1]FCPs *rac*-**36** and S_p,S_p-**37**. Following a common synthetic route to prepare sila[1]ferrocenophanes,[90] *rac*-**36** and S_p,S_p-**37** were prepared (Scheme 3-3 and 3-4). The replacement of *i*Pr groups in *rac*-**38** and S_p,S_p-**39** by Et groups in *rac*-**41** and S_p,S_p-**42** afforded highly soluble species that could not be crystallized.

Scheme 3-3. Synthesis of the racemic silicon-bridged [1]FCP *rac*-**36**.

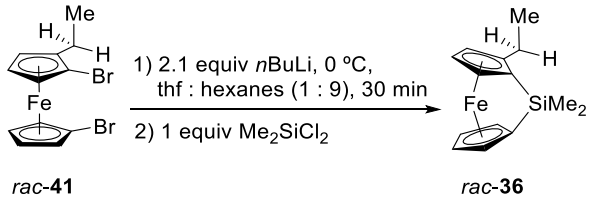

Scheme 3-4. Synthesis of the enantiopure silicon-bridged [1]FCP S_p,S_p-**37**.

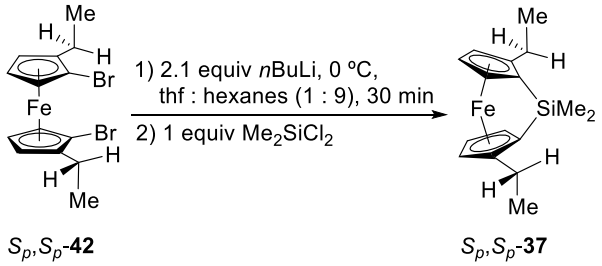

S_p,S_p-**42** S_p,S_p-**37**

Similarly, salt-metathesis reaction of the dilithio derivative of the known dibromoferrocene derivative *rac*-**40** with Et_2SiCl_2 gave the new silicon-bridged [1]FCP *rac*-**35** (Scheme 3-5). Species *rac*-**35** was crystallized and suitable single crystals for X-ray analysis were obtained.

Scheme 3-5. Synthesis of the racemic silicon-bridged [1]FCP *rac*-**35**.

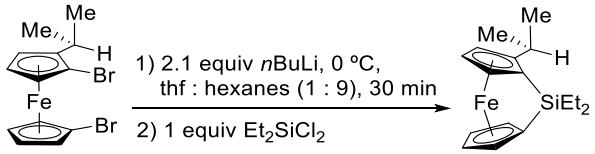

rac-**40** *rac*-**35**

3.3. Metallopolymers

3.3.1. Thermal ROP of Sila[1]ferrocenophanes

T-ROP of sila[1]ferrocenophane *rac*-**35** resulted in the PFS (*rac*-**35**)$_n$. The polymer was soluble in CH_2Cl_2, thf, CD_3Cl, and benzene and precipitated into MeOH and acetone. The quality of the ^{29}Si NMR spectrum was not sufficient. Consequently, the signals could not be analyzed correctly. However, GPC analysis revealed a significant lower M_w compared to that from T-ROP of *rac*-**38**, which could come from the increase of the steric bulkiness on the silicon atom. Therefore, the replacement of Me groups on the silicon with Et groups did affect the T-ROP outcome affording a metallopolymer with significantly lower M_w.

T-ROP of sila[1]ferrocenophanes *rac*-**36** and S_p,S_p-**37** resulted in the PFSs (*rac*-**36**)$_n$ and (S_p,S_p-**37**)$_n$, respectively. Polymer (*rac*-**36**)$_n$ was soluble in CH_2Cl_2, thf, CD_3Cl, and benzene and precipitated into hexanes, MeOH, and acetone. ^{29}Si NMR spectroscopy revealed that the T-ROP of *rac*-**36** is less selective with respect to the addition of new monomers to the propagating chain end compared to the T-ROP of *rac*-**38**. On the other hand, GPC analysis suggests a similar M_w for polymer (*rac*-**36**)$_n$ in comparison to that from T-ROP of *rac*-**38**, meaning that reducing the bulkiness of the alkyl groups on the Cp rings do not affect significantly the M_w. The ^{29}Si NMR spectroscopy showed four signals for (*rac*-**36**)$_n$ (Figure 2-12), further supporting that the T-ROP of sila[1]ferrocenophanes proceed through the cleavage of Si−Cp^{alkyl} and Si−Cp^{H} bonds.[90]

The PFS (S_p,S_p-**37**)$_n$ was insoluble in CH_2Cl_2, thf, benzene, hexanes, MeOH, and acetone. Solubility was observed in heated TCB at 150 ^{o}C. Unfortunately, the lack of solubility of this polymer prevented its characterization. Although it was expected that the replacement of the *i*Pr groups by Et groups would improve the solubility of the polymers, this expectation was proven wrong. Probably, longer alkyl chains are required to increase the solubility.

T-ROP of monomers *rac*-**38** and S_p,S_p-**39** toward copolymers **49** and **50** was performed. However, the formation of the polymers could not be concluded as the ^{29}Si NMR spectroscopy data did not show a similar pattern to that of (*rac*-**38**)$_n$ obtained from T-ROP.

3.3.2. Transition-Metal-Catalyzed ROP of Sila[1]ferrocenophanes

TMC-ROP of species *rac*-**38** afforded a polymer that was soluble in CH_2Cl_2, thf, and benzene and precipitated into hexanes, MeOH, and acetone. ^{29}Si NMR spectroscopy resulted in four signals with the same chemical shifts but different intensity ratios compared to those of the polymer obtained from T-ROP. The more intense peak at δ = -7.4 ppm for the S_p-Si-Cp / R_p-Si-Cp environments led to the conclusion that TMC-ROP affords a more regular polymer than T-ROP.

Nevertheless, GPC analysis showed a trimodal distribution, whereas the polymer obtained from T-ROP shows a monomodal distribution. The trimodal distribution is indicative of the homogeneous and heterogeneous catalysis occurring at the same time.

TMC-ROP of S_p,S_p-**39** afforded a polymer that was insoluble in CH_2Cl_2, thf, benzene, $CDCl_3$, hexanes, MeOH, and acetone, and only swelling and partial solubility were observed in heated TCB. Consequently, the expectation of improving the solubility of (S_p,S_p-**39**)$_n$ by decreasing the M_w was proven wrong.

CHAPTER 4

EXPERIMENTAL

4.1. General Procedures

If not mentioned otherwise, all syntheses were carried out using standard Schlenk and glovebox techniques. Solvents were dried using an MBraun Solvent Purification System and stored under nitrogen over 3 Å molecular sieves. All solvents for NMR spectroscopy were prepared by pump-freeze-thaw cycles and stored under nitrogen over 3 Å molecular sieves. Unless otherwise noted, temperatures refer to that of the bath. Flash chromatography was performed with neutral aluminum oxide and silica gel 60; mixed solvent eluents are reported as vol : vol solutions. ^{1}H, ^{13}C, and ^{29}Si NMR spectra were recorded on a 500 MHz Bruker Avance, a 500 MHz Bruker Avance III HD, and a 600 MHz Bruker Avance III HD NMR spectrometer at 25 ºC in C_6D_6 and $CDCl_3$. ^{1}H chemical shifts were referenced to the residual protons of the deuterated solvents (δ = 7.15 ppm for C_6D_6; δ = 7.26 ppm for $CDCl_3$, δ = 4.79 ppm for D_2O); ^{13}C chemical shifts were referenced to the C_6D_6 signal at δ = 128.00 ppm and the $CDCl_3$ signal at δ = 77.00 ppm. Coupling constants are reported to the nearest 0.5 Hz (^{1}H NMR spectroscopy). ^{29}Si NMR chemical shifts were referenced to $ClSiMe_3$ in $CDCl_3$ at 30 ppm (relative to primary reference TMS at 0 ppm). Each ^{29}Si NMR spectrum was acquired over 16 h. Assignments for *rac*-**35**, *rac*-**36**, S_p,S_p-**37**, *rac*-**41**, S_p,S_p-**42**, *rac*-**44**, *rac*-**45**, *rac*-**46,** *R*,*R*,S_p,S_p-**48**, (*rac*-**35**)$_n$, (*rac*-**36**)$_n$, (S_p,S_p-**37**)$_n$, (*rac*-**38**)$_n$, **49**, and **50** were supported by additional NMR experiments (DEPT, HMQC, COSY). Simulations for second order system multiplets in *rac*-**36**, S_p,S_p-**37**, *rac*-**41**, S_p,S_p-**42**, and *rac*-**46** were performed with SpinWorks software. Mass spectra were measured on a JEOL AccuTOF GCv 4G using field desorption ionization (FDI) and reported in the form *m/z* (rel intens) [M^+] where '*m/z*' is the observed mass. The intensities are reported relative to the most intense peak and [M^+] is the

molecular-ion peak or a fragment; only characteristic mass peaks are listed. For the isotopic pattern, only the mass peak of the isotopoloque or isotope with the highest natural abundance is listed.

4.2. Reagents

The compounds oxazaborolidine catalyst,[95] *rac*-**40**,[85] *rac*-**38**,[90] S_p,S_p-**12**,[1] S_p,S_p-**39**,[1] and **14**[91] were prepared as described in the literature. *n*BuLi (2.5 M in hexanes), dichlorodimethylsilane (98%), ferrocene (98%), trimethylaluminum (2.0 M in hexanes), and 1,2-dibromotetrachloroethane (Acros, 97%) were purchased from Sigma-Aldrich. N,N,N',N'-tetramethylethylenediamine (Alfa Aesar, 99%) and acetic anhydride (EMD, ACS grade, 99%) were purchased from VWR. Silica gel 60 (EMD, Geduran, particle size 0.040-0.063 mm) and aluminium oxide (Sigma-Aldrich, activated, neutral, Brockmann I, 58 Å pore size) were used for flash column chromatography.

4.3. Gel-Permeation-Chromatography (GPC) Analyses

Chromatograms were recorded on a Viscotek 350 HT-GPC system (Malvern) that was used at low temperature (column temperature of 45.1 ºC; thf; flow rate = 1.0 mL.min^{-1}; calibrated for polystyrene standards). The instrument was equipped with the following Viscotek components: auto-sampler (Model 430 Vortex), degasser (model 7510), two pumps (model 1122), 7° and 90° light scattering detectors, refractometer, and viscometer. GPC columns cover the range of M_w of 500 to 10,000,000 g.mol^{-1} (three main columns: Plgel 10 μM MIXED-B LS 300 x 7.5 mm; one guard column: 10 μM GUARD 50 x 7.5 mm; Agilent Technologies). Samples were dissolved in thf and filtered through 0.45 μm syringe PTFE filters before GPC analysis.

4.4. Syntheses

4.4.1. Synthesis of *rac*-1,1'-Dibromo-2-ethylferrocene (*rac*-41)

Synthesis of *rac*-2-[1-(Trimethylamino)ethyl]-1,1'-dibromoferrocene iodide (*rac*-44)

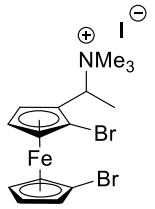

rac-**44**

To a stirred solution of *rac*-2-[1-(dimethylamino)ethyl]-1,1'-dibromoferrocene (*rac*-**43**) (0.83 g, 2.0 mmol) in CH_3CN (12 mL) was added dropwise CH_3I (0.38 mL, 6.0 mmol) at r.t. After 1 h stirring at r.t. the resulting solution was added dropwise to stirring Et_2O (20 mL) and kept stirring for 30 min. A yellow suspension is formed that ends up being a clear yellow solution with brown precipitate. The solution was decanted and followed by drying the solid under high vacuum. The product was afforded as a yellow powder (1.06 g, 95%). ^{1}H NMR ($CDCl_3$, 500.3 MHz): δ = 2.17 [d, 3H, *J* = 8.0 Hz, $CH(NMe_3)C\underline{H}_3$], 3.29 [s, 9H, $CH(N\underline{Me}_3)CH_3$], 4.24 (m, 1H, CH of Cp) 4.46 (m, 1H, CH of Cp), 4.49 (m, 1H, CH of Cp), 4.52 (t, 1H, *J* = 2.5 Hz, CH of Cp), 4.57 [q, 1H, *J* = 7.0 Hz, $C\underline{H}(NMe_3)CH_3$], 4.65 (m, 1H, CH of Cp), 4.69 (m, 1H, CH of Cp). ^{13}C {^{1}H} NMR ($CDCl_3$, 125.8 MHz): δ = 17.9 [$CH(NMe_3)\underline{C}H_3$], 51.9 [$CH(N\underline{Me}_3)CH_3$], 69.2 (<u>C</u>H of Cp), 70.3 ($\underline{C}H(NMe_3)CH_3$), 71.79 (<u>C</u>H of Cp), 71.83 (<u>C</u>H of Cp), 72.1 (<u>C</u>H of Cp), 74.0 (<u>C</u>H of Cp), 74.8 (<u>C</u>H of Cp), 75.0 (<u>C</u>H of Cp), 78.9 (*ipso*-Cp) 80.6 (*ipso*-Cp), 81.2 (*ipso*-Cp). Elemental Anal. Calcd. for $C_{15}H_{20}Br_2FeIN$ (556.8895) C, 32.35; H, 3.62; N, 2.52. Found: C, 32.41; H, 3.32; N, 2.53.

Synthesis of *rac*-1,1'-Dibromo-2-ethylferrocene (*rac*-41)

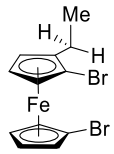

rac-**41**

To a stirred solution of *rac*-**44** (0.65 g, 1.2 mmol) in CH_3CN (6 mL) was added portionwise $NaBH_4$ (0.13 g, 3.5 mmol) at r.t. followed by stirring at 80 °C for 4 h. The resulting solution was quenched with water and extracted with Et_2O (2 x 50 mL). The organic layers were washed with water (3 x 50 mL) and brine. The combined organic layers were dried over anhydrous Na_2SO_4, filtered, and concentrated using a rotatory evaporator. The yellow oil crude material (0.40 g, 93%) was purified by flash column chromatography (hexanes/EtOAc, 9 : 1) affording a yellow oil (0.33 g, 81%). This oil was dissolved in hexanes (3 ml) and stored at -80 ºC. Brown solid was obtained that melted at r.t. affording a dark yellow oil (0.26 g, 62%). ^{1}H NMR ($CDCl_3$, 500.3 MHz): δ = 1.18 (t, 3H, *J* = 7.5 Hz, $CH_2C\underline{H}_3$), 2.43, 2.46 (nonet, ABX_3 system, 2H, J = 15.0, 7.5, 7.5 Hz, $C\underline{H}_2CH_3$), 4.08 (m, 4H, Cp), 4.30 (m, 1H, Cp), 4.34 (m, 1H, Cp), 4.40 (m, 1H, Cp), ^{13}C {^{1}H} NMR ($CDCl_3$, 125.8 MHz): δ = 14.3 ($CH_2\underline{C}H_3$), 20.5 ($\underline{C}H_2CH_3$), 67.9 (<u>C</u>H of Cp), 68.5 (<u>C</u>H of Cp), 70.0 (<u>C</u>H of Cp), 70.5 (<u>C</u>H of Cp), 71.8 (<u>C</u>H of Cp), 72.4 (<u>C</u>H of Cp), 73.0 (<u>C</u>H of Cp), 78.7 (*ipso*-Cp^{Br}), 80.1 (*ipso*-Cp^{Br}), 90.7 (*ipso*-Cp^{Et}). MS (FDI): m/z (%) 372 (100) [M^+]. HRMS (FDI; m/z): [M^+] calcd for $C_{12}H_{12}FeBr_2$, 371.8643; found, 371.8635. Elemental Anal. Calcd. for $C_{12}H_{12}Br_2Fe$ (371.8810): C, 38.76; H, 3.25; Found: C, 38.86; H, 2.81.

4.4.2. Synthesis of *rac*-1,1'-Dibromo-2-(hydroxyethyl)ferrocene (*rac*-46)

Synthesis and Characterization of *rac*-1,1'-Dibromo-2-vinylferrocene (*rac*-45)

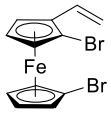

rac-**45**

rac-2-[1-(Dimethylamino)ethyl]-1,1'-dibromoferrocene (*rac*-**43**) (0.95 g, 2.3 mmol) was dissolved in acetic anhydride (12.8 mL, 136 mmol) and acetic acid was added (1.3 mL; 20.6 mmol). The resulting mixture was thoroughly degassed and stirred for 10 h at 140 ºC. All volatiles were removed at 50 ºC under high vacuum to give a brown oil. The brown oil was dissolved in Et_2O (50 mL) and washed with saturated aqueous $NaHCO_3$ solution, water, and brine. The organic layer was dried over anhydrous Na_2SO_4, filtered, and concentrated using a rotatory evaporator. The brown oil crude material (0.80 g, 94 %) was purified by flash column chromatography (hexanes). The product was obtained as a dark red oil (0.60 g, 71%, Note: *rac*-**45** contained ca. 3% of *rac*-1-bromo-2-vinylferrocene as an impurity). ^{1}H NMR ($CDCl_3$, 500.3 MHz): δ = 4.08 (m, 2H, Cp), 4.27 (t, 1H, J = 3.0 Hz, Cp), 4.31 (m, 1H, Cp), 4.32 (m, 1H, Cp), 4.47 (m, 1H, Cp), 4.50 (m, 1H, Cp), 5.29 (dd, 1H, J = 11.0, 1.5 Hz, C<u>H</u>CH_2) 5.54 (dd, 1H, J = 17.5, 1.5 Hz, CHC<u>H</u>$_2$) 6.57 (dd, 1H, J = 18.0, 11.0 Hz, CHC<u>H</u>$_2$) ^{13}C {^{1}H} NMR ($CDCl_3$, 125.8 MHz): δ = 66.1 (<u>C</u>H of Cp), 69.7 (<u>C</u>H of Cp), 71.2 (<u>C</u>H of Cp), 71.5 (<u>C</u>H of Cp), 73.16 (<u>C</u>H of Cp), 73.22 (<u>C</u>H of Cp), 73.7 (<u>C</u>H of Cp), 78.7 (*ipso*-Cp^{Br}), 79.8 (*ipso*-Cp^{Br}), 83.4 (*ipso*-Cp^{vinyl}), 114.5 (CH<u>C</u>H_2), 131.1 (<u>C</u>HCH_2). MS (FDI): m/z (%) 370 (100) [M^+]. HRMS (FDI; m/z): [M^+] calcd for $C_{12}H_{10}FeBr_2$, 367.8499; found, 367.8499.

Synthesis of *rac*-1,1'-Dibromo-2-(hydroxyethyl)ferrocene (*rac*-46)

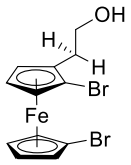

rac-**46**

$BH_3{\cdot}SMe_2$ (0.11 mL, 1.7 mmol) was added dropwise to a solution of *rac*-**45** (0.22 g, 0.60 mmol) in thf (6 mL) at r.t. The mixture is stirred at r.t. for 2 h. followed by the addition of NaOH solution (2.0 mL, 3.0 M, 6.1 mmol) and dropwise addition of H_2O_2 (1.5 g, 30% water, 13.2 mmol). CH_2Cl_2 (15 mL) was added and the phases were separated. The aqueous phase was extracted with CH_2Cl_2 (2 x 15 mL). The organic layers were washed with water, and brine. The combined organic layers were dried over anhydrous Na_2SO_4, filtered, and concentrated using a rotatory evaporator. The red oil crude material (0.21 g, 91%) was purified by flash column chromatography (hexanes/EtOAc; 6 : 4). The product was obtained as an orange oil [0.13 g, 54%]. ^{1}H NMR ($CDCl_3$, 500.3 MHz): δ = 1.40 (t, 1H, *J* = 6.0 Hz, $CH_2CH_2O\underline{H}$), 2.71, 2.80 (m, ABCDE system, 2H, *J* = 14.5, 7.0, 6.0, 6.0, 6.0 Hz, $C\underline{H}_2CH_2OH$), 3.77, 3.83 (m, ABCDE system, 2H, *J* = 11.5, 7.0, 6.0, 6.0, 6.0, 6.0, 6.0 Hz, $CH_2C\underline{H}_2OH$, 4.11 (m, 2H, CH of Cp), 4.16 (m, 2H, CH of Cp), 4.30 (m, 1H, CH of Cp), 4.35 (m, 1H, CH of Cp), 4.43 (t, 1H, J = 2.0 Hz, CH of Cp). ^{13}C {^{1}H} NMR ($CDCl_3$, 125.8 MHz): δ = 30.8 ($\underline{C}H_2CH_2OH$), 62.5 ($CH_2\underline{C}H_2OH$), 68.5 (<u>C</u>H of Cp), 69.8 (<u>C</u>H of Cp), 70.1 (<u>C</u>H of Cp), 70.6 (<u>C</u>H of Cp), 72.1 (<u>C</u>H of Cp), 72.4 (<u>C</u>H of Cp), 73.4 (<u>C</u>H of Cp), 78.8 (*ipso*-Cp^{Br}), 80.4 (*ipso*-Cp^{Br}), 85.1 (*ipso*-$Cp^{Alcohol}$). MS (FDI): *m/z* (%): 388 (100) [M^+]. HRMS (FDI; m/z): calcd for $C_{12}H_{12}Br_2FeO$, 385.8604; found, 385.8616.

4.4.3. Synthesis of (S_p,S_p)-1,1'-Dibromo-2,2'-diethylferrocene

Synthesis of (*R*,*R*,S_p,S_p)-2,2'-Bis[1-(trimethylamino)ethyl]-1,1'-dibromoferrocene iodide (*R*,*R*,S_p,S_p-48)

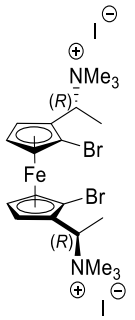

R,*R*,S_p,S_p-**48**

To a stirred solution of (*R*,*R*,S_p,S_p)-2,2'-bis[1-(dimethylamino)ethyl]-1,1'-dibromoferrocene (*R*,*R*,S_p,S_p-**47**) (1.20 g, 2.5 mmol) in CH_3CN (14 mL) was added dropwise CH_3I (0.92 mL, 14.9 mmol) at r.t. The solution was stirred for 10 min at r.t. and a yellow suspension was obtained that was stirred for additional 20 min. Appox. 80% of the solvents were removed under vacuum and Et_2O was added (25 mL). The suspension was stirred for 10 min and vacuum filtered. The product was afforded as a yellow powder (1.52 g, 80%). ^{1}H NMR (D_2O, 500.3 MHz): δ = 1.95 [d, 6H, *J* = 6.5 Hz, $CH(NMe_3)C\underline{H}_3$], 2.93 [s, 18H, $CH(N\underline{Me}_3)CH_3$], 4.66 [m, 2H, $C\underline{H}(NMe_3)CH_3$], 4.69 – 4.86 (m, 6H, CH of Cp). ^{13}C {^{1}H} NMR ($CDCl_3$, 125.8 MHz): δ = 16.2 [$CH(NMe_3)\underline{C}H_3$], 51.0 [$CH(N\underline{Me}_3)CH_3$], 68.5 [$\underline{C}H(NMe_3)CH_3$], 69.9 ($\underline{C}$H of Cp), 72.5 ($\underline{C}$H of Cp), 79.3 (*ipso*-Cp) 81.4 (*ipso*-Cp), 82.6 (*ipso*-Cp).

Synthesis of (S_p,S_p)-1,1'-Dibromo-2,2'-diethylferrocene (S_p,S_p-42)

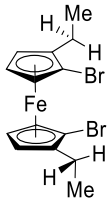

S_p,S_p-**42**

To a stirred solution of *R*,*R*,S_p,S_p-**48** (1.35 g, 1.8 mmol) in CH_3CN (30 mL) was added portionwise $NaBH_4$ (0.39 g, 11 mmol) at r.t. followed by stirring at 80 °C for 48 h. The resulting solution was quenched with water and extracted with Et_2O (2 x 50 mL). The organic layers were washed with water (3 x 50 mL) and brine. The combined organic layers were dried over anhydrous Na_2SO_4, filtered, and concentrated using a rotatory evaporator. The yellow oil crude material (0.67 g, 95%) was purified by flash column chromatography (hexanes/EtOAc, 9 : 1) affording a dark yellow oil (0.60 g, 86%). ^{1}H NMR ($CDCl_3$, 500.3 MHz): δ = 1.13 [t, 6H, J = 7.5 Hz, ($CH_2C\underline{H}_3)_2$], 2.36, 2.38 [m, ABX_3 system, 4H, J = 15.0, 7.5, 7.5 Hz, ($C\underline{H}_2CH_3)_2$], 4.00 (m, 4H, C<u>H</u> of Cp), 4.28 (m, 2H, C<u>H</u> of Cp) ppm; $^{13}C\{^1H\}$ NMR ($CDCl_3$, 125.8 MHz): δ = 14.4 [($CH_2\underline{C}H_3)_2$], 20.0 [($\underline{C}H_2CH_3)_2$], 68.2 (CH of Cp), 68.3 (CH of Cp), 71.9 (CH of Cp), 80.8 (*ipso*-Cp^{Br}), 90.3 (*ipso*-Cp^{Et}) ppm. MS (FDI): m/z (%) 400 (100) [M^+]. HRMS (FDI; m/z): [M^+] calcd for $C_{14}H_{16}FeBr_2$, 397.8950; found, 397.8968.

4.4.4. Synthesis of the Racemic Sila[1]ferrocenophane *rac*-35.

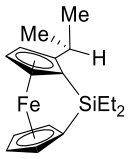

rac-**35**

rac-1,1'-Dibromo-2-isopropylferrocene (*rac*-**40**) (0.40 g, 1.0 mmol) was dissolved in a mixture of thf (0.94 mL) and hexanes (8.4 mL) and cooled to 0 °C. A solution of *n*BuLi (2.5 M in hexanes, 0.88 mL, 2.2 mmol) was added dropwise and the reaction mixture was stirred at 0 °C for 30 min. Et_2SiCl_2 (0.16 mL, 1.1 mmol) was added dropwise via syringe within 1 min at 0 °C and the color of the solution changed from orange to red, along with formation of a white precipitate. After stirring of the reaction for 15 min at 0 °C, all volatiles were removed under vacuum and the resulting red residue was dissolved in hexanes (10 mL). Solids were removed by filtration and solvents were removed under vacuum. The crude material was purified by flash column chromatography (neutral alumina; hexanes/Et_3N, 10 : 1) and crystallization in hexanes (3 mL) at -80 °C resulted in *rac*-**35** as red crystals (0.24 g, 75%). ^{1}H NMR (C_6D_6, 600.2 MHz): δ = 0.92 [two overlapping quartets, 2H, *J* = 8.0 Hz, Si(C<u>H</u>$_2$CH$_3$)$_2$], 1.08 [m, 2H, Si(C<u>H</u>$_2$CH$_3$)$_2$; overlaps with doublet at 1.10], 1.10 [d, 3H, *J* = 7.0 Hz, CH(C<u>H</u>$_3$)$_2$], 1.16 [t, 3H, *J* = 8.0 Hz, Si(CH$_2$C<u>H</u>$_3$)$_2$; overlaps with triplet at 1.19], 1.19 [t, 3H, *J* = 8.0 Hz, Si(CH$_2$C<u>H</u>$_3$)$_2$; overlaps with triplet at 1.16 and doublet at 1.19] 1.19 [d, 3H, *J* = 7.0 Hz, CH(C<u>H</u>$_3$)$_2$;], 2.60 [sept, 1H, *J* = 7.0 Hz, C<u>H</u>(CH$_3$)$_2$], 3.65 (m, 1H, H-α of Cp), 3.86 (m, 1H, H-α of Cp), 3.93 (m, 1H, H-α of Cp), 4.33 (m, 1H, H-β of Cp), 4.36 (t, 1H, *J* = 2.0 Hz, H-β of Cp), 4.40 (td, 1H, *J* = 2.0, 1.0 Hz, H-β of Cp), 4.52 (td, 1H, *J* = 2.0, 1.0 Hz, H-β of Cp) ppm; ^{13}C{^{1}H} NMR (C_6D_6, 150.9 MHz): δ = 3.1 [Si(<u>C</u>H$_2$CH$_3$)$_2$], 5.1 [Si(<u>C</u>H$_2$CH$_3$)$_2$], 6.5 [Si(CH$_2$<u>C</u>H$_3$)$_2$], 6.6 (Si(CH$_2$<u>C</u>H$_3$)$_2$), 21.5 (CH(<u>C</u>H$_3$)$_2$), 27.8 (CH(<u>C</u>H$_3$)$_2$), 29.3 (<u>C</u>H(CH$_3$)$_2$), 30.4 (*ipso*-Cp^{Si}), 33.2 (*ipso*-Cp^{Si}), 74.0 (<u>C</u>H of Cp), 75.2 (<u>C</u>H of Cp), 75.8 (<u>C</u>H of

Cp), 76.3 (CH of Cp), 76.6 (CH of Cp), 77.8 (CH of Cp), 80.8 (CH of Cp) 105.6 (*ipso*-Cp^{iPr}) ppm; ^{29}Si NMR (C_6D_6, 119.2 MHz): 1.0 ppm. MS (FDI): m/z (%) 312 (100) [M^+]. HRMS (FDI; m/z): [M^+] calcd for $C_{17}H_{24}FeSi$, 312.0997; found, 312.1010. Elemental Anal. Calcd. for $C_{17}H_{24}FeSi$ (312.31): C, 65.38; H, 7.75. Found: C, 65.24; H, 6.98.

4.4.5. Synthesis of the Racemic Sila[1]ferrocenophane *rac*-36

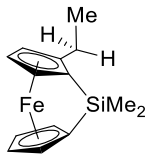

rac-**36**

Species *rac*-**41** (0.75 g, 2.0 mmol) was dissolved in a solvent mixture (18 mL; hexanes : thf, 9 : 1) and cooled to 0 ºC. A solution of *n*BuLi (2.5 M in hexanes, 1.71 mL, 4.2 mmol) was added dropwise and the reaction mixture was stirred at this temperature for 30 min, resulting in a red solution followed by dropwise addition of Me_2SiCl_2 (0.27 g, 2.1 mmol) at 0 ºC . All volatiles were removed, followed by addition of hexanes (10 mL) and filtration. After removing all the volatiles, the red solution resulted in a red oil. The compound was purified by flash column chromatography on alumina (neutral alumina; hexanes/Et_3N, 10 : 1), which resulted in a red oil (0.35 g, 65%). ^{1}H NMR (C_6D_6, 600.2 MHz): δ = 0.36 [s, 3H, Si(CH$_3$)$_2$], 0.50 [s, 3H, Si(CH$_3$)$_2$], 1.06 [t, 3H, *J* = 7.5 Hz, (CH$_2$CH$_3$)], 2.21, 2.28 (m, ABX$_3$ system, 2H, *J* = 15.0, 7.5, 7.5 Hz, CH$_2$CH$_3$), 3.60 (m, 1H, H-α of Cp), 3.84 (m, 1H, H-α of Cp), 3.90 (m, 1H, H-α of Cp), 4.32 (m, 1H, H-β of Cp), 4.35 (t, 1H, *J* = 2.0 Hz, H-β of Cp), 4.39 (td, 1H, *J* = 2.0, 1.0 Hz, H-β of Cp), 4.56 (td, 1H, *J* = 2.0, 1.0 Hz, H-β of Cp) ppm; ^{13}C{^{1}H} NMR (C_6D_6, 150.9 MHz): δ = -2.7 [Si(CH$_3$)$_2$], -0.6 [Si(CH$_3$)$_2$], 16.4 (CH$_2$CH$_3$), 24.0 (CH$_2$CH$_3$), 31.3 (*ipso*-Cp^{Si}), 33.9 (*ipso*-Cp^{Si}), 74.9 (CH of Cp), 75.5 (CH of Cp), 76.3 (CH of Cp), 76.6 (CH of Cp), 77.2 (CH of Cp), 78.0 (CH of Cp), 81.1 (CH of Cp) 99.5 (*ipso*-

Cp^{Et}) ppm; ^{29}Si NMR (C_6D_6, 119.2 MHz): -5.7 ppm. MS (FDI): *m/z* (%): 270 (100) [M^+]. HRMS (FDI; m/z): calcd for $C_{14}H_{18}FeSi$: 270.0527; found: 270.0523.

4.4.6. Synthesis of the Chiral Sila[1]ferrocenophane S_p,S_p-37

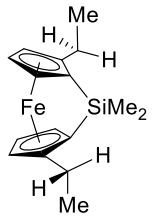

S_p,S_p-**37**

Species S_p,S_p-**42** (0.54 g, 1.3 mmol) was dissolved in a solvent mixture (12 mL; hexanes : thf, 9 : 1) and cooled to 0 ºC. A solution of *n*BuLi (2.4 M in hexanes, 1.20 mL, 2.8 mmol) was added dropwise and the reaction mixture was stirred at this temperature for 30 min, resulting in a red solution followed by dropwise addition of Me_2SiCl_2 (0.18 g, 1.4 mmol) at 0 ºC . All volatiles were removed, followed by addition of hexanes (7 mL) and filtration. After removing all the volatiles, the red solution resulted in a red oil. The compound was purified by flash column chromatography on alumina (neutral alumina; hexanes/Et_3N, 10 : 1), which resulted in a mixture of red oil (0.31 g, 76%). ^1H NMR (C_6D_6, 600.2 MHz): δ = 0.51 [s, 6H, Si($C\underline{H}_3$)$_2$], 1.07 [t, 6H, *J* = 7.5 Hz, ($CH_2C\underline{H}_3$)$_2$], 2.21, 2.28 [m, ABX_3 system, 4H, *J* =15.0, 7.5, 7.5 Hz, ($C\underline{H}_2CH_3$)$_2$], 3.50 (m, 2H, H-α of Cp), 4.30 (m, 2H, H-β of Cp), 4.50 (m, 2H, H-β of Cp) ppm; $^{13}C\{^1H\}$ NMR (C_6D_6, 150.9 MHz): δ = -0.2 [Si($\underline{C}H_3$)$_2$], 16.4 [($CH_2\underline{C}H_3$)$_2$], 23.7 [($\underline{C}H_2CH_3$)$_2$], 32.2 (*ipso*-Cp^{Si}), 76.3 (CH of Cp), 76.6 (CH of Cp), 80.7 (CH of Cp), 98.9 (*ipso*-Cp^{Et}) ppm; ^{29}Si NMR (C_6D_6, 119.2 MHz): -5.9 ppm. MS (FDI): *m/z* (%): 298 (100) [M^+]. HRMS (FDI; m/z): calcd for $C_{16}H_{22}FeSi$: 298.0840; found: 298.0852.

4.4.7. Thermal ROP of *rac*-35

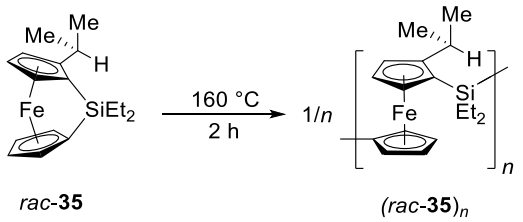

rac-**35** (*rac*-**35**)$_n$

Monomer *rac*-**35** (207 mg; 0.66 mmol) was heated to 160 ºC for 2 h in a flame-sealed Pyrex NMR tube. After letting the sample cool down to r.t., a red-orange glassy solid was obtained. From this point on the manipulation was done under air. The resulting red-orange glassy solid slowly dissolved in thf (3.0 mL). Precipitation into methanol (12 mL) in a vial afford an orange solid and a yellow supernatant. Re-dissolved in thf (3.0 mL) and precipitated into methanol (12 mL). The polymer was re-dissolved in thf (2 x 3.0 mL) and precipitated into methanol (2 x 12 mL). The obtained orange solid was dried under high vacuum for 16 h, to give the product as an orange powder (188 mg, 90%). ^{1}H NMR (C_6D_6, 600.2 MHz): δ =1.02 – 1.16 [br, 3H, CH(C<u>H</u>$_3$)$_2$], 1.15 – 1.55 [br, 3H, CH(C<u>H</u>$_3$)$_2$; 10H, Si(C<u>H</u>$_2$C<u>H</u>$_3$)$_2$], 2.38 – 2.72 [br, 1H, C<u>H</u>(CH$_3$)$_2$], 3.94 – 4.61 (br, 7H, C<u>H</u> of Cp) ppm; ^{13}C{^{1}H} NMR (C_6D_6, 150.9 MHz): δ = -0.6 to -0.2(br), 0.2, 0.3, 0.5, 1.0 2.2 [Si(<u>C</u>H$_2$<u>C</u>H$_3$)$_2$], 23.0, 23.3, 23.8, 26.7, 27.2, 27.3 [CH(<u>C</u>H$_3$)$_2$], 28.1, 28.27, 28.32, 30.2 [<u>C</u>H(CH$_3$)$_2$], 68.3, 68.5, 70.8, 71.5, 72.6, 73.2, 73.6, 73.9, 74.0, 74.2, 74.3, 75.0 (<u>C</u>H of Cp), 70.2, 70.5 (*ipso*-Cp^{Si}), 102.3, 102.6 (*ipso*-Cp^{iPr}) ppm; GPC: M_w = 4.96 × 10^4 Da, M_n = 2.13 × 10^4 Da, $Đ$ = 2.32.

4.4.8. Thermal ROP of *rac*-36

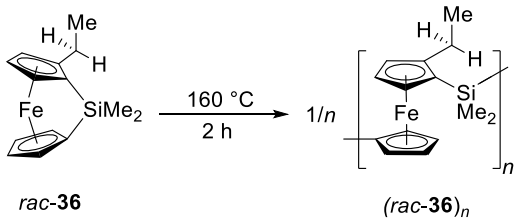

rac-**36** (*rac*-**36**)$_n$

Monomer *rac*-**36** (107 mg; 0.40 mmol) was heated to 160 ºC for 2 h in a flame-sealed Pyrex NMR tube. After letting the sample cool down to r.t., a red-orange glassy solid was obtained. From this point on the manipulation was done under air. The resulting red-orange glassy solid slowly dissolved in CH_2Cl_2 (2.0 mL). Precipitation into methanol (8 mL) in a vial afford an orange solid and a yellow supernatant. Re-dissolved in CH_2Cl_2 (2 × 2.0 mL) and precipitated into methanol (2 × 8 mL). The polymer was re-dissolved in thf (2 x 2.0 mL) and precipitated into hexanes (2 x 8 mL). The obtained yellow solid was dried under high vacuum for 16 h, to give the product as a yellow powder (93 mg, 87%).^{1}H NMR (C_6D_6, 600.2 MHz): δ =0.35 – 0.78 [br, 6H, Si(C$\underline{H}_3$)$_2$], 0.85 – 1.02 [br, 2H, $CH_2C\underline{H}_3$], 1.06 – 1.23 [br, 1H, $CH_2C\underline{H}_3$], 2.16 – 2.50 [br, 2H, $C\underline{H}_2CH_3$], 3.93 – 4.43 (br, 7H, C$\underline{H}$ of Cp) ppm; ^{13}C{^{1}H} NMR (C_6D_6, 150.9 MHz): δ = -0.5 to -0.3(br), -0.2, -0.1, 0.3, 0.4, 0.5, 1.0, 2.0 [Si($\underline{C}H_3$)$_2$], 15.5, 15.6, 16.0[$CH_2\underline{C}H_3$], 23.4 [$\underline{C}H_2CH_3$], 70.7, 71.4, 71.5, 72.4, 73.1, 73.6, 73.8, 73.9, 74.5, 74.6 ($\underline{C}$H of Cp) 70.3, 70.4 (*ipso*-Cp^{Si}), 95.6, 95.8 (*ipso*-Cp^{iPr}) ppm; ^{29}Si NMR (C_6D_6, 119.2 MHz): δ = -7.3, -7.1, -6.8, -6.1 ppm; GPC: M_w = 4.02 × 10^5 Da, M_n = 2.20 × 10^5 Da, $Đ$ = 1.83.

4.4.9. Thermal ROP of S_p,S_p-37

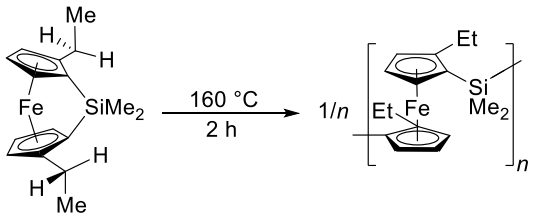

S_p,S_p-**37** $(S_p,S_p\text{-}\mathbf{37})_n$

Monomer S_p,S_p-**37** (205 mg; 0.34 mmol) was heated to 160 ºC for 2 h in a flame-sealed Pyrex NMR tube. After letting the sample cool down to r.t., a dark red glassy solid was obtained. From this point on the manipulation was done under air. The resulting dark red glassy solid was dissolved in heated TCB (3 mL) at 150 ºC. Precipitation into methanol (12 mL) in a vial afford a dark brown solid and a brown supernatant. Re-dissolved in heated TCB (6 × 3.0 mL) at 150 ºC and precipitated into methanol (6 × 12 mL). The obtained dark brown solid was dried under high vacuum for 16 h, to give the product as a dark brown powder (110 mg, 54%).

4.4.10. Thermal ROP toward 49

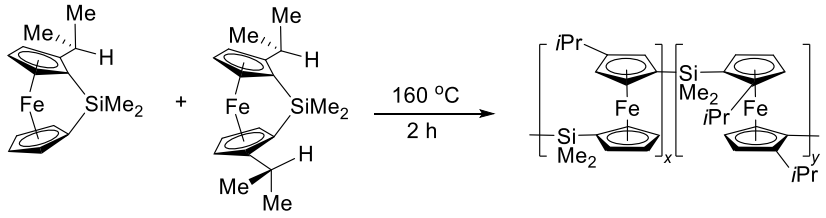

rac-**38** S_p,S_p-**39** **49**

Monomer *rac*-**38** (100 mg; 0.35 mmol) and S_p,S_p-**39** (11 mg; 0.035 mmol) was heated to 160 ºC for 2.0 h in a flame-sealed Pyrex NMR tube. After letting the sample cool down to r.t., a red-orange glassy solid was obtained. From this point on the manipulation was done under air. The resulting red-orange glassy solid slowly dissolved in thf (2.0 mL). Precipitation into methanol (8 mL) in a vial afford an orange solid and a yellow supernatant. The orange solid was washed with methanol (2 x 10 mL). Re-dissolved in thf (2 × 2.0 mL) and precipitate into methanol (2 × 8 mL). The

obtained orange solid was dried under high vacuum for 16 h, to give product as an orange powder (92 mg, 83%). ^{1}H NMR (C_6D_6, 600.2 MHz): δ =0.52 – 0.86 [br, 6H, Si(C<u>H</u>$_3$)$_2$], 1.01 – 1.19 [br, 2H, CH(C<u>H</u>$_3$)$_2$], 1.21 – 1.40 [br, 3H, CH(C<u>H</u>$_3$)$_2$], 2.57 – 2.75 [br, 1H, C<u>H</u>(CH$_3$)$_2$], 4.03 – 4.52 (br, 7H, C<u>H</u> of Cp) ppm; ^{13}C{^{1}H} NMR (C_6D_6, 150.9 MHz): δ = -0.6 to -0.2 (br), 0.2, 0.3, 0.5, 1.3 2.3 [Si(<u>C</u>H$_3$)$_2$], 23.0, 23.3, 23.8, 26.7, 27.1, 27.3 [CH(<u>C</u>H$_3$)$_2$], 28.1, 28.27, 28.31, 30.2 [<u>C</u>H(CH$_3$)$_2$], 68.3, 68.5, 70.3, 70.8, 71.6, 72.4, 72.6, 73.2, 73.6, 73.9, 74.0, 74.2, 74.4, 75.1 (<u>C</u>H of Cp), 70.2, 70.5 (*ipso*-Cp^{Si}), 102.3, 102.6 (*ipso*-Cp^{iPr}) ppm; ^{29}Si NMR (C_6D_6, 119.2 MHz): δ = -8.2, -7.4, -6.7, -5.8 ppm; GPC: M_w = 3.56 × 10^6 Da, M_n = 1.70 × 10^6 Da, $Đ$ = 2.09.

4.4.11. Thermal ROP toward 50

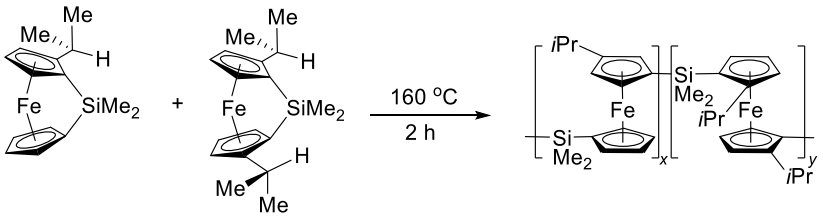

rac-**38** S_p,S_p-**39** **50**

Monomer *rac*-**38** (78.0 mg; 0.28 mmol) and S_p,S_p-**39** (27 mg, 0.083 mmol) was heated to 160 ºC for 2 h in a flame-sealed Pyrex NMR tube. After letting the sample cool down to r.t., a red-orange glassy solid was obtained. From this point on the manipulation was done under air. The resulting red-orange glassy solid slowly dissolved in thf (2.0 mL). Precipitation into methanol (8 mL) in a vial afford an orange solid and a yellow supernatant. Re-dissolved in thf (2 × 2.0 mL) and precipitate into methanol (2 × 8 mL). The obtained orange solid was dried under high vacuum for 16 h, to give product as an orange powder (85.4 mg, 81%). ^{1}H NMR (C_6D_6, 600.2 MHz): δ =0.52 – 0.87 [br, 6H, Si(C<u>H</u>$_3$)$_2$], 0.99 – 1.22 [br, 2H, CH(C<u>H</u>$_3$)$_2$], 1.20 – 1.44 [br, 3H, CH(C<u>H</u>$_3$)$_2$], 2.56 – 2.78 [br, 1H, C<u>H</u>(CH$_3$)$_2$], 3.97 – 4.59 (br, 7H, C<u>H</u> of Cp) ppm; ^{13}C{^{1}H} NMR (C_6D_6, 150.9 MHz): δ = -0.6 to -0.2 (br), 0.3, 0.5, 1.3 2.2 [Si(<u>C</u>H$_3$)$_2$], 23.0, 23.2, 23.8, 26.6, 26.7, 27.2, 27.3 [CH(<u>C</u>H$_3$)$_2$],

28.1, 28.3, 30.2, 30.4 [CH(CH$_3$)$_2$], 68.3, 68.4, 70.0, 70.5, 71.6, 72.5, 73.2, 73.6, 74.0, 75.1 (CH of Cp), 70.2, 70.5 (*ipso*-Cp^{Si}), 102.3, 102.6 (*ipso*-Cp^{iPr}) ppm; ^{29}Si NMR (C$_6$D$_6$, 119.2 MHz): δ = -8.2, -7.4, -6.7, -5.8 ppm; GPC: M_w = 2.20 × 10^6 Da, M_n = 1.06× 10^6 Da, $Đ$ = 2.08.

4.4.12. Transition-Metal-Catalyzed ROP of *rac*-38

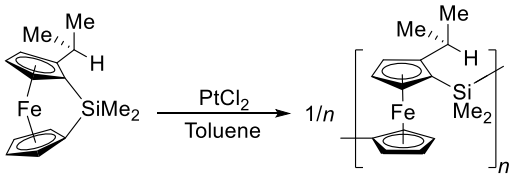

rac-**38** (*rac*-**38**)$_n$

A solution of monomer *rac*-**38** (188 mg, 0.66 mmol) in toluene (2.80 mL) was stirred for 5.5 h in the presence of $PtCl_2$ (1 mol %) at r.t. The resulting red-brown thick solution was precipitated into MeOH to afford an orange solid and brown-green supernatant. The polymer was re-dissolved in CH_2Cl_2 (4 × 3.0 mL) and precipitated into methanol (4 × 12 mL). After this, the polymer was re-dissolved in CH_2Cl_2 (2 x 3.0 mL) and precipitate into acetone (2 x 12 mL) to afford a brown ball and a yellow supernatant. The polymer was re-dissolved one more time in CH_2Cl_2 (3.0 mL) and precipitate into methanol (12 mL). The obtained orange solid was dried under high vacuum for 16 h, to give the product as an orange powder (148 mg, 79%). ^{1}H NMR (C$_6$D$_6$, 600.2 MHz): δ =0.54 – 0.88 [br, 6H, Si(CH$_3$)$_2$; 1H, CH(CH$_3$)$_2$], 1.02 – 1.18 [br, 2H, CH(CH$_3$)$_2$], 1.23 – 1.42 [br, 3H, CH(CH$_3$)$_2$], 2.57 – 2.75 [br, 1H, CH(CH$_3$)$_2$], 4.00 – 4.52 (br, 7H, CH of Cp) ppm; ^{13}C{^{1}H} NMR (C$_6$D$_6$, 150.9 MHz): δ = -0.6 to -0.2 (br), 0.2, 0.3, 0.5, 1.0 2.3 [Si(CH$_3$)$_2$], 23.0, 23.3, 23.8, 26.7, 27.2, 27.3 [CH(CH$_3$)$_2$], 28.1, 28.27, 28.32, 30.2 [CH(CH$_3$)$_2$], 68.3, 68.5, 70.8, 71.5, 72.6, 73.2, 73.6, 73.9, 74.0, 74.2, 74.3, 75.1 (CH of Cp), 70.2, 70.5 (*ipso*-Cp^{Si}), 102.3, 102.6 (*ipso*-Cp^{iPr}) ppm; ^{29}Si NMR (C$_6$D$_6$, 119.2 MHz): δ = -8.2, -7.4, -6.7, -5.8 ppm; GPC: M_w ~ 5.8 × 10^6, 3.9 x 10^5, 6.7 x 10^4 Da.

4.4.13. Transition-Metal-Catalyzed ROP of S_p,S_p-39

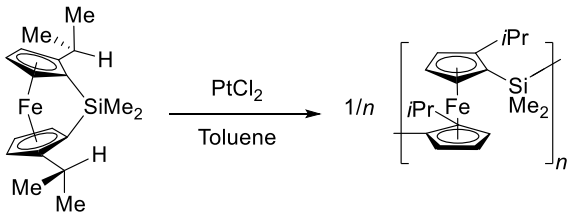

S_p,S_p-**39** $(S_p,S_p\text{-}\mathbf{39})_n$

A solution of monomer S_p,S_p-**39** (133 mg, 0.41 mmol) in toluene (1.70 mL) was stirred for 24 h in the presence of $PtCl_2$ (1 mol %) at r.t. The resulting red-brown thick solution was precipitated into hexanes to afford a dark orange solid and brown supernatant. The resulting polymer was insoluble in thf, CH_2Cl_2, or benzene, and only swelling and partial solubility were observed in heated TCB. The yellow solid was re-dissolved in TCB (3 × 10 mL) at 150 ºC and precipitated into methanol (3 × 50 mL). The obtained yellow solid was dried under high vacuum for 16 h, to give product $(S_p,S_p\text{-}\mathbf{39})_n$ as a tan yellow solid (41 mg, 31%).

4.4.14. Transition-Metal-Catalyzed ROP of S_p,S_p-39

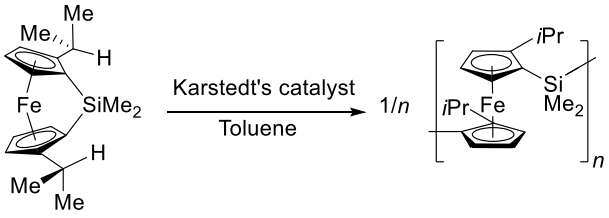

S_p,S_p-**39** $(S_p,S_p\text{-}\mathbf{39})_n$

A solution of monomer S_p,S_p-**39** (63 mg, 0.19 mmol) in toluene (0.35 mL) was stirred for 24 h in the presence of Karstedt's catalyst (1 mol %) at r.t. The resulting dark red solution was precipitated into hexanes to afford an orange solid and yellow supernatant. The resulting polymer was insoluble in thf, CH_2Cl_2, or benzene, and only swelling and partial solubility were observed in heated TCB. The yellow solid was re-dissolved in TCB (3 × 6 mL) at 150 ºC and precipitated into methanol

(3 × 30 mL). The obtained yellow solid was dried under high vacuum for 16 h, to give product (S_p,S_p-**39**)$_n$ as a tan yellow solid (11 mg, 17%).

APPENDIX A

Table A-1. Bond lengths [Å] and bond angles [°] for compound *rac*-**35**.

Fe(1)-C(1)	2.0097(18)	C(11)-C(13)	1.531(3)
Fe(1)-C(6)	2.0111(17)	C(11)-C(12)	1.532(3)
Fe(1)-C(5)	2.0219(19)	C(14)-C(16)	1.523(3)
Fe(1)-C(10)	2.0242(18)	C(15)-C(17)	1.531(3)
Fe(1)-C(7)	2.0326(19)	C(1)-Fe(1)-C(6)	88.94(7)
Fe(1)-C(2)	2.0359(18)	C(1)-Fe(1)-C(5)	42.23(8)
Fe(1)-C(9)	2.0713(19)	C(6)-Fe(1)-C(5)	108.16(7)
Fe(1)-C(4)	2.0729(19)	C(1)-Fe(1)-C(10)	108.57(8)
Fe(1)-C(8)	2.075(2)	C(6)-Fe(1)-C(10)	42.04(7)
Fe(1)-C(3)	2.0803(18)	C(5)-Fe(1)-C(10)	145.22(8)
Fe(1)-Si(1)	2.6995(6)	C(1)-Fe(1)-C(7)	111.55(8)
Si(1)-C(14)	1.867(2)	C(6)-Fe(1)-C(7)	41.97(8)
Si(1)-C(15)	1.8688(19)	C(5)-Fe(1)-C(7)	101.13(8)
Si(1)-C(6)	1.8887(19)	C(10)-Fe(1)-C(7)	68.95(8)
Si(1)-C(1)	1.8976(18)	C(1)-Fe(1)-C(2)	42.22(7)
C(1)-C(5)	1.452(3)	C(6)-Fe(1)-C(2)	111.91(7)
C(1)-C(2)	1.457(2)	C(5)-Fe(1)-C(2)	69.43(7)
C(2)-C(3)	1.424(3)	C(10)-Fe(1)-C(2)	101.89(8)
C(2)-C(11)	1.513(3)	C(7)-Fe(1)-C(2)	149.80(8)
C(3)-C(4)	1.419(3)	C(1)-Fe(1)-C(9)	148.59(8)
C(4)-C(5)	1.415(3)	C(6)-Fe(1)-C(9)	70.10(8)
C(6)-C(10)	1.448(2)	C(5)-Fe(1)-C(9)	166.30(8)
C(6)-C(7)	1.448(3)	C(10)-Fe(1)-C(9)	40.57(8)
C(7)-C(8)	1.423(3)	C(7)-Fe(1)-C(9)	68.17(8)
C(8)-C(9)	1.418(3)	C(2)-Fe(1)-C(9)	124.13(8)
C(9)-C(10)	1.420(3)	C(1)-Fe(1)-C(4)	70.05(8)
C(6)-Fe(1)-C(4)	147.96(8)	C(2)-Fe(1)-Si(1)	75.72(5)
C(5)-Fe(1)-C(4)	40.42(7)	C(9)-Fe(1)-Si(1)	111.33(6)
C(10)-Fe(1)-C(4)	167.50(8)	C(4)-Fe(1)-Si(1)	110.50(6)

C(7)-Fe(1)-C(4)	123.42(8)	C(8)-Fe(1)-Si(1)	111.80(6)
C(2)-Fe(1)-C(4)	68.42(8)	C(3)-Fe(1)-Si(1)	112.61(6)
C(9)-Fe(1)-C(4)	138.14(8)	C(14)-Si(1)-C(15)	110.81(9)
C(1)-Fe(1)-C(8)	151.97(8)	C(14)-Si(1)-C(6)	110.38(9)
C(6)-Fe(1)-C(8)	69.97(8)	C(15)-Si(1)-C(6)	112.80(9)
C(5)-Fe(1)-C(8)	126.32(8)	C(14)-Si(1)-C(1)	116.78(9)
C(10)-Fe(1)-C(8)	68.06(8)	C(15)-Si(1)-C(1)	109.26(9)
C(7)-Fe(1)-C(8)	40.52(8)	C(6)-Si(1)-C(1)	96.13(8)
C(2)-Fe(1)-C(8)	163.58(8)	C(14)-Si(1)-Fe(1)	127.77(6)
C(9)-Fe(1)-C(8)	40.00(8)	C(15)-Si(1)-Fe(1)	121.39(7)
C(4)-Fe(1)-C(8)	119.27(9)	C(6)-Si(1)-Fe(1)	48.10(5)
C(1)-Fe(1)-C(3)	69.74(7)	C(1)-Si(1)-Fe(1)	48.04(5)
C(6)-Fe(1)-C(3)	152.32(8)	C(5)-C(1)-C(2)	105.18(15)
C(5)-Fe(1)-C(3)	67.90(8)	C(5)-C(1)-Si(1)	114.64(13)
C(10)-Fe(1)-C(3)	127.56(8)	C(2)-C(1)-Si(1)	122.82(13)
C(7)-Fe(1)-C(3)	162.95(8)	C(5)-C(1)-Fe(1)	69.34(10)
C(2)-Fe(1)-C(3)	40.45(7)	C(2)-C(1)-Fe(1)	69.86(10)
C(9)-Fe(1)-C(3)	120.22(8)	Si(1)-C(1)-Fe(1)	87.35(7)
C(4)-Fe(1)-C(3)	39.96(7)	C(3)-C(2)-C(1)	108.57(16)
C(8)-Fe(1)-C(3)	135.56(8)	C(3)-C(2)-C(11)	124.93(16)
C(1)-Fe(1)-Si(1)	44.60(5)	C(1)-C(2)-C(11)	126.32(16)
C(6)-Fe(1)-Si(1)	44.35(5)	C(3)-C(2)-Fe(1)	71.46(11)
C(5)-Fe(1)-Si(1)	72.03(6)	C(1)-C(2)-Fe(1)	67.93(10)
C(10)-Fe(1)-Si(1)	73.18(5)	C(11)-C(2)-Fe(1)	130.34(13)
C(7)-Fe(1)-Si(1)	74.07(6)	C(4)-C(3)-C(2)	108.74(16)
C(4)-C(3)-Fe(1)	69.74(10)	C(6)-C(7)-Fe(1)	68.22(10)
C(2)-C(3)-Fe(1)	68.10(10)	C(9)-C(8)-C(7)	108.12(18)
C(5)-C(4)-C(3)	107.88(17)	C(9)-C(8)-Fe(1)	69.87(11)
C(5)-C(4)-Fe(1)	67.85(10)	C(7)-C(8)-Fe(1)	68.14(11)
C(3)-C(4)-Fe(1)	70.30(11)	C(8)-C(9)-C(10)	107.86(18)
C(4)-C(5)-C(1)	109.62(16)	C(8)-C(9)-Fe(1)	70.13(11)

C(4)-C(5)-Fe(1)	71.73(11)	C(10)-C(9)-Fe(1)	67.93(11)
C(1)-C(5)-Fe(1)	68.44(10)	C(9)-C(10)-C(6)	109.69(17)
C(10)-C(6)-C(7)	104.91(16)	C(9)-C(10)-Fe(1)	71.50(11)
C(10)-C(6)-Si(1)	117.92(13)	C(6)-C(10)-Fe(1)	68.50(10)
C(7)-C(6)-Si(1)	120.09(14)	C(2)-C(11)-C(13)	109.47(16)
C(10)-C(6)-Fe(1)	69.46(10)	C(2)-C(11)-C(12)	112.48(17)
C(7)-C(6)-Fe(1)	69.80(10)	C(13)-C(11)-C(12)	110.73(18)
Si(1)-C(6)-Fe(1)	87.55(7)	C(16)-C(14)-Si(1)	114.52(16)
C(8)-C(7)-C(6)	109.40(17)	C(17)-C(15)-Si(1)	114.38(15)
C(8)-C(7)-Fe(1)	71.34(11)		

REFERENCES

(1) Sadeh, S.; Schatte, G.; Müller, J. *Chem. Eur. J.* **2013**, *19*, 13408–13417.

(2) Mark, J. E.; Allcock, H. R.; West, R. *Inorganic Polymers*, Oxford Uni.; New York, 2005.

(3) Segal, D. *Chemical Synthesis of Advanced Ceramic Materials*, Cambridge.; New York, 1991.

(4) Crabtree, R. H. *The Organometallic Chemistry of the Transition Metals*; Wiley and Sons, Ed.; New York, 2001.

(5) Manners, I. *Synthetic Metal-Containing Polymers*, WILEY-VCH.; Toronto, 2003.

(6) Barlow, S.; Drewitt, M. J.; Dijkstra, T.; Green, J. C.; O'Hare, D.; Whittingham, C.; Wynn, H. H.; Gates, D. P.; Manners, I.; Nelson, J. M.; Pudelski, J. K. *Organometallics* **1998**, *17*, 2113–2120.

(7) Herberhold, M. *Angew. Chem. Int. Ed.* **1995**, *34*, 1837–1839.

(8) Herbert, D. E.; Mayer, U. F. J.; Manners, I. *Angew. Chem. Int. Ed.* **2007**, *46*, 5060–5081.

(9) Rinehart, K. L.; Curby, R. J. *J. Am. Chem. Soc.* **1957**, *79*, 3290–3291.

(10) Rinehart, K. L.; Frerichs, A. K.; Kittle, P. A.; Westman, L. F.; Gustafson, D. H.; Pruett, R. L.; McMahon, J. E. *J. Am. Chem. Soc.* **1960**, *82*, 4111–4112.

(11) Osborne, A. G.; Whiteley, R. H. *J. Organomet. Chem.* **1975**, *101*, 27–28.

(12) Schachner, J. A.; Lund, C. L.; Quail, J. W.; Müller, J. *Organometallics* **2005**, *24*, 4483–4488.

(13) Schachner, J. A.; Lund, C. L.; Quail, J. W.; Müller, J. *Organometallics* **2005**, *24*, 785–787.

(14) Lund, C. L.; Schachner, J. A.; Quail, J. W.; Müller, J. *Organometallics* **2006**, *25*, 5817–5823.

(15) Bagh, B.; Gilroy, J. B.; Staubitz, A.; Müller, J. *J. Am. Chem. Soc.* **2010**, *132*, 1794–1795.

(16) Bagh, B.; Schatte, G.; Green, J. C.; Müller, J. *J. Am. Chem. Soc.* **2012**, *134*, 7924–7936.

(17) Schachner, J. A.; Tockner, S.; Lund, C. L.; Quail, J. W.; Rehahn, M.; Müller, J. *Organometallics* **2007**, *26*, 4658–4662.

(18) Braunschweig, H.; Burschka, C.; Clentsmith, G. K. B.; Kupfer, T.; Radacki, K. *Inorg. Chem.* **2005**, *44*, 4906–4908.

(19) Schachner, J. A.; Orlowski, G. A.; Quail, J. W.; Kraatz, H.-B.; Müller, J. *Inorg. Chem.* **2006**, *45*, 454–459.

(20) Bhattacharjee, H.; Müller, J. *Coord. Chem. Rev.* **2016**, *314*, 114–133.

(21) Sadeh, S.; Bhattacharjee, H.; Khozeimeh Sarbisheh, E.; Quail, J. W.; Müller, J. *Chem. Eur. J.* **2014**, *20*, 16320–16330.

(22) Rulkens, R.; Lough, A. J.; Manners, I. *J. Am. Chem. Soc.* **1994**, *116*, 797–798.

(23) Marquard, D.; Klusacek, H.; Gokel, G.; Hoffmann, P.; Ugi, I. *J. Am. Chem. Soc.* **1970**, *92*, 5389–5393.

(24) Kuhnen T.; Ruffolo R.; Stradiotto, M.; Ulbrich D.; McGlinchey, M. J. *Organometallics* **1997**, *15*, 5042–5047.

(25) Musgrave, R. A.; Russell, A. D.; Manners, I. *Organometallics* **2013**, *32*, 5654–5667.

(26) Foucher, D. A.; Tang, B. Z.; Manners, I. *J. Am. Chem. Soc.* **1992**, *114*, 6246–6248.

(27) Pudelski, J. K.; Rulkens, R.; Foucher, D. A.; Lough, A. J.; Macdonald, P. M.; Manners, I. *Macromolecules* **1995**, *28*, 7301–7308.

(28) Musgrave, R. A.; Russell, A. D.; Whittell, G. R.; Haddow, M. F.; Manners, I. *Organometallics* **2015**, *34*, 897–907.

(29) Ni, Y. Z.; Rulkens, R.; Pudelski, J. K.; Manners, I. *Macromol. Rapid Commun.* **1995**, *16*, 637–641.

(30) Reddy, N. P.; Yamashita, H.; Tanaka, M. *J. Chem. Soc., Chem. Commun.* **1995**, *22*, 2263–2264.

(31) Arimoto, F. S.; Haven, J. R. A. C. *J. Am. Chem. Soc.* **1955**, *77*, 6295–6297.

(32) Rosenberg, H.; Rausch, M. D. *US Pat. 3060215* **1962**.

(33) Rosenberg, H. *US Pat. 3426053* **1969**.

(34) Pudelski, J. K.; Manners, I. *J. Am. Chem. Soc.* **1995**, *117*, 7265–7266.

(35) Bellas, V.; Rehahn, M. *Angew. Chem. Int. Ed.* **2007**, *46*, 5082–5104.

(36) Rulkens, R.; Ni, Y. Z.; Manners, I. *J. Am. Chem. Soc.* **1994**, *116*, 12121–12122.

(37) Ni, Y.; Rulkens, R.; Manners, I. *J. Am. Chem. Soc.* **1996**, *118*, 4102–4114.

(38) Hailes, R. L. N.; Oliver, A. M.; Gwyther, J.; Whittell, G. R.; Manners, I. *Chem. Soc. Rev.* **2016**, *45*, 5358–5407.

(39) Sheridan, J. B.; Temple, K.; Lough, A. J.; Manners, I. *Dalt. Trans* **1997**, *5*, 711–713.

(40) Temple, K.; Jäkle, F.; Sheridan, J. B.; Manners, I. *J. Am. Chem. Soc.* **2001**, *123*, 1355–1364.

(41) Mizuta, T.; Onishi, M.; Miyoshi, K. *Organometallics* **2000**, *19*, 5005–5009.

(42) Herbert, D. E.; Tanabe, M.; Bourke, S. C.; Lough, A. J.; Manners, I. *J. Am. Chem. Soc.* **2008**, *130*, 4166–4176.

(43) Chan, W. Y.; Lough, A. J.; Manners, I. *Chem. Eur. J.* **2007**, *13*, 8867–8876.

(44) Manners, I. *Science (80-.).* **2001**, *294*, 1664–1666.

(45) Holliday, B. J.; Stanford, T. B.; Swager, T. M. *Chem. Mater.* **2006**, *18*, 5649–5651.

(46) Lammertink, R. G. H.; Hempenius, M. A.; Chan, V. Z. H.; Thomas, E. L.; Vancso, G. J. *Chem. Mater.* **2001**, *13*, 429–434.

(47) Massey, J. A.; Winnik, M. A.; Manners, I.; Chan, V. Z. H.; Ostermann, J. M.; Enchelmaier, R.; Spatz, J. P.; Möller, M. *J. Am. Chem. Soc.* **2001**, *123*, 3147–3148.

(48) Mizoguchi, K.; Tanaka, S.; Ogawa, T.; Shiobara, N.; Sakamoto, H. *Phys. Rev. B - Condens. Matter Mater. Phys.* **2005**, *72*, 1–4.

(49) Kealy, T. J.; Pauson, P. L. *Nature* **1951**, *168*, 1039–1040.

(50) Miller, S. A.; Tebboth, J. A.; Tremaine, J. F. *J. Chem. Soc.* **1952**, 632–635.

(51) Ruch, E., Fischer, E. O. *Z. Naturforsch., B* **1952**, *7*, 676.

(52) Wilkinson, G.; Rosenblum, M.; Whiting, M. C.; Woodward, R. B. *J. Am. Chem. Soc.* **1952**, *74*, 2125–2126.

(53) Eiland, P. F.; Pepinsky, R. *J. Am. Chem. Soc.* **1952**, *74*, 4971.

(54) Heinze, K.; Lang, H. *Organometallics* **2013**, *32*, 5623–5625.

(55) Schlögl, K.; Fried, M. *Monatsh. Chem.* **1964**, *95*, 558–575.

(56) *IUPAC Compend. Chem. Terminol.* **2014**, *2193*, 4681.

(57) Schlögl, K. *Top. Stereochem.* **1967**, *1*, 39–91.

(58) Hayashi, T.; Mise, T; Mitachi, S; Yamamoto, K.; Kumada, M. *Tetrahedron Lett.* **1976**, *17*, 1133–1134.

(59) Hayashi, T.; Matsumoto, Y.; Morikawa, I.; Ito, Y. *Tetrahedron: Asymmetry* **1990**, *1*, 151–154.

(60) Hayashi, T.; Yamamoto, K.; Kumada, M. *Tetrahedron Lett.* **1974**, *15*, 4405–4408.

(61) Ito, Y.; Sawamura, M.; Hayashi, T. *J. Am. Chem. Soc.* **1986**, *108*, 6405–6406.

(62) Sawamura, M.; Hamashima, H.; Ito, Y. *J. Org. Chem.* **1990**, *55*, 5935–5936.

(63) Sawamura, M.; Nagata, H; Sakamoto, H.; Ito, Y. *J. Am. Chem. Soc.* **1992**, *114*, 2586–2592.

(64) Hayashi, T; Hayashizaki, K.; Kiyoi, T.; Ito, Y. *J. Am. Chem. Soc.* **1988**, *110*, 8153–8156.

(65) Watanabe, M.; Araki, S.; Butsugan, Y.; Uemura, M. *J. Org. Chem.* **1991**, *56*, 2218–2224.

(66) Togni A., T. H. T. *Ferrocenes: homogeneous catalysis, organic synthesis, material science.*, VCH: Weinh.; Germany, 1995.

(67) Long, N. J. *Angew. Chem. Int. Ed. Eng.* **1995**, *34*, 21–38.

(68) Ryabov, A. D. *Angew. Chem. Int. Ed.* **1991**, *30*, 931–941.

(69) Woodward, R. B.; Rosenblum, M.; Whiting, M. C. *J. Am. Chem. Soc.* **1952**, *74*, 3458–3459.

(70) Weinmayr, V. *J. Am. Chem. Soc.* **1955**, *77*, 3009–3012.

(71) Benkeser, R. A.; Melzer, M. S.; Fitzgerald, W. P. *J. Org. Chem.* **1961**, *26*, 2569–2571.

(72) Benkeser, R. A.; Bach, J. L. *J. Am. Chem. Soc.* **1964**, *86*, 890–895.

(73) Rinehart, K. L.; Motz, K. L.; Moon, S. *J. Am. Chem. Soc.* **1957**, *79*, 2749–2754.

(74) Feng, X.; Pugin, B.; Küsters, E.; Sedelmeier, G.; Blaser, H.-U. *Adv. Synth. Catal.* **2007**, *349*, 1803–1807.

(75) Rausch, M. D.; Ciappene.Dj. *J. Organomet. Chem.* **1967**, *10*, 127–136.

(76) Sanders, R.; Mueller-Westerhoff, U. T. *J. Organomet. Chem.* **1996**, *512*, 219–224.

(77) Guillaneux, D.; Kagan, H. B. *J. Org. Chem.* **1995**, *60*, 2502–2505.

(78) Haush, M.; Vogei, M.; Rosenberg, H. *Chem. Commun.* **1957**, *22*, 900–903.

(79) Slocum, D. W.; Rockett, B. W.; Hauser, C. R. *J. Am. Chem. Soc.* **1965**, *87*, 1241–1246.

(80) Battelle, L. F.; Bau, R.; Gokel, G. W.; Oyakawa, R. T.; Ugi, I. K. *J. Am. Chem. Soc.* **1973**, *95*, 482–486.

(81) Schwink, L.; Knochel, P. *Chem. Eur. J.* **1998**, *4*, 950–968.

(82) Gleiter, R.; Bleiholder, C.; Rominger, F. *Organometallics* **2007**, *26*, 4850–4859.

(83) Lednicer, D.; Lindsay, J. K.; Hauser, C. R. *J. Org. Chem.* **1958**, *23*, 653–655.

(84) Lednicer, D.; Hauser, C. R. *J. Org. Chem.* **1959**, *24*, 43–46.

(85) Khozeimeh Sarbisheh, E.; Esteban Flores, J.; Zhu, J.; Müller, J. *Chem. Eur. J.* **2016**, *22*, 16838–16849.

(86) Zirakzadeh, A.; Schuecker, R.; Weissensteiner, W. *Tetrahedron: Asymmetry* **2010**, *21*, 1494–1502.

(87) SpinWorks version 4.1.

(88) Gschwend, B.; Pugin, B.; Bertogg, A.; Pfaltz, A. *Chem. Eur. J.* **2009**, *15*, 12993–13007.

(89) Nguema Edzang, R. W.; Lejars, M.; Brisset, H.; Raimundo, J.-M.; Bressy, C. *RSC Adv.* **2015**, *5*, 77019–77026.

(90) Khozeimeh Sarbisheh, E.; Esteban Flores, J.; Anderson, B. J.; Zhu, J.; Müller, J. *Organometallics* **2017**, *36*, 2182–2189.

(91) Fischer, A. B.; Kinney, J. B.; Staley, R. H.; Wrighton, M. S. *J. Am. Chem. Soc.* **1979**, *101*, 6501–6506.

(92) Osborne, A. G.; Whiteley, R. H. *J. Organomet. Chem.* **1980**, *193*, 345–357.

(93) Herbert, D. E.; Mayer, U. F.; Manners, I. *Angew. Chem. Int. Ed.* **2007**, *46*, 5060–5081.

(94) Finckh, W.; Tang, B. Z.; Foucher, D. A.; Zamble, D. B.; Ziembinski, R.; Lough, A.; Manners, I. *Organometallics* **1993**, *12*, 823–829.

(95) Corey, E. J.; Bakshi, R. K.; Shibata, S. *J. Am. Chem. Soc.* **1987**, *109*, 5551–5553.